An Experimental Study of Pool Fires and Validation of Different CFD Fire Models

Lars Roar Skarsbø

A thesis submitted in partial fulfilment of the requirements for the degree of Master of Science in the subject of Physics; Process Safety Technology

Department of Physics and Technology
University of Bergen
Bergen Norway
June 2011

Preface

This thesis is the final part of work in connection with my master programme in process technology, at the University of Bergen (UoB). During the work with my thesis, I have performed experiments in the fire laboratory at SHUC (Stord/Haugesund University College) and at RESQ training facility outside Haugesund. Computer simulations, using the CFD model FLACS, are performed at Gexcon in close cooperation with the developers of the code.

There are many people I would like to thank for helping me through all the work with this thesis. First I would like to thank my teaching supervisor Bjørn J. Arntzen for help, discussions and indication of what to focus on during the thesis. Thanks to Jens A. Melheim, Idar E. Storvik, Deiveegan Muthusamy, Olav Roald Hansen and Trygve Skjold for help and support with FLACS simulations. I also appreciate the good collaboration between UoB and SHUC making it possible to perform my own experiments for validations use in the CFD codes. In this context I would specially like to thanks Frode A. Halrynjo, a fellow student working with his Master's degree, and Arjen Kraaijenveld for helping me in the accomplishment of the experiments. The experimental work could not have been performed unless RESQ and SHUC had let me used their facilities and experimental apertures. I would also like to thank the Mechanical workshop at UoB for helping me building the rig used in the experiments.

I am grateful to Bjarne Paulsen Husted, Arild Grov and Maja Aarland who have been proofreading parts of the thesis.

Also thanks to my employer, Aker Solutions, who has given me the possibility to complete my master's degree beside work.

And finally thanks to Torhild Høgheim who has supported me and put up with me even though much of my spare time has gone into the work with this thesis.

Bergen 6.June 2011

_____
Lars Roar Skarsbø

Department of Physics and Technology
University of Bergen
Bergen Norway

III

Abstract

Computer programs developed to predict a possible fire scenario is today an important tool when working with fire safety. In this context different Computational Fluid Dynamics models, so called CFD models, where the domain of interest is divided into thousands of small control volumes, is widely used.

An important task when developing fire models are validation against experiments. This involves recreating the experimental setup in the CFD models and comparisons of the results from the simulation with the experimental results. Initially, in the work with this thesis, literature from previous pool fire experiments was collected and organized through a literature search. Even if there are a lot experimental data available for validation, it was decided to perform additional pool fire experiments in order to compare results with the CFD models FLACS (FLame Accelerator Simulator) and FDS (Fire Dynamic Simulator). From the literature search amongst existing experiments it was noticed that there were little experimental data available on pool fires with equipment other than tanks above the pool.

Several 0.5m x 0.5m heptane pool fire experiments with pipes obstructing above the fire were studied in the fire laboratory at SHUC (Stord/Haugesund University College). Different obstruction areas in different heights above the obstruction were tested in order to verify what effect it had on the fire. A cone calorimeter analysed the smoke from the fire. Additionally, temperature, radiative heat flux and mass loss rate were measured. These experiments showed that when a pipe obstruction is located close to the pool fire it has a decreasing effect on the heat release rate and thermal radiation from the fire. In order to verify if this also was the case with increased fire diameter, outdoor pool fire experiments with increased area were performed. Due to wind conditions during these experiments the results were not valid for use in verification. However, the outdoor experiments showed that the pipe effect can be neglected for windy conditions.

In the validation process of the CFD models FLACS and FDS, two additional experiments performed by Steckler et al. (1982) and Gutiérrez-Montez et al. (2009) are studied. Following parameters are validated against experiments; heat release rate, radiative heat flux, temperatures and velocity in flame, hot smoke gases and air. Simulations revealed that temperature and velocity in the hot smoke layer is close to experimental results for both FLACS and FDS. In FDS, radiative heat flux is well predicted when the fire is defined with mass loss rate or heat release rate. When using the liquid fuel model, where FDS calculated the evaporation rate, results are very grid dependent. This is also stated in the FDS User Guide. It seems that both simulations programs over predict the flame temperatures. Since small grid resolution is necessary in the flame region, further reduction in grid size probably would have improved these results. The pipe effects observed in the experimental work are not fully reproduced in the simulations. Some reductions in HRR and thermal radiation as well as narrower flame are observed in FDS using the liquid fuel model.

Nomenclature

Symbol	Description	Unit
A_f	Fuel surface area	m^2
d	Pipe (release) diameter	m
d	Sphere diameter	m
D	Pool diameter	m
E	Radiative power	W/ m^2
g	Gravitational acceleration	m^2/s
h	Convective heat transfer coefficient	W/(m^2 K)
h_v	Heat of vaporization	J/mol
H_f	Flame length	m
k	Turbulent kinetic energy	J/kg = m^2/s^2
k	Thermal conductivity	W/(m K)
k	Extinction coefficient	-
K	Effective emission coefficient	-
L	Flame thickness	m
L_v	Latent heat of evaporation or gasification	J/g
l_o	Integral length scale	-
l_u	Kolmogorov length scale	-
$\dot{m}$	Rate of mass loss	g/s
Nu	Nusselt number	-
Pr	Prandtl number	-
Q	Turbulent kinetic energy	$m^2 s^{-2}$
$\dot{Q}_c$	Rate of heat release	J/s = W
R	Universal gas constant	J/(mol K)
R	Regression rate	mm/min
R	Distance	m
Re	Reynolds number	-
R_l	Turbulent Reynolds number	-
t	Time	s
T	Temperature	K
v	Velocity	m/s
V	Volume	m^3
X_f	Volume fraction of fuel vapour	-
W_f	Molecular weight	g/mol

Greek letters

β	Mean beam length corrector	-
ΔH_c	Heat of combustion	kJ/mol or kJ/g
ε	Emissivity	-
ε	Dissipation rate of turbulent kinetic energy	$W/kg = m^2/s^3$
θ	Angle	°
μ	Dynamic viscosity	kg/(m s)
ρ	density	kg/m^3
ν	Kinematic viscosity	m^2/s
σ	Stefan-Boltzmann constant	$W/(m^2\ K^4)$
χ	Combustion efficiency	-
ϕ	Configuration factor	-

Subscripts

a	ambient
C	Combustion
ch	Chemical reaction
conv	convection
E	External
f	Flame
F	Flame
g	Gas
l	liquid
L	Losses
rad	Radiation
R	Radiative
TC	Thermo couple
∞	Final value

Superscripts

·	Signifies rate of change as in $\dot{m}$
″	Double prime (signifies 'per unit area')

x

Table of content

Definitions and word explanations

Auto ignition – Lowest temperature of spontaneously ignition in a normal atmosphere without any external ignition sources (flame, spark etc.).

Electromagnetic spectrum – Range of all possible frequencies of electromagnetic radiation, from low frequencies used in modern radios to gamma radiation at the short wavelength end.

Evaporation – Vaporization of a liquid that occurs only on the surface of a liquid (not boiling).

Flash point liquid - lowest temperature at which a volatile liquid can vaporize to form an ignitable mixture in air.

Hydrocarbon (HC) – An organic compound consisting entirely of hydrogen and carbon.

Pyrolysis – Thermo chemical decomposition of organic material at elevated temperatures in the absence of oxygen.

Thermal radiation/convection/conduction – "Thermal Radiation", "Thermal Conduction" and "Thermal Convection" are mainly used as "Radiation", "Conduction " and "Convection" in this report.

TNO – Netherlands Organisation for Applied Scientific Research TNO.

Two- phase flow – Flow containing both gas and liquid.

Volatiles - Tendency of a substance to vaporize (low boiling point).

Validation and Verification - The terms Verification and Validation are often used interchangeably to mean the process of checking the accuracy of a numerical model. For many, this entails comparing model predictions with experimental measurements. However, there is now a fairly broad-based consensus that comparing model and experiment is largely what is considered Validation (FDS official website).

1   Introduction

1.1   Motivation

In process systems or other systems containing flammable liquids there are always a risk for an accidental leak. Ignition of a flammable liquid might result in a fire with potential to threaten humans, structures and surrounding nature. Risks of liquid fires (pool fires) are present during all stages of handling petroleum products. Starting with exploration and production both in onshore and offshore installations, refining and processing the crude petroleum and during transportation at sea or land to the end users. Size of the pool fire dependents on; ground features, existence of a confining bund or by balance between the release rate and the evaporation rate. A possible scenario in the petroleum production or processing stage could be a relative small liquid fire that impinges on a vessel. If the vessel is not dimensioned to withstand the fire loads from the fire, this could result in an escalation potential where the vessel ruptures and a much larger incident is developing.

In the design of new installations, or modification of existing, an important part of the safety evaluation is to calculate Dimensional Accidental Loads (DAL). Regarding liquid releases this requires assessing: amount of potential release, dispersion of the release, duration of a fire after the leak ignites and fire loads that affect the surroundings. To get as realistic fire loads as possible engineers use computer simulations software where all available input data is defined and resulting fire scenarios given as output data.

1.2   Objective

When developing computer programs for fire simulation an important part is validation against results from experimental work. In this thesis liquid pool fire experiments for use in such validation work have been constructed. These experiments, together with some of the experiments performed by Steckler et al. (1982) and Gutiérrez-Montez et al. (2009), are used in validation of the CFD models FLACS (Flame Accelerator Simulator) and FDS (Fire Dynamic Simulator). The main objective of this work is to clarify how adequate the CFD models correlate with the experiments, and identify possible weaknesses.

1.3   Limitations

The work is limited to validation of the CFD models towards experimental work only. This means that weaknesses and improvement suggestions are only described. Models are not modified and tested.

1.4   Overview of thesis

A theoretical background of the fire phenomena, with focus on pool fires, is given in Chapter 2. In Chapter 3, the numerical models FLACS and FDS are described, and in Chapter 4, a literature search of existing work is presented. Chapter 5 constitutes of a description of the experimental test facilities with experimental results and discussions. Simulation results using the CFD models and discussion of these results are presented in Chapter 6, while Chapter 7 contains the overall conclusion. Recommendation for further work is described in Chapter 8.

1 Introduction

2   Background

From (FARLEX) a fire can be defined as a: *"rapid, persistent chemical change that releases heat and light and is accompanied by flame, especially the exothermic oxidation of a combustible substance"*. The flame is the visible part of the fire and consists mainly of glowing hot soot. Historical as well as today the fire phenomena is used in controlled conditions like cooking, generating heat, signalling and propulsion purposes. But if a fire is not intended it can easy escalate to an uncontrolled dangerous situation where human, material,-and environmental values are threaten. This chapter starts with an introduction of the fire phenomena and different types of fires. Thereafter liquid fires, from now on called pool fires are handled in more detail.

2.1   Fire square and combustion of fuels

There are several factors that are essential for a fire to occur and continue burning. An easy way to illustrate these factors is by looking at the fire square illustrated in Figure 2-1. As the figure shows, a fire can start when flammable fuel in combination with a sufficient quantity of an oxidizer such as oxygen, is exposed to a source of heat. This could be a sparking source or ambient temperature above the flash point for the fuel/oxygen (air) mix. Continuous burning after ignition requires rapid oxidation process that produces chain reactions. For many years a fire triangle was used to illustrate the concept of a fire. But further fire research determined that a fourth element, chemical chain reaction in the combustion zone, was a necessary fire component. Anyway, the triangle is still sufficient for those who just want an introduction in fire technical subjects. In English and American literature the four factors are illustrated as a fire tetrahedron.
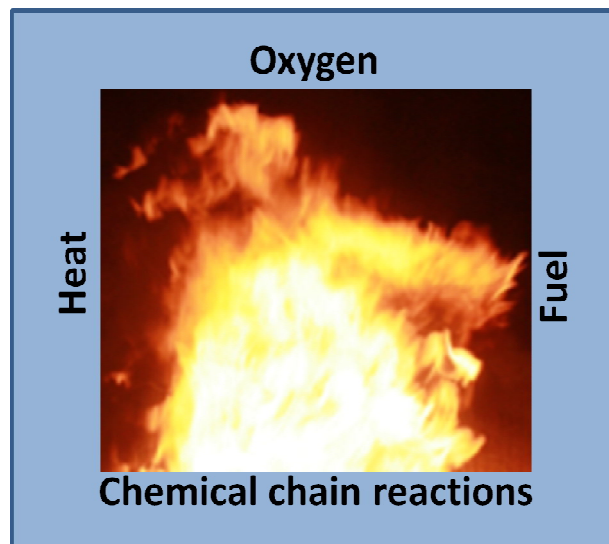
Figure 2-1 *Fire square*

Fuel exists in three aggregate states: solid, liquid and gas. Flame is a gas phase phenomena, this means that liquid and solid fuels must be transformed to gaseous form in flaming combustion. To yield products that can volatilize from a solid surface and enter the flame, a chemical decomposition or pyrolysis is necessary for almost all solids. For liquids this process is normally simple evaporating from the surface. Pyrolysis requires much

_____

more energy than evaporation, which results in high surface temperatures (around 400°C) of the burning solids (Drysdale, 1999).

Oxygen and heat (energy) are both central factors in a combustion process. Air contains approximately 21% oxygen and therefore supplies the combustion with oxygen as long as the air supply is not avoided. In non-premixed flames (see Section 2.3) air is feed into the combustion zone by suction forces due to pressure-and density differences between the fire and surrounding air. Energy to maintain the combustion is produced in the combustion zone. The energy production should give enough energy to maintain the temperature in the combustion zone and contribute to sufficient evaporation of the fuel (Hagen, 2004).

During chemical reactions between two or more substances chemical reactions equations are used to describe amount of reactants and products, see equation (2-1) for heptane combustion in air. In these reaction equations intermediate processes called *chain reactions* are not included. Since chain reactions include free radicals (atoms, molecules, or ions) that don't consumes or disappear from the reaction zone, they are necessary for a chemical process to keep going. Free radicals are characterized as unpaired electrons where the outermost electron shell is unfilled (Hagen, 2004). As described in Warnatz, Maas et al. (2006) the radical chain reactions can be divided into *chain initiation steps* (radicals formed from stable species), *chain propagation steps* (one reactive species formed when reactive intermediate species reacting with stable species), *chain branching steps* (two reactive species formed when a reactive species react with a stable species) and *chain termination steps* (reactive species react to stable species). This means that the chain branching steps where only free radicals are formed is of high importance in a combustion process

In combustion where a compound reacts with an oxidizing element, such as oxygen or fluorine, and the products are compounds of each element in the fuel with the oxidizing element, is called a *complete combustion*. For hydrocarbon (HC) combustion processes reacting with oxygen this will result in only CO_2 and H_2O in the combustion products. In fires the rate of mixture between fuel and air will result in *incomplete combustion* where some of the reactants are parts of the products from the fire. Incomplete combustion is either *fuel lean* or *fuel rich*. In *lean combustion* there is not enough fuel to react all the oxygen, this results in oxygen in the combustion products as shown in equation (2-2). In *fuel rich combustion* there is not enough oxygen (air) to react all the fuel, this is shown in equation (2-3). In these cases it is not possible ascertain exact the combustion products, but typical products are CO and H_2 in addition to CO_2 and H_2O (Hagen, 2004).

$$C_7H_{16} + 11(O_2 + 3,76N_2) \rightarrow 7CO_2 + 8H_2O + 82,72N_2 \qquad \textbf{(2-1)}$$

$$C_7H_{16} + 12(O_2 + 3,76N_2) \rightarrow 7CO_2 + 8H_2O + 82,72N_2 + O_2 \qquad \textbf{(2-2)}$$

$$2C_7H_{16} + 11(O_2 + 3,76N_2) \rightarrow xCO_2 + yH_2O + zN_2 + wCO + uH_2 + vC_7H_{16} \qquad \textbf{(2-3)}$$
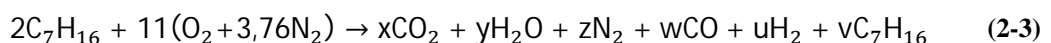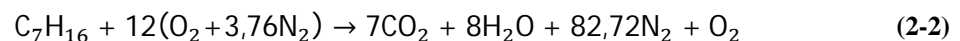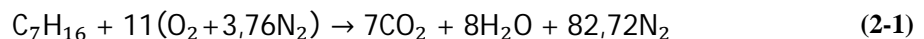
2.2   Heat transport

This section is based on theory from the book "An introduction to fire dynamics" by Drysdale (1999).

To be able to interpret the fire phenomena it's required to understand several branches of physics as; fluid dynamics and heat and mass transfer. The three basic mechanisms of heat transfer, namely conduction, convection and radiation are further described in this section. In a fire all three mechanism may contribute, but according Drysdale (1999) it is often found that one of the mechanism dominates at a given location or given stage of the fire development.

Conduction is the rate of heat flow in and through solids and is by this important during ignition and spread of flame over combustible solids. It can also occur in fluids, but it is normally masked by convective motion where heat is dissipated by a mixing process driven by buoyancy. Conduction is also important in connection with fire safety measures to prevent fire spread through fire walls, heating of structure above yield strength etc.

Heat exchange between gas or liquid and a solid, involving movement of the fluid is called *convection*. In fires this method of heat transfer is most important in early stage due to thermal radiation levels are low. Movement of gases by convection in natural fires is determined by buoyancy, which also influence the shape and behaviour of diffusion flames.

Radiation heat transfer on the other hand involves transfer of heat by electromagnetic waves and thereby no intervening medium between the heat source and the receiver. Radiation can be absorbed, transmitted or reflected at a surface in all parts of the electromagnetic spectrum. In fires, radiation becomes the dominant mode of heat transfer as the fuel diameter increases above about 0.3m. Because radiation is not dependent of contact between heat source and the receiver, objects located away from the fire itself can be heated and auto ignites after some time. Fire spread between buildings is a typical radiation phenomenon.

When a body is heated the temperature rises. The body will then partly loose heat by convection and partly by radiation. At low temperatures (150-200°C) convection dominated but above 400°C the radiation becomes increasingly dominant. Radiation heat transfer can be described by a reference to the so-called "black body" which is defined as a body that absorbs all that falls on its surface. This is a hypothetic body that completely absorbs all wavelengths of thermal radiation incident on it. Radiation energy per unit time from a black body is proportional with fourth power of absolute temperature and can be expressed with Stefan Boltzmann law as:

$$E = \varepsilon \sigma T^4 \quad [W/m^2] \tag{2-4}$$

Where ε is the efficiency of the surface as a radiator, called emissivity (black body has emissivity of 1). σ is the Stefan- Boltzmann constant (5.67 x 10^{-8} W/m^{2}K^4) and T is the temperature of the black body (K). By inserting a factor that account for geometrical relationship between the emitter and the receiver, called the configuration factor (ϕ), the effect on a surface remote from the emitter can be calculated by following equation:

$$\dot{q}''_{radiation} = \phi \varepsilon \sigma T^4 \quad [W/m^2] \tag{2-5}$$

Conductive and convective heat transfers are also expressed by heat transfer equations. For conduction, the following equation, also called Fourier's law of heat conduction, is used:

$$\dot{q}''_{conduction} = -k\frac{dT}{dx}\ [W/m^2]\qquad\qquad\text{(2-6)}$$

where k (W/mK) is the thermal conductivity of the material, dT is the difference in temperature (K) between the exposed side (normally fire side) and not exposed side (e.g. other side of a fire wall), and dx is the distance the heat is transferred (e.g. thickness of a wall). A good heat conductor like copper has a k value of 387 W/mk (Table 2.1 in (Drysdale, 1999)) while for concrete which often is used in fire walls, and low heat conduction is of importance, the thermal conductivity is in the range 0.8-1.4 W/mk (Table 2.1 in (Drysdale, 1999)).

Heat transfer by natural convection can be described by Newton's law of cooling:

$$\dot{q}''_{convection} = hdT\ [W/m^2]\qquad\qquad\text{(2-7)}$$

where h (W/m^{2}K) is the convective heat transfer and dT is the temperature difference between the hot and cold medium, e.g. hot smoke and wall or hot wall and surrounding cold air. Unlike thermal conductivity, h is not a material constant. It (h) depends on geometry of the solid, properties of the fluid, flow parameters and characteristics of the system. A major problem in heat transfer and fluid dynamics is therefore evaluation of h in different situations.

2.3   Flame behaviour

According Warnatz et al. (2006) a combustion process could be divided into different categories This based upon whether the fuel and oxidizer (typical air) is mixed first and burned later (premixed), or whether combustion and mixing occur simultaneous in the combustion zone (non-premixed). Non-premixed flames are also called diffusion flames since oxygen and fuel diffuse into each other and the flame occur where they meets. Premixed and non-premixed combustion are further divided into laminar and turbulent combustion. Figure 2-2 contains examples of different combustions in each category.
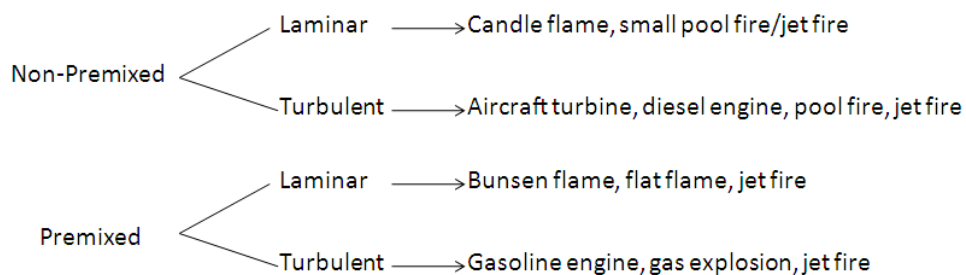

Figure 2-2 *Combustion ordered based on mixing between fuel and oxidizer and fluid motion. Figure based on Table 1.2 in (Warnatz, Maas et al., 2006).*

If the combustion consists of flow, e.g. jet flame or flame in pipe, laminar flames are obtained at low flow rates. When the flow rate increases the flame transforms gradually to turbulent. The Reynolds number is often used to characterize the laminar or turbulent flow regimes. Laminar flow occurs at low Reynolds number, e.g. less than 2000 for jet flames (Drysdale, 1999) and 2300 in pipe flow. In the laminar flow regime viscous forces are

dominant, and the flame characterized as smooth with constant motion. Increased velocity (flow rate) results in increased Reynolds number, see equation (2-8) below;

$$Re = \frac{\rho v d}{\mu} = \frac{v d}{\mu} \quad [-] \tag{2-8}$$

where ρ is the density (kg/m^3) of the fluid, v is the velocity, d is the diameter of the pipe or release diameter, μ is the dynamic viscosity and ν is the kinematic viscosity. According Drysdale (1999) turbulence occurs when Reynolds number is significantly greater than 2000 in jet flames (nozzles), and about 4000 in pipe flow. Turbulence is dominated by inertial forces, which tend to produce chaotic eddies, vortices and other flow instabilities.

The above definition of the Reynolds number (R_e) is as described geometry-dependent. To universally describe the degree of turbulence, a turbulence Reynolds number (R_l) from (Warnatz, Maas et al., 2006) can be used:

$$Rl = \frac{\bar{\rho}\sqrt{2q}l_0}{\bar{\mu}} \quad [-] \tag{2-9}$$

where l_0 is the integral length scale, or largest turbulent structure and q is the turbulent kinetic energy (m^{2}s^{-2}).

In contrast to jet flames (fires) where momentum of the fuel stream is dominating the behaviour, buoyancy is the dominating driving force in natural flames. These flames are more susceptible to external influences (air movement), which lead to less ordered flame structures. As described further in Section 2.4.1.3 studies by Blinov and Khudiakov (1957) reported in Drysdale (1999) concluded that for pool fires with diameter less then 0.03m, flames are laminar. In the region with pool diameters from 0.03m to 1.0m they observed a transitional behaviour between laminar and turbulent. For larger diameters ($D>1$m) the flames are fully turbulent.

When flammable combustibles are released from a reservoir different combustion scenarios may occur. Depending on different parameters such as; how the combustible are released, if the combustibles are in gas/liquid or two-phase and ignition time (delayed ignition) accidents as showed in Figure 2-3 may occur.
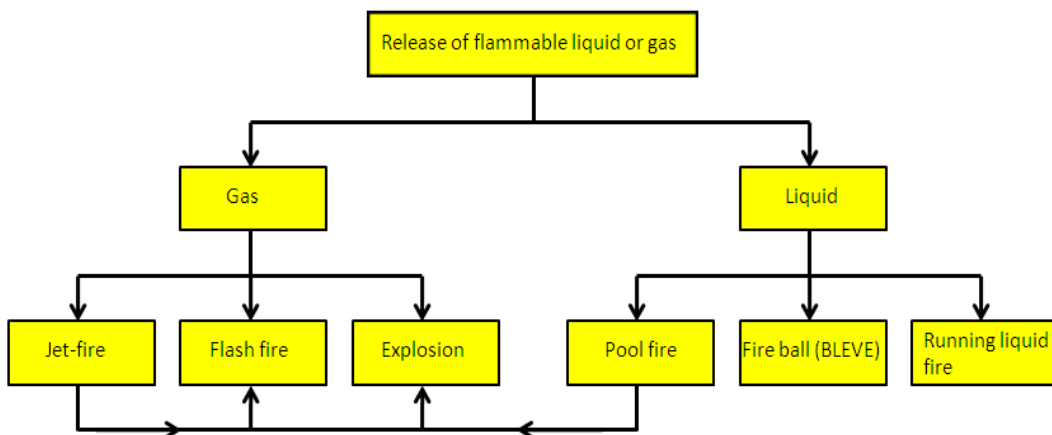

Figure 2-3 *Possible scenarios from release of flammable combustibles (modified from (Casal, 2008)).*

_____

A *liquid fire* occurs when a spill of liquid fuel is ignited. This is a diffusion fire (normally turbulent, see Section 2.4.1.3) that burns above a vaporizing fuel (normally hydrocarbon fuel) with zero or low initial momentum. Fires in the open will be well ventilated (fuel-controlled), but fires within enclosures may become under-ventilated (ventilation-controlled). According Drysdale (1999) stable liquids tend to burn as pools with uniform horizontal surfaces. But a *running liquid fire*, where the leak of fluid at high level produces a flow of burning liquid over the surface below, is experienced in petrochemical and related industries. These fires can cause very substantial damage to structural steel work and are difficult to extinguish.

If a pool-or jet fire is not ignited within some time, it increases the possibility of creating an explosive vapour (gas)/air mixture that could lead to a flash fire or explosion. A *flash fire* can be defined as (NFPA, 2002) : *"fire involving the delayed ignition of a dispersed vapour cloud, which does not cause blast damage. That is, the flame speed is not as high as in an unconfined vapour cloud explosion, but the fire spreads quickly throughout the flammable zone of the cloud and is usually associated with near-field damage effects and remote personnel effects"*. An *explosion* on the other hand creates a shock wave (blast wave) that has supersonic velocity (detonation) or subsonic velocity (deflagration). In explosion the blast wave is the cause of serious damage of surrounding equipment.

According to D.A. Crowl & J.F. Louvar (1990) a *BLEVE* (boiling liquid expanding vapour explosion) occurs when a vessel containing a pressurized liquid above its boiling point ruptures. This results in an explosive vaporization of a large fraction of the tank contents. When BLEVE involves a flammable substance, it is usually followed by a *fireball* consisting of a two-phase cloud that can burn only on its outer surface as inside there is no oxygen. This fire ball has a short duration, but the thermal radiation intensity can be very strong (Casal, 2008). BLEVE is often caused by a surrounding fire heating up the content in the vessel leading to pressure build up. If a tank is heated in the area of no liquid it ruptures faster due to less absorption of heat. Vessels are often passive fire protected to prevent these ruptures.

If flammable gas/vapour or two phases flows are released through a hole, flange etc. at a relatively high speed, followed by ignition, a *jet fire* occurs. Compared with pool fires they normally emit higher heat fluxes (temperatures) but a smaller area is exposed by the fire. Requirements regarding peak heat loads from a fire is according the Norwegian safety standard for offshore installations (Norsok(S-001), 2008) 150 kW/m^2 for pool fires and 350 kW/m^2 for jet fires. According HSE (2011) properties of a jet fire depends on release conditions, release rate, fuel composition, release geometry, direction and ambient wind conditions. For instance will a low velocity two-phase release of condensate material be more wind affected, sootier and therefore highly more radiative than a high velocity (sonic) release of natural gas that are less buoyant, less sootier and thus less radiative.

2.4   Pool fires (liquid fires)

In this section liquid fires (pool fires) are further described. The main focus is to give a more detail understanding in burning-behaviour of these kinds of fires.

2.4.1   Heat Release Rate

The rate of which energy is released in a fire ($\dot{Q}_c$) is the most important single factor characterizing its behaviour (Babruskas and Peacick (1992) reported in Drysdale (1999)). If the Heat Release Rate (HRR) is known, it can among other things be used to estimate the flame size and radiation to surroundings, and assess likely flame behaviour in practical situations. In (NFPA, 2002) it is stated that the energy released (convective and radiative component) in a fire is the total amount of heat generated as a result of chemical reactions in the combustion.

$$E_{ch} = E_{convective} + E_{radiative} \qquad \textbf{(2-10)}$$

Today it is possible to determine the rate of heat release experimentally by using the method of oxygen consumption calorimeter (cone calorimeter). This method is widely used throughout the world and it is recognized as the most accurate and practical technique for measuring heat release rate from experimental fires. A short introduction of this method based on information from (Drysdale, 1999) and (NFPA, 2002) is further described.

The basis of this method is that most gases, liquids, and solids release a constant amount of energy for each unit mass of oxygen consumed. This constant is found to be 13.1 kJ/g oxygen consumed and is considered to be accurate within ±5 percent for most hydrocarbon fuels. After ignition, the combustion products are collected in a hood and removed through an exhaust duct in which the flow rate and composition of the gases is measured to determine how much oxygen has been consumed. HRR is then calculated using the constant relationship between oxygen consumed and energy released.

There are limitations in fire sizes when using the cone calorimeter. As an alternative method, HRR is measured based on mass loss rate using simple a scale (weight equipment). The time dependent mass loss rate measured from the fire experiment can then be used in equation (2-11) to calculated the HRR (Drysdale, 1999).

$$\dot{Q}_c = \chi \cdot \Delta H_c \cdot \dot{m}'' \cdot A_f \quad \text{[kW]} \qquad \textbf{(2-11)}$$

where χ is a factor (<1.0) which is included to account for incomplete combustion. ΔH_c is the heat of combustion of the volatiles (kJ/g), $\dot{m}''$ is the rate of burning or mass flux given as (g/m^{2}s) and A_f is the fuel surface area (m^2).

2.4.1.1   Heat of combustion and combustion efficiency

The heat of combustion (ΔH_c) value describes amount of energy released or consumed during complete combustion between fuel and oxygen. A reaction where energy is released (negative ΔH_c) is called exothermic.

Heat of combustion (ΔH_C) is normally determined using a 'bomb' calorimeter. In this method the volume is constant and a known mass of fuel is burnt completely in an atmosphere of pure oxygen. The change in enthalpy (ΔH_c) can also be calculated using the heat of formation (ΔH_f) values for all reactants and products in the chemical reaction, see equation (2-12). The heat of formation (ΔH_f) is defined as the enthalpy change when a compound is formed in its standard state (Temperature 298K and Pressure 1atm) from its constituent elements also in their standard states (Drysdale, 1999).

_____

$$\Delta H_c = \frac{\sum \Delta H_{f\,products} - \sum \Delta H_{f\,reactants}}{n_{fuel}} \quad \text{[kJ/mol]} \tag{2-12}$$

Since the enthalpy change is given for complete combustion it is necessary to correct it for incomplete combustion in a fire scenario. From (NFPA, 2002) the combustion efficiency factor χ which account for incomplete combustion are defined as:

$$\chi_{ch} = \frac{\dot{Q}_{ch}{}''}{\dot{Q}_T{}''} = \frac{\dot{m}'' \Delta H_{ch}}{\dot{m}'' \Delta H_T} = \frac{\Delta H_{ch}}{\Delta H_T} = \frac{\Delta H_{convection} + \Delta H_{radiation}}{\Delta H_T} \tag{2-13}$$

Where $\dot{Q}_T{}''$ and ΔH_T are for complete combustion and $\dot{Q}_{ch}{}''$ and ΔH_{ch} are the chemical rates for the given fire. As described in (NFPA, 2002) combustion efficiency generally depends on the fuel, ventilation conditions, soot production and flame size. The distribution of the chemical heat into convective and radiative components changes with fire size. Generally, larger fire size gives larger fraction of the chemical heat distributed into the radiative component. A clear sign of incomplete combustion is when the flame produces soot. Clean burning gaseous fuels such as methane has χ close to 1.

As described above the combustion efficiency (χ) is not only dependent of the fuel. For heptane liquid different combustion efficiency values are documented in literature, see Table 2-1 below. Experiments performed by Tewarson (2004) shows that for well ventilated pool fires within the range 0.1-2m, χ is weakly dependent of fire diameter. McCaffrey and Harkleroad (1989) studied heptane among other fuels in a O_2 depletion calorimetry. They found that the combustion efficiency varied with pool diameter. Work performed by Koseki and Mulholland (1991) showed that increased pan diameter lead to increased CO/CO_2 ratio. This increase in smoke and CO lead to decreased combustion efficiency.

Table 2-1 *Combustion efficiency (χ) values for heptane and crude oil*

χ	χ$_{rad}$	χ$_{conv}$	Conditions	Reference
0.69	0.316	0.374	Small diameter (ca. 0.1m) External heat flux controlled	Table 5.12 (Drysdale, 1999)
0.924	0.305	0.619	Small diameter (ca. 0.1m) Well ventilated External heat flux controlled	Table 3-4.14 (NFPA, 2002)
0.94	-	-	Diameter of 0.5m	McCaffrey and
0.80	-	-	Diameter of 0.3m	Harkleroad (1989)
0.8±0.1	-	-	Diameter 0.71-1.60m	Simo Hostika (2001)
0.90	-	-	Crude oil diameter 1.0m	Koseki and
0.75	-	-	Crude oil 2.7m x 2.7m	Mulholland (1991)

2.4.1.2 Mass burning rate

This section is based on theory from the book "An introduction to fire dynamics" by Drysdale (1999).

_____

The rate of supply of volatiles from a fuel surface is dependent of the rate of heat transfer from the flame to the fuel. In fire scenarios where radiation from surrounding equipment or smoke layer (outdoor) is neglected, the mass flux ($\dot{m}''$) is described by following equation:

$$\dot{m}'' = \frac{Q''_F - Q''_L}{L_v} \quad [\text{kg/s}]$$

(2-14)

where $\dot{Q}''_F$ is the heat flux supplied by the flame (kW/m^2) and must in turn be related to the rate of energy released within the flame and the mechanism of heat transfer involved. $\dot{Q}''_L$ represents the losses expressed as a heat flux through the fuel surface (kW/m^2) and L_v is the heat required to produce the volatiles (kJ/kg). This means that liquids have a lower L_v value than solids where chemical decomposition is involved.

In liquid pool fires the heat flux $\dot{Q}''_F$ from the flame to the liquid is expressed as the sum of the three terms, these are; conduction, convection and radiation. Conduction refers to heat transfer through the rim of the container, expressed as:

$$\dot{q}''_{conduction} = k_1 \pi D (T_F - T_l) \quad [\text{W}]$$

(2-15)

where T_F is the flame temperature, T_l the liquid temperature, D is the diameter of the pool and k_1 is a constant which incorporate a number of heat transfer terms. Convection direct to the fuel surface is given by:

$$\dot{q}''_{convection} = k_2 \frac{\pi D^2}{4} (T_F - T_l) \quad [\text{W}]$$

(2-16)

where k_2 is the convective heat transfer coefficient (h). The radiation to the surface can be expressed as (re-radiation from fuel surface is included):

$$\dot{q}''_{radiation} = k_3 \frac{\pi D^2}{4} (T^4_F - T^4_l)(1 - \exp(-k_4 D)) \quad [\text{W}]$$

(2-17)

where k_3 contains the Stefan-Boltzmann constant (σ) and the configuration factor(ϕ) for heat transfer from the flame to the surface, while $(1 - exp(-k_4 D))$ is the emissivity of the flame. The factor k_4 must contain a factor of proportionality relating the mean beam length to the pool diameter, but also concentration and emission coefficients of the radiating species in the flame. Rasbash (1956), reported in Drysdale (1999), discovered in experiments that for hydrocarbon fires there was a vapour zone above the liquid that would be expected to attenuate (the cool vapour layer will absorb radiation from the hot flame) the radiation reaching the surface. This vapour zone varies for different fuels and pool sizes. The k_4 constant must also incorporate a factor for this 'radiation blocking' when the vapours zone above the fuel becomes sufficiently thick to attenuate the flux falling on the surface.

Conductive heat transfer determines the mass burning rate when D is very small, but provided that the emissivity is of sufficient magnitude, radiation dominates for large pool diameters. The heat conduction through the rim of the container (if the pool has a surrounding rim) is also a minimalistic contribution in a pool fire. This means that for most

_____

pool fires (no radiation from surroundings) it is only relevant to consider the radiation contribution from the flame back to the liquid and losses from the liquid surface.
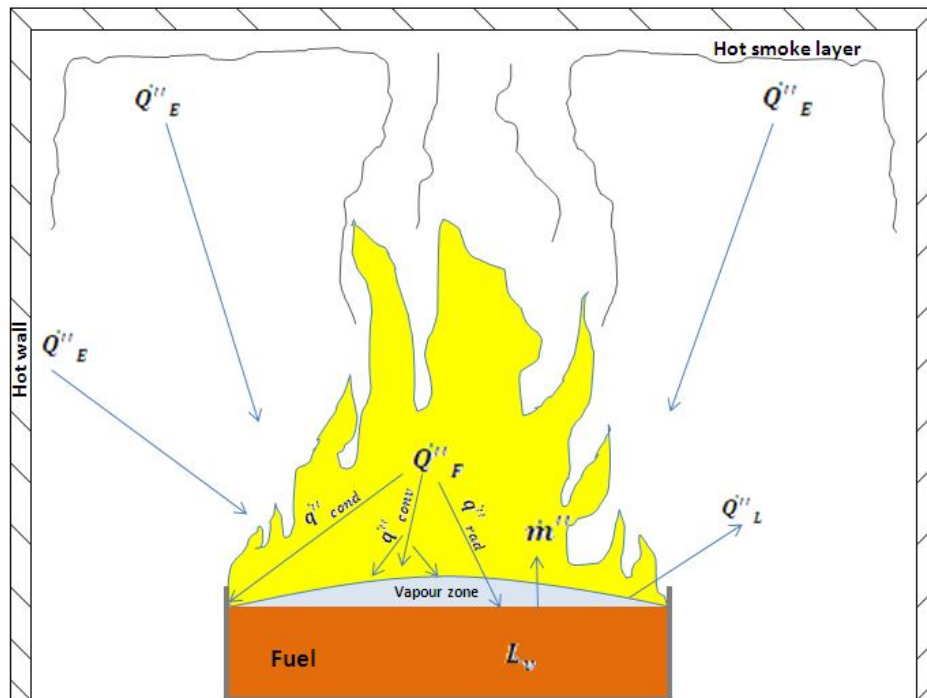

Figure 2-4 *Mass burning rate pool fires.*

In many situations surroundings will affect the pool fires mass burning rate. As Figure 2-4 illustrates this could for instance be surrounding equipment that is heated by the fire or a growing smoke layer above the fire. Both the surrounding equipment and the smoke layer will radiate back to the liquid pool and lead to further evaporation. By assuming that the smoke layer and surroundings radiates as a horizontal surface, the external heat flux $\dot{Q}''_E$ (W/m^2) back to the fuel surface, are calculated by replacing T^4 with $(T^4_s - T^4_l)$ in equation (2-5). This includes the temperature difference between the hot smoke layers or surrounded equipment temperature (T_s) and the liquid (T_l).

Rewriting the mass flux equation to include heat effect from the smoke layer (surroundings) gives the following expression:

$$\dot{m}'' = \frac{\dot{Q}''_F + \dot{Q}''_E - \dot{Q}''_L}{L_v} \quad [\text{kg/sm}^2] \tag{2-18}$$

If the mass burning rate from a liquid pool fire is unknown, not found by experiments, it has to be estimated. Zabetakis and Burgess reported in Drysdale (1999), proposed a correlation which is valid for pool fires with larger diameter than 0.2m:

$$\dot{m}'' = \dot{m}_\infty''(1 - exp(-k\beta D)) \quad [\text{kg/sm}^2] \tag{2-19}$$

The above equation require knowledge about the fuels extinction coefficient (k), mean beam length corrector (β) and limiting burning rate ($\dot{m}_\infty$). Table 2-2 includes some proposed heptane values.

Table 2-2 *Proposed heptane values from Table 5.2 in (Drysdale, 1999)*

Liquid	$\dot{m}_\infty$ (kg/m^{2}s)	$k\beta$ (m^{-1})
Heptane	0.101	1.1

When using proposed heptane values from Table 2-2 in equation (2-19), Figure 2-5 shows that the mass burning rate will increase rapidly until the diameter reach about 3m where it stabilizes around $\dot{m}_\infty''$.
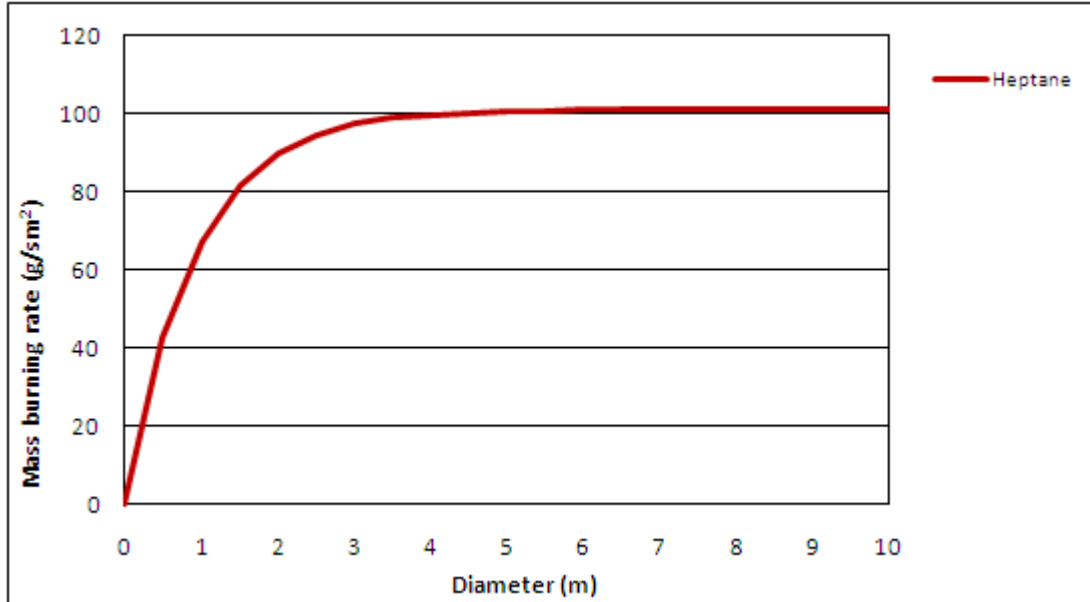

Figure 2-5 *Heptane mass burning rate dependence of pool diameter using Zabetakis and Burgess (1961) expression reported in (Drysdale, 1999)*

2.4.1.3   Regression rate and flame behaviour

Blinov and Khudiakov (1957) (reported in Drysdale (1999)) studied the rates of burning for different pool sizes with different hydrocarbon liquids, see Figure 2-6. In their study they discovered that the rate of burning expressed as a 'regression rate' R (mm/min) was high for small-scale laboratory pools and exhibited a minimum around 0.1m diameter. From their results the regression rate dependents of pool sizes seems to be distinguished in three regimes. When the diameter is less then 0.03m, the flames are laminar and the regression rate, R, falls with increase in diameter. For larger diameters (D>1m) the flames are fully turbulent and R becomes independent of diameter. In the region with pool diameters from 0.03m to 1.0m transitional behaviour, between laminar and turbulent, is observed.

Figure 2-6 also shows that different fuels reach their maximum regression rate at different pool diameters.
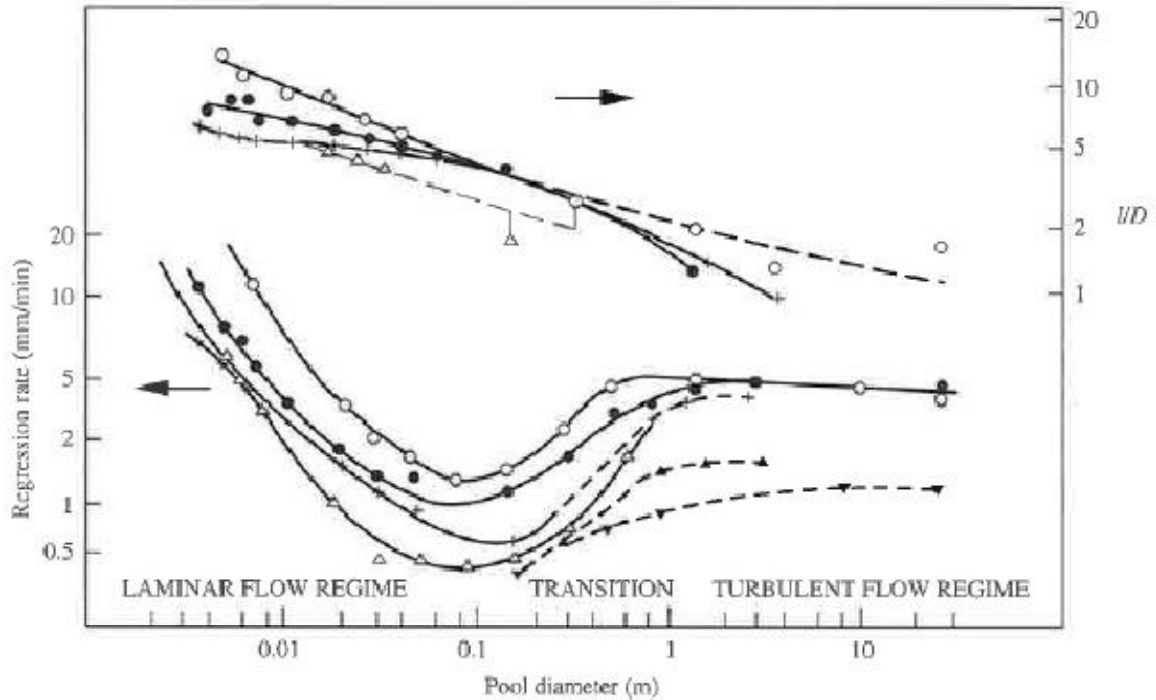
Figure 2-6 *Regression rates and flame height results for liquid pool fires with diameters in the range 3.7 x 10⁻³m to 22m Gasoline (○), tractor kerosene (●), diesel oil (+), petroleum oil (▲), mazut oil (▼), solar oil(△) ((Blinov and Khudiakov, 1957, 1961; Hottel, 1959) reported in Drysdale (1999))*

2.4.2   Radiation

Thermal radiation from flame and its smoke layer has partly been described in Section 2.2, but due to its importance in pool fires a further description is necessary. This section is based on theory from the book "An introduction to fire dynamics" by Drysdale (1999).

Liquids (except methanol) normally burn with luminous diffusion flames. The characteristic yellow luminosity is the net effect of emission from minute carbonaceous particle, known as "soot". These particles (diameter of 10-100nm) are formed within the flame, mainly on the fuel side of the reaction zone. If the particle does not burn as they pass through the oxidative region of the flame they will escape from the flame tip to form smoke. Generally the sootier the flame is the lower is the flames average temperature. This mainly because the soot particles in the flame will attain high temperatures and act as minute black or grey bodies that radiate energy away from the flame.

As described in equation (2-4) the emissivity (ε) is an important parameter when describing the radiation from a flame. Emissivity can be expressed with the following equation (Drysdale, 1999):

$$\varepsilon = 1 - \exp\left(-KL\right)$$ **(2-20)**

where L is the thickness of the flame or smoke layer and K is the effective emission coefficient which is dependent of the particle concentration of soot. In Table 2-3 some experimental values (fuel bed around 0.3m square) which show the connection between carbon appearing as soot and emissivity are presented.

14

_____

Table 2-3 *Experimental values from Table 2.10 in (Drysdale, 1999)*

Fuel	Emissivity (ε)	Emission coefficient K (m^{-1})	Carbon appearing as soot (%)
Polystyrene	0.81	5.3	18
PMMA	0.26	1.3	0.30

How radiation from a flame affects the surroundings is an interesting aspect regarding fire safety. In a fire scenario radiation from the fire could prevent people using escape routes or lead to fire spread from one fire area to another. As an example a radiation heat flux of 12.5 kW/m^2(Drysdale, 1999) could pilot ignite volatiles from wood after prolonged exposure.

To consider the radiation effect from a pool fire to a point in a distance *R* (m) from the fire, equation (2-21) from (Drysdale, 1999) can be used:

$$\dot{q}''_R = \frac{\chi_{rad} \cdot \dot{m}'' \cdot \Delta H_c \cdot A_f \cdot \cos\theta}{4\pi R^2} \quad [W/m^2] \qquad\qquad \textbf{(2-21)}$$

In the above equation it is assumed that the radiation originates from a point source on the flame axis at a height of *0,5l* above the pool surface. However, if the receiving point is at an angle θ, the heat flux $\left(\dot{q}''_R\right)$ will be reduced by a factor *cos θ*. If the amount of radiation (radiation fraction, χ_{rad}) from a fire is unknown it's sometimes assumed to be 0.30 (Drysdale, 1999). Looking at heptane liquid χ_{rad} values of 0.316 and 0.305 are proposed in Table 2-1. Heptane experiments performed by Hamins et al. (1991) also concluded with χ_{rad} values around 0.3. Koseki and Mulholland (1991) observed that thermal radiation increases for increasing pan size up to 2m, then decrease for larger pans.

2.4.3   Flame height

When working with fire safety design the flame height of a pool fire is an important factor that needs to be considered. Flame height may for instance affect fire heating of building structure, fire suppression systems, fire ventilation and escape possibilities. The height of the flame typically depends on the mass burning rate and the ventilation conditions. There are different methods defining the flame height, i.e. based on temperature criteria or visible flame height criteria. From Naeem Iqbal (2004) researcher defined the flame height as the height at which the flame is observed at least 50-percent of the time. As shown in Figure 2-7 the flame from a pool fire has highly intermittent pulsing structure, particularly along its perimeter and near its top. This intermittence is driven largely by the turbulent mixing of air and subsequent combustion.
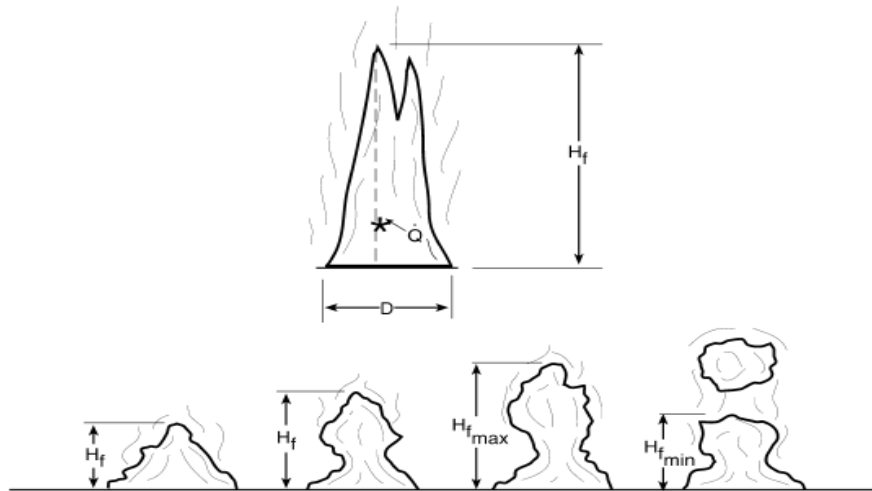
_____

Figure 2-7 *Flame structures from (Naeem Iqbal, 2004)*

From (NFPA, 2002) two correlation defined by Heskestad and Thomas can be used to calculate the flame height of pool fires with no cross-wind;

$$H_f = 0{,}235\dot{Q}_c^{\,2/5} - 1{,}02D \quad [m] \tag{2-22}$$

$$H_f = 42D\left(\frac{\dot{m}''}{\rho_a\sqrt{gD}}\right)^{0{,}61} \quad [m] \tag{2-23}$$

where D is the pool diameter (m), ρ_a is the ambient air density (kg/m³) and $\dot{m}''$ is the rate of burning given as (g/m²s). Equation (2-22) is only valid for normal atmospheric conditions (293K and 1atm) and where the heat liberated per unit mass of air entering the combustion reactions $\Delta H_c/r$ is about 3000 kJ/kg. This is for a large number of gaseous and liquid fuels. For instance heptane has $\Delta H_c = 44700$ kJ/kg and r=15.1 (see appendix B for calculation), this gives $\Delta H_c/r$ value of 2959 kJ/kg and the constant 0.235 is therefore valid for heptane pool fires.

If the pool in the above equations is non circular, an effective diameter could be calculated based on the area (A) of the non circular pool:

$$D_{eff} = \sqrt{\frac{A \cdot 4}{\pi}} \quad [m] \tag{2-24}$$

2.4.4   Air entrainment and flame temperatures

The maximum possible theoretical temperature in fuel/oxidant combustion is called the adiabatic flame temperature. This theoretical temperature is based on no heat losses to the surroundings. This means that all energy released by the chemical reaction is used to raise the temperature of the products (CO_2, H_2O and N_2 in fuel/air reaction). For instance, the adiabatic flame temperature for a heptane/air mixture is given as 1419°C (Table 1-5.6 in (NFPA, 2002)). If the fuel is burnt in pure oxygen these temperatures are higher due to the heat of combustion (ΔH_c) is not used to raise the temperature of nitrogen.

_____

Unlike a premixed flame where the mixing between fuel and air is quite homogeneous the flame zone of diffusion flames (pool fires) is highly heterogeneous as a result of the inadequate preparation of reactants before the combustion zone (Hagen, 2004). This results in generally variations in temperatures depending on the position in the flame. The main reason for this temperature difference is the narrow combustion zone in diffusion fires. Regions of the flame that are not part of the combustion zone have lower temperatures. Turbulent mixing of air in pool fires also leads to pulsing behaviour which in turns affects the temperature of the flame. This involves widely temperature fluctuations at a fixed position, particularly around the edges and near the top of the flame. This is why flame temperature is usually reported in terms of the average centreline temperature or average flame temperature (Naeem Iqbal, 2004).

In Naeem Iqbal (2004) some of the early work on temperatures in turbulent diffusion flames studied by McCaffrey is described. McCaffrey studied various characteristics of a fire plume from a gas burner (methane) in pool fire mode (non-premixed). From his work tree different regimes are described for such a fire plume, this is:
1) Continuous flame region which begins slightly above the base of the fire. In this region the temperature is some below 900°C.
2) Intermittent flame region above the continuous flame region. Temperature drops as a function of distance up the plume. A temperature around 320°C in the visible flame tip.
3) Thermal plume region. No visible flames, temperature continuous to drop.

Naeem Iqbal (2004) also writes that French researchers at the University of Poitiers obtained very similar results in their experiments. They measured temperatures of 900°C in the continuous flame region and temperatures around 340°C at the flame tips.

From the above documentation Naeem Iqbal (2004) concluded that the flame tip temperature for turbulent diffusion flames could be expected to be around 320-400°C. For small flames (diameter less than about 1 m), continuous flame region temperatures around 900 °C should be expected. In large pool fires, these values can rise to 1.100 to 1.200 °C.

Flame temperature is as described earlier dependent of the emissivity (ε) of the flame. In Table 2-4 experimental values for kerosene and alcohol flames are compared. Reading from the table the relation between the emissivity (ε) and flame temperatures is quite clear. Low emissivity value in the alcohol flame result in high temperature. Kerosene on the other hand has a higher emissivity value; it therefore radiates more and the flame temperature is low compared with the alcohol flame. The main reason for this emissivity difference is the emission coefficient (*K*), described in Section 2.4.2, which is directly dependent of the soot appearance in the flame.

Table 2-4 *Experimental values from Table 5.4 in (Drysdale, 1999)*

Fuel	Flame temperature (°C)	Emissivity (ε)	Emission coefficient K (m^{-1})
Alcohol	1218	0.066	0.37
Kerosene	990	0.37	2.6

3   Fire modelling

When working with fire safety of buildings, offshore installations, boats and other constructions, full scale fire tests to verify the design is neither possible nor reasonable to perform. In this way, fire simulation software has been developed to validate the design against realistic fire scenarios. To get a successful result it is important that correct input data is used, that the fire model is validated and approved for use in the defined scenario, and that the people performing the simulations knows how to make use of the results. It's also important that the purpose for doing the modelling is clarified.

Fire modelling can for instance be used to:
- Simulate smoke spread to find available escape time. This could be the time before critical values for toxic gases occur, or the view is unacceptable reduced. Then, the available escape time is compared with the time necessary to escape to verify whether the safety is satisfying or not.
- Simulate fire spread. This could be fire spread from small fires in building to large pool or jet fires in the process industry. In these cases simulations are for instance used to verify if the design is sufficiently good to prevent a small and "uncritical fire" to escalate to a large and "critical fire".
- Find measurements if the existing design is not satisfying. This could for instance be to study the effect of; installing a new fire wall, use passive fire protection on existing walls and equipment or install active fire protection systems as fire water and smoke control.
- Reduce the amounts of fire protection. This by applying the fire modelling input in structural analyzes to verify if amount of passive fire protection can be reduced but the design still fall within acceptable safety values.

Before analyzing the results from fire simulations it is important that critical values called acceptance criteria are defined. According Norsok Z-013 the risk acceptance criteria is defined as *"criteria that are used to express a risk level that is considered as the upper limit for the activity in question to be tolerable"*. The acceptance criteria could be different from one case to another based on the purpose of the simulation. When performing fire simulations this could be:

Structural acceptance criteria when for instance a wall is exposed to a fire. In both onshore regulations and offshore regulation there are given criteria for walls function as a fire wall. According to Petroleum Safety Authority Norway (2010), a fire wall which section different main areas (for instance process area and utility area) could be stated as a H- firewall, if:
- It is sufficiently braced.
- It prevents propagation of flames and smoke for a minimum of two hours of the standardised fire test
- It is designed so that the average temperature and the temperature at any single point on the unexposed side does not exceed 140°C and 180 °C respectively above the initial temperature within the time limits stated below:
  - Class H- 120: 120 minutes,
  - Class H-60: 60 minutes
  - Class H-0: 0 minutes
- Insulation materials, if any, are fire tested at an institution which is internationally or nationally recognised in the specific technical field

Human acceptance criteria is based on factors that prevent escape, this could be; maximum exposure of thermal radiation or temperature from the fire or smoke layer, maximum amount of smoke that reduce the view or influence of toxic gases.

Heat exposure and thermal radiation values from DNV Technica & Scandpower (2001) can be used to define the acceptance criteria in the simulations. Physical responses for human when exposed to high temperatures are presented in Table 3-1.

Table 3-1 *Physical responses for human exposed to high temperatures (recreated from (DNV Technica & Scandpower, 2001))*

Temperature	Physical influence on human
127 °C	Difficult breathing
140 °C	5-min tolerance limit
149 °C	Mouth breathing difficult, temperature limit for escape
160 °C	Rapid, unbearable pain with dry skin
182 °C	Irreversible injury in 30 seconds
203 °C	Respiratory systems tolerance time less than 4 minutes (wet skin)

From the same report by DNV Technica and Scandpower (2001) it is stated that the amount of radiation (radiative heat flux) a person close to a fire can be exposed to is dependent of the exposure time, this is showed in Table 3-2 below:

Table 3-2 *Fatality rate as a function of radiation level and exposure time (recreated from (DNV Technica & Scandpower, 2001))*

Exposure time (s)	TNO probit model (Naked human skin) Fatality rate (%)		
	10 kW/m^2	20 kW/m^2	30 kW/m^2
10	0	5	39
20	1	53	93
30	11	87	100
40	31	97	100
50	53	99	100
60	71	100	100

According to Table 3-2 personnel staying in an area with a radiation of 20 kW/m^2 in 60 seconds have a death-rate of 100%.

There are two types of widely used fire models; namely zone models and field models. Zone models comprise of two control volumes, one for upper hot gas layer and one for lower cold air. Field models (CFD models) divide the room volume into many small cells (control volumes). Differential equations are solved for each control volume in space and time (Hasib, Kumar et al., 2007). In CFD models momentum-conservation by using Navier-Stokes equation is solved while zone models use empirical equations when finding the velocities.

One of the most important parameter in CFD simulations is the selection of numerical grid. Finer grid normally gives better results, but more grid cells involve longer simulations time. It is therefore important to do a grid sensitivity study to verify the optimal grid size.

_____

In general, a study starts with a coarse grid, and then gradually refines the grid until the difference in results between two grid resolutions become small. The spatial resolution of the grid will vary with the phenomena and case that is studied. For example, a cell size of 10cm may be sufficient in evaluation of smoke spread through a building, but it may not be sufficient to study a small fire.

When working with fire simulations there are different CFD models that can be used. Further in this chapter software used for simulations in this thesis, FLACS and FDS, are described, and some of the other fire models available on the marked are shortly mentioned.

3.1   CFD modelling general equations and principals

This section is based on theory from the text book "Combustion" by Warnatz, Maas et al. (2006) unless other references are stated.

The fundamental bases of almost all CFD problems are the Navier–Stokes (NS) equations, which define any single-phase fluid flow. Since most fire scenarios includes turbulence behaviour this is an important parameter to include in simulations. In contrast to laminar flow, turbulent flow with fluctuations of velocity, leads to fluctuation in density, temperature and mixture composition. For this reason numerical solution of the NS equations for turbulent flow is extremely difficult. Turbulence flow can be implemented in the NS equations and solved as Direct Numerical Simulations (DNS), but this will require prohibitive amount of computational time. The main reason for this time-consume is that the small scales in turbulent flows require far more grid points than analogous laminar flow.

$$\frac{l_0}{l_K} = R_l^{3/4}$$

(3-1)

A typical turbulent flow with turbulent Reynolds number (R_l) of 500 gives a ratio of about 100 between largest turbulent structure *(integral length scale, l_o)* and smallest turbulent structure *(kolmogorow length scale, l_k)*, see equation (3-1) above. In this situation about 1000 grid points in one direction, and by 10^9 grid cells in all three directions, are required to resolve the smallest turbulent eddies. The conclusion is then that DNS in 3 dimensions is possible for low R_l, but mainly used in detail researching of turbulent flows. Solutions of the NS equations of turbulent reacting flows in practical purpose are therefore not yet possible. Even if DNS was possible for these practical cases it would give a vast amount of details.

In practical CFD modelling of turbulent flow time-average equations such as Reynolds average Navier Stokes (RANS) equations or Large Eddy Simulations (LES) method are used. In contrast to RANS equations which do not solve any scale of the turbulence, the LES method resolves the largest scales (eddies). Both methods require additional turbulence models for the unsolved eddies to close the system of equations. Among different turbulence models the two-equation model called *k-ε* model is one of the most popular. Two extra transport equations represent the turbulent properties of the flow. *k* represents the turbulent kinetic energy and ε represent the dissipation rate of turbulent kinetic energy dissipation. In the LES method more primitive turbulence models (Sub-Grid

_____

models) can be used to handle the unsolved eddies, for instance Smagorinsky model which is used in FDS.

"Since turbulence also has an effect on the non-premixed combustion process and on radiation, the accuracy and reliability of field modelling results is highly dependent on the quality of the turbulence model applied. Large Eddy-type simulations are considered as a promising next step in fire modelling, as they offer a deeper insight in the various flow phenomena which occur during a fire (Van Maele and Merci, 2006)".

Van Maele and Merci (2006) still has the opinion that RANS simulations have their benefit in the fire community, and the search for improved sub-models should not be abandoned. The main reason for this statement is that LES simulations require higher computational power due to the time dependency of the simulations, and the finer grid that is required.

In fires (except jet fires) the buoyancy effect is of high importance due to the fire-generated flows are mainly driven by this force (large density variation due to temperature differences). According Van Maele and Merci (2006) this effect concerns an increase of the turbulence level in unstably stratified situations and suppression of turbulence production in stably stratified flow regions. k-ε models were originally developed for constant density flows, but the effect of buoyancy is commonly accomplished by adding buoyancy source terms to the transport equations for k and ε.

3.2   FLame ACcelator Simulator (FLACS)

Gexcon AS, which is a wholly owned subsidiary of Chrsitian Michelsen Research (CMR), develops, maintains and supports the CFD software FLACS. The development of FLACS started in 1980 at the Department of Science and Technology at Christian Michelsen Institute (became CMR in 1992). FLACS-86 was the first version distributed, and the first test version of FLACS-Fire was included in FLACS v9.0, released in 2008.

The FLACS software used to simulate process safety cases such as; dispersion of flammable and toxic gases, gas and dust explosions, propagation of blast and shock waves, and feature for the simulation of industrial fires (pool/jet fires) are under development. As most of the CFD software FLACS is divided into a "pre-processor" where the scenario is defined, a "solver" where the scenario is calculated and a "post-processor" where the results are visualized.

In the pre-processor "CASD" the user defines a FLACS simulation. The input to the simulation includes geometry-and grid definition, fuel (gas cloud composition), size and location of leakage, ignition location and output specifications. The post processor FLOWVIS is used to visualize results such as temperature, pressure and radiation in 2D/3D plots, time series of probes (monitor points) and simple line plots.

3.2.1   Models included in FLACS-Fire

As described in the previous excerpt, fire modelling in FLACS-Fire is still under development. One important improvement that has been ongoing in parallel with the work on this thesis is a new radiation model. In this section the main features in FLACS-Fire are shortly described. More details about the models in FLACS-Fire can be found in the FLACS-Fire test release manual (Gexcon-Software, 2007).

_____

Combustion model and radiation

The combustion rate in non premixed flames, which is the case for most fires, is controlled by the mixing of fuel and air. For turbulent diffusion flames, the Eddy Dissipation Concept (EDC) model is implemented in FLACS. The (EDC) model is the default combustion model for calculation of the fuel source term in turbulent diffusion flames in FLACS. For fires with little or no turbulence a simple *mixed is burnt* (MIB) model will be sufficient. It is possible to use the MIB model in FLACS, but it has been observed that the flame has blown out with very little turbulence (Gexcon-Software, 2007).

The present radiation model used in FLACS-fire is a six-flux radiation transport equation. Fire modelling performed by Nilsen (2010) concluded that this radiation model need to be revised. Nilsen observed both that the radiation was not correctly distributed, which was not unexpected from the six-flux radiation model, and that the radiative heat flux values were inaccurate. A new radiation model is today going through a validating process. In this model radiative intensity is calculated with the discrete transfer radiation model (DTM) and the properties of the radiating media are calculating using the Mixed Gary Gas Model (Muthuswamy, Hansen et al., 2011). *"The major computational effort in the discrete transfer method is to trace the ray through the hexahedral volumes in the descretised radiation space"* (Muthusamy, 2011).

Turbulence model

Turbulence is modelled using the k-ε model which is shortly described in Section 3.1. The buoyancy term in the dissipation equation (ε) ensures that buoyant turbulence production is limited. The strength of buoyant dissipation production is regulated by the value of the constant $C_{3\varepsilon}$. In standard FLACS gas dispersion account for the buoyancy effect by modifying the ε-equation according the method by Rodi (1980) with the default values $C_{1\varepsilon}$ =1.44, $C_{2\varepsilon}$ =1.92 and $C_{3\varepsilon}$ =0.8, more details about this method can be found in (Van Maele and Merci, 2006). Using FLACS-Fire $C_{3\varepsilon}$ =1 is used.

Soot model

There are two models for soot handling in FLACS-Fire. The default model is the *formation-oxidation* (FOX) soot model. This model has two source terms in the transport equation for soot, where one term models the formation of soot and the other term models the oxidation (combustion) of soot. The other model is called the *fixed conversion factor model* (CFM). This model only reveals how much of the carbon in the fuel that is converted to soot in the products. This is independent of the equivalence ratio, temperature, time, etc. The only input for this model is the soot yield, which gives the fraction of carbon that is converted to soot. This is a crude model, but a similar model is used in FDS, see Section 3.3.1. It is also possible to run simulations without any soot model.

Grid definition

The grid does not need to be uniform (i.e. equally spaced grid lines), nor does it have to be isotropic (i.e. equal grids in all three directions). After the grid cells are defined it is possible to stretch them in all directions. It is still advised that the grid is uniform and isotropic in the area of interests. This means that stretching the grid should only be applied to extend the grid beyond the area of interest (FLACS User Guide).

Output data handling

Parameters such as temperature, velocity, pressure and heat flux can be measured with monitor points. Alternatively, heat flux and temperature on walls are measured by defining

_____

TWALL and QWALL in the input file. It's possible to get 2D/ 3D plots and graphs from all the defined input parameter in the simulations.

3.2.2   Limitations

The present radiation model used in FLACS-Fire (6-flux model) has various limitations. A ray tracing model, which soon will be in place, will probably perform better.

Light hydrocarbon fuels are preferred and there are no models available for sprinkler sprays running FLACS-fire.

It is possible to model pool leaks in FLACS, but the modelling of the heat feedback, which determines the evaporation rate is premature (Lokna, 2008).

3.3   Fire Dynamic Simulator (FDS)

This Section is generally based on information from FDS User Guide and FDS Technical Reference Guide which both are attached in the FDS download package. These documents can also be found on (FDS official website).

FDS, developed by the National Institute of Standard and Technology (NIST), is a CFD model of fire-driven fluid flow. FDS is free to download on NIST home pages. The simulator has been under development for about 25 years, but the first public software was released in February 2000.

When describing a scenario to simulate with FDS the input file is created as a single text file, with for instance Notepad (pre-processor), or by the graphical user interface PyroSim. This input file contains information about the numerical grid, geometry, ambient environment, combustion kinetics, material properties and desired output data as for instance heat release rate (normally defined), temperature, radiative heat flux i.e. The geometric must conform to the numerical grid. This means that objects smaller than a single cell are either approximated as a single cell, or rejected. The building geometry is defined as rectangular blocks and materials are defined by their thermal conductivity, specific heat, density, thickness and burning behaviour.

FDS is the "solver" which solves numerically a form of Navier-Stokes equations appropriate for low-speed, thermally-driven flow with an emphasis in smoke and heat transport from fire (Hydrodynamic model).

The program Smoke View is the "post processor" which produces images and animations of the results from the FDS simulation (Kevin McGrattan, 2010).

In FDS it is possible to simulate:
- Low speed transport of heat and combustion products from fire
- Pyrolysis
- Radiative and convective heat transfer between the gas and solid surfaces
- Flame spread and fire growth
- Sprinkler sprays and suppression by water
- Sprinkler, heat detector and smoke detector activation.
- Low speed fluid flow simulations that do not necessary include fire or thermal effects.

_____

Each release of FDS or Smokeview is identified by a version number such as FDS_5.5.3 which is the version used in this thesis. The first number (5) is a major release that includes dramatically changes the functionality or capabilities of the model, the second number (5) is a minor release that may cause minor changes in the functionality. The third number (3) indicates a maintenance release and are just bug fixes or small refinements, and should not affect code functionality (Kevin McGrattan, 2010).

3.3.1   Models included in FDS

In the below descriptions of FDS and its limitation, information is collected from the FDS User Guide (Kevin McGrattan, 2010) and FDS Technical Reference Guide.

Combustion model and radiation in FDS
Two types of combustion models can be applied in FDS. The default model uses mixture fraction (quantity representing the fuel and the products of combustion) and in the second model individual gas species react according to specified Arrhenius reaction parameter (Only DNS simulations). The combustion model based on the mixture fraction concept is used for most applications. This is a conserved scalar quantity that represents the mass fraction of one or more components of the gas at a given point in the flow field. By default, the mass fraction of unburned fuel and burned fuel are explicitly computed. The major reactants and products of combustion – fuel, O_2, CO_2, H_2O, N_2, CO and soot – are all pre-tabulated functions of the mixture fraction (Kevin McGrattan, 2010). If the fuel is not specified on a reaction line in the input file, propane is used as default. Following yield values are default unless the user specify these values: CO(0.0), soot(0.01), H_2(0.0) and amount of hydrogen in the soot H_{frac}(0.1).

In FDS there are two ways of modelling a fire. The method that is most used and predicts the best results require that the mass loss rate or heat release rate of the fire is known. The Mass Loss Rate Per Unit Area (MLRPUA) or Heat Release Rate Per Unit Area (HRRPUA) is then connected to an obstruction or vent which represents the fire. This creates a gas burner where the amount of fuel is controlled.

In the other method FDS predicts the heat release rate from the material properties of the fuel. In this case the burning rate of the fuel depends on the net heat feedback to the surface. The liquid fuel evaporation, when burning, is a function of the liquid temperature and the concentration of fuel vapour above the pool surface. The evaporation rate of the fuel is governed by the Clausius-Clapeyron equation where the volume fraction of the fuel vapour above the surface is given as:

$$X_f = \exp\left[-\frac{h_v W_f}{R}\left(\frac{1}{T_s} - \frac{1}{T_b}\right)\right]$$
(3-2)

where h_v is the heat of vaporization, W_f is the molecular weight, T_b is the boiling temperature of the fuel and T_s is the surface temperature. When the simulations start there is no temperature and an initial guess is made for the fuel vapour mass flux. During the simulation, the evaporation mass flux is updated based on the difference between current close-to-the surface volume fraction of fuel vapour and the equilibrium value given in equation (3-2) above (Kevin McGrattan, 2010). The mixture fraction combustion model is used by default in both methods.

_____

Thermal radiation is included in the model via the solution of the radiation transport equation for a gray gas. The equation is solved using a technique similar to a finite volume method (FVM) for convective transport (Kevin McGrattan, 2010). Thermal radiation transport is computed by default for most FDS simulations, but there are situations where it is important to be aware of issues related to the radiative transport solver. Fraction of energy released from the fire as thermal radiation (radiative fraction) is the most important issue. The thermal radiation from the flame is a function of both the flame temperature and chemical composition. In large scale fire calculation, the flame sheet is not well-resolved (large grid cells) and these parameters are therefore not reliably calculated. Because of fourth power of absolute temperature (T^4) dependence in radiation transport equations it is important that the temperature near the flame surface is correct. In FDS calculations where mesh cells are in order of a centimetre or larger the temperature near the flame surface cannot be relied. As an alternative, the fraction of total combustion energy that is released as thermal radiation can be specified in the input file. It should be emphasized that some of that energy can be reabsorbed elsewhere, resulting in a net radiative loss from the fire less than the specified radiative fraction. By defining the radiative fraction as zero, the radiation transport equation uses the gas temperature and chemical compositions of the flame to calculate the radiation (only for mesh cells smaller than on centimetre). Default radiation fraction value for LES calculations is 0.35 and for DNS calculations 0.

Turbulence model
As default turbulence is treated by means of the Smagorinsky form of Large Eddy Simulation (LES). It is also possible to handle turbulence as Direct Numerical Simulation (DNS) if the grid is fine enough. There is not capability to handle Reynolds-Averaged Navier-Stokes (RANS) in FDS.

Smoke production
By default (using mixture fraction) smoke generation is in direct proportion to the defined HRR. The default smoke (soot) production value is 1% of the fuel burning rate (SOOT_YIELD=0.01). In this way the smoke production is assumed to be a function of the mixture fraction and not explicitly tracked by FDS. If the SOOT_YIELD value is changed it only impinge upon the net smoke production from the fire, it is not applicable in the processes of soot growth and oxidation. It is possible to define the smoke production rate independently of the HRR. In these cases the SOOT_YIELD is set to zero to prevent FDS including smoke as a mixture fraction species.

Grid definition (meshes)
All FDS calculations must be performed within a domain that is made up of rectilinear volumes called meshes and each mesh is divided into rectangular cells. By default the mesh cells that fill the computational domain are uniform in size, but it is possible to specify the cells to be non-uniform in one or two of the tree coordinates directions. The LES technique is based on the assumption that the numerical mesh should be fine enough to allow the formation of eddies that are responsible of the mixing. Since eddy formation is limited by the largest dimension of the mesh cell, it may not necessarily lead to a better simulation by shrinking the mesh in one direction. It is also possible to run multiple meshes in FDS. In this way different grid sizes can be used and the workload can be divided among available processors. In order to accomplish good results using multiple meshes, there are several conditions stated in Section 6.3.4 in FDS User Guide (Kevin McGrattan, 2010) that must be followed.

Output data handling

Overall energy budget (HRR from fire and radiative, convective- and conductive losses) is generated automatically in FDS.

It is possible to measure temperature by inserting thermocouples. When defining a "THERMOCOUPLE" in FDS, the temperature of the thermocouple itself, and not the gas temperature is measured. This temperature is determined by solving the following equation iteratively:

$$\varepsilon_{TC}\left(\sigma T_{TC}{}^4 - \frac{U}{4}\right) + h\left(T_{TC} - T_g\right) = 0 \tag{3-3}$$

where ε_{TC} is the emissivity of the thermocouple, U is the integrated radiative intensity, T_g is the true gas temperature, and h is the heat transfer coefficient to a small sphere;

$$h = \frac{k_a Nu}{\mathrm{Pr} \cdot \mathrm{d_{TC}}}/ \tag{3-4}$$

According FDS User Guide this temperature is usually close to the gas temperature, but not always.

There are various ways of recording the heat flux (radiation) at a solid boundary. To measure radiative heat flux a radiometer that is not attached to a surface can be defined as a 'RADIATIVE HEAT FLUX GAS'. This quantity integrates the incoming radiative flux over 2π solid angles around the vector defined by the orientation of the device. As an example ORIENTATION = 0.0, -1.0, 0.0 means that the device points in the negative y direction. Orientation of the device can also be defined by IOR if the device is in one of the three coordinate angles (x, y, and z). For instance by defining IOR=-2 the device is turned in negative y-direction.

In FDS the value of the QUANTITY (temperature, radiative heat flux etc.) is measured in the cell where the point XYZ is located.

3.3.2   Limitations

FDS is only valid for low speed flow with an emphasis on smoke and heat transport from fires. This means that FDS cannot be applied in situation where the flow speed approaches the speed of sound (explosions, detonations and high momentum jet fires).
It is recommended to use cells that are almost cubical. The number of grid cells in y-and z-direction must be factorable with 2, 3 and 5. This is caused by Fast Fourier Transformers (FFTs) used in the Poisson solver.

The uncertainty of the model is higher when the heat release rate is predicted instead of specified. For most applications, FDS uses a mixture fraction-based combustion model where a fraction of gas at a given point in the flow field originates as fuel. The model assumes, in its simplest form that combustion is mixing controlled, and that the reaction of fuel and oxygen is infinitely fast, regardless of the temperature. This is a good assumption for large scale well-ventilated fires, but not in cases where fuel and oxygen are allowed to mix and not burn (under ventilated compartments or in cases where a extinguish system

_____

like water mist or CO_2 is introduced). However simply empirical rules can be used to prevent burning from taking place.

Radiation transport is discretized via many solid angles (100 of more). For targets far away from the fire (radiation source) the discretization can lead to non-uniform distribution of the radiant energy, showing as "hot spots". This problem might be solved by including more solid angles, but this will increase the simulation time.

3.4   Other CFD models

This section contains a short description of some available CFD models used in Fire modelling.

Kameleon (KFX):
The Kameleon FireEx KFX® is a CFD simulator, dedicated to gas dispersion, flare and fire simulations (Computit). The code was originally developed by ComputIT/ NTNU/ SINTEF with partners, and is today owned by ComputeIT. KFX® has continuously been developed since the seventies, and is also today going through a R&D program for further improvement.

According ComputeIT home page (Computit) it is possible to use KFX modelling in all kinds of fires (pool fires, jet fires, two phase spray fires, flares, fire in enclosures, in complex geometries, in open space, in still air or in windy conditions) and detail calculations of temperatures, radiation, smoke, visibility, concentrations of species, toxic gases, noise etc. is included. KFX uses the *k-ε* turbulence model and Eddy Dissipations Soot model. Different sub models are available, e.g. pool model (evaporation due to flashing, convection and boiling), spray model (LaGrangian model), radiation model (The discrete transfer model of Shah and Lockwood).

Ansys (CFX and Fluent):
According Ansys home page (Ansys) the software can be applied to examine fire suppression systems, low- and high-momentum fires, flashovers, back drafts etc. The software incorporates among other things:

- A wide range of turbulence models including RANS and LES
- A variety of combustion models
- State-of-the-art grey and spectral radiation solvers

Other CFD models available for fire simulation are e.g. Sofie and Jasmine.

_____

4   Previous work

Publications regarding pool fire experiments are collected and organized through a literature search performed early in the thesis. The object of this search was to find experimental pool fire data that could be recreated through FLACS and FDS simulations, but also to get ideas regarding setup and measurements for the experiments performed in this work. There is a lot of available literature on pool fire experiments. Some of the experiments collected from the literature search are organized in Table 4-1 below. All these experiments are relevant in a validation process of a fire model. To recreate the experimental setup as realistic as possible and compare with accurate results, it is necessary to collect more details for some of the experiments. Even if it could have been interesting to simulate all the experiments described in Table 4-1, it was decided to limit the simulations to the two first experiments in addition to the experiments performed in the work with this thesis (see Chapter 5).

The FLACS fire model is under development. Simulations performed on jet fires by Nilsen (2010) concluded that FLACS gave good results on flame length and flame temperature in the centreline of vertical flames, but the radiation intensity was too high and incorrectly distributed. One of the main focuses in development work with the software today is therefore to improve the radiation model.

Table 4-1 *Overview of previous experiments*

Description	Measurements	Simulations		Comments/ Experimental data
		FLACS	FDS	
Medium Heptane pool fires in a 20m cubic atrium.	Temperature Velocity Mass loss rate	Yes	Yes	(Gutiérrez-Montes, Sanmiguel-Rojas et al., 2009)
Flow Induced by Fire in a Compartment	Temperature Velocity	Yes	Yes	(Steckler, Quintiere et al., 1982)
Simulations of an experimental compartment fire by CFD	Temperature Velocity	No	No	Very low temperature results (300K)/ (Hasib, Kumar et al., 2007)
Validation of FDS for the prediction of medium-scale pool fires	Temperature Velocity	No	No	(Wen, Kang et al., 2007) and (Weckman and Strong, 1996)
Analysis of the geometric and radiative characteristics of hydrocarbon pool fires	Temperature Mass loss rate Flame height/tilt Emissive power	No	No	Experiment for large pool fire simulations, possible to recreate with some more details/ (Muñoz, Arnaldos et al., 2004), (Muñoz, Planas et al., 2007) and (Chatris, Quintela et al., 2001)
Flame temperature distribution in a pool fire	Temperature Mass burning rate Flame height/tilt Emissive power	No	No	Experiment for large pool fire simulations/ (Planas-Cuchi and Casal, 1998) and (Planas-Cuchi, Casal et al., 1996)
Thermal Measurements from a Series of Tests with a Large Cylindrical Calorimeter on the Leeward Edge of a JP-8 Pool Fire in Cross-Flow	Temperature Heat flux Pressure Wind conditions	No	No	(Jill M. Suo-Anttila, July 2001) and (Miles Greiner, August 2004)

_____

5   Experimental work

According to pool fire literature (see Section 2.4.1.3) the diameter of a pool fire affects the rate of turbulence and the regression rate (mm/min). Based on this it was decided to carry out experiments with pool fires both in the transition area (D=0.03-1m), and fully turbulent pool fires with diameter around 1m. Due to restrictions in the ventilations capacity and safety reasons it was only possible to perform indoor experiments with pool fire diameter within the transition area (below 1m). Wind condition during the outdoor experiments involves large uncertainties in measurements from these experiments.

Fire experiments were carried out in collaboration with Frode A. Halrynjo, a fellow student working with his Master's degree at UoB.

5.1   Purpose of the fire experiments

When developing computer programs for fire simulations an important part of this work is to perform experiments for validation of the programs. In this validation process physics from experiments and corresponding simulations are compared. As described earlier (Chapter 4) in this report a lot of pool fire experiments have been performed by other scientists, and in this way a lot of data is available for performing validation simulations. The purpose of the pool fire experiments performed in this report is therefore not just to get data for performing own validation simulations, but also to get the understanding in constructing an experimental setup in order to compare with simulations. From a literature survey performed early in the work process, it was noticed that there hasn't been done much experimental work on structure (piping) located above a pool fire. Therefore it was decided to build a rig where it was possible to look at what effects pipe obstruction located in different heights above the pool have on the physics of the fire.

5.2   Indoor experiments

The small scale fire tests were performed in the fire laboratory of Stord/Haugesund University College.

The test facility used in the experiments is built according to "ISO 9705 – Room corner test", but the ISO room itself was not used in the experiments. The pool fire was located outside the ISO room below the exhaust hood, see Figure 5-1. A total of 11 experiments were performed. Two experiments (1 and 2) without structure above the pool and nine experiments (3 to 11) with 40mm pipes obstruction in different heights and with different obstruction area above the fire. Except from location of the pipe rack in experiment 3-11, all experiments were performed under approximate the same conditions and with similar location of measuring equipment. For more details of the test setup, see Figure 5-2, Figure 5-3 and Figure 5-4.

The fire:
Heptane (C_7H_{16}) fuel located in a pan with square sides of 0.5m and with depth of 0.1m was used in the experiments. About 13 litres of water was added in the pan before each experiment. This to provide more stable steady burning regime and insulate the pan from the intense heat from the fire.

Temperature measurements:
3mm Type K Thermocouples were used to measure the temperature at different heights in the pool fire. The flame temperature itself is difficult to measure due to flame fluctuations. Thermocouples were therefore located strategic at different height in the centre of the fire plume where the temperatures area more stabile. In experiment 1 and 2 a total of eight thermocouples were used, and in experiment 3-5 two more thermocouples were added to measure temperatures on inside- and outside the pipes. In experiments 6-11 thermocouples 1, 3, 6, 8, and 10 were not used, but instead a thermocouple was located close to the flux sensor to verify temperature around the sensor. This in order to calculate its measuring error due to convection. Heights of all thermocouples located inside the fire plume is illustrated in Figure 5-4.

Flame height measurements:
A high speed camera, type Casio Exilim EX-F1, was used for flame height measurements. The flame height of each experiment was measured based on the definition; the flame height is the height at which the flame is observed at least 50-percent of the time. The observed flame height was also compared with flame height calculated using the maximum HRR and mass burning rate from each experiment in equations (2-22) and (2-23).

Radiative heat flux measurements:
Radiative heat flux from the fire was measured using the "SBG01-10 Water Cooled Heat Flux Sensor According to Schmidt-Boelter". The sensor has a measuring range up to 10 kW/m^2 and according (User manual SBG01, 2008) it is recommended that the measured radiative heat flux is above 50% of the maximum measuring range due to its calibrated at full range. In all experiments the flux sensor was located approximately 0.9m above the pool in a distance of 1.25m from the pool fires centre. This height was decided since it was desirable to measure the radiation from the middle of the flame. The flame height was measured from equation (2-22) using diameter of 0.56m calculated from area of 0.25m^2. HRR was calculated using heptane values from Table 2-2 in equation (2-19) assuming (χ) of 0.69 in equation (2-11).

$$\dot{m}'' = \dot{m}_\infty''(1 - exp(-k\beta D)) = 101 \cdot (1 - exp(-1.1 \cdot 0.56)) \approx 46.4 \; g/s$$
$$\dot{Q}_c = \chi \cdot \Delta H_c \cdot \dot{m}'' \cdot A_f = 0.69 \cdot 44.6 \cdot 46.4 \cdot 0.25 \approx 357 \; kW$$
$$H_f = 0.235 \dot{Q}_c^{2/5} - 1.02D = 0.235 \cdot 357^{2/5} - 1.02 \cdot 0.56 \approx 1.9m$$

Weight measurements (evaporation rate)
Weight loss due to evaporation was measured using a weight type VEGA (weight indicator, VDI 137).

Velocity measurements:
Before experiment 5-11 velocity directly above the test rig and by the flux sensor (for use in uncertainness calculations) was measured by using a VelociCalc Plus Meter (Model: 8386-M-S).

Thermo camera:
Before each experiment a thermo camera, type Fluke Ti20, was utilized to verify that the temperature on the surroundings was approximately unchanged from initial temperatures in experiment 1.

_____

Heat release rate measurements:

The heat release rate was both measured directly by a cone calorimeter and calculated with equation (2-11) based on the mass loss rate from weight measurements. The cone calorimeter fire test method is built according to "ISO 9705 Room-Corner test". In these tests the fire is located in the corner inside the ISO room. The fire experiments performed in this report are, as shown Figure 5-1, located directly below the exhaust hood to the cone calorimeter. The pool fire was lifted with pallets so that it was on the same elevation as the ISO room floor.
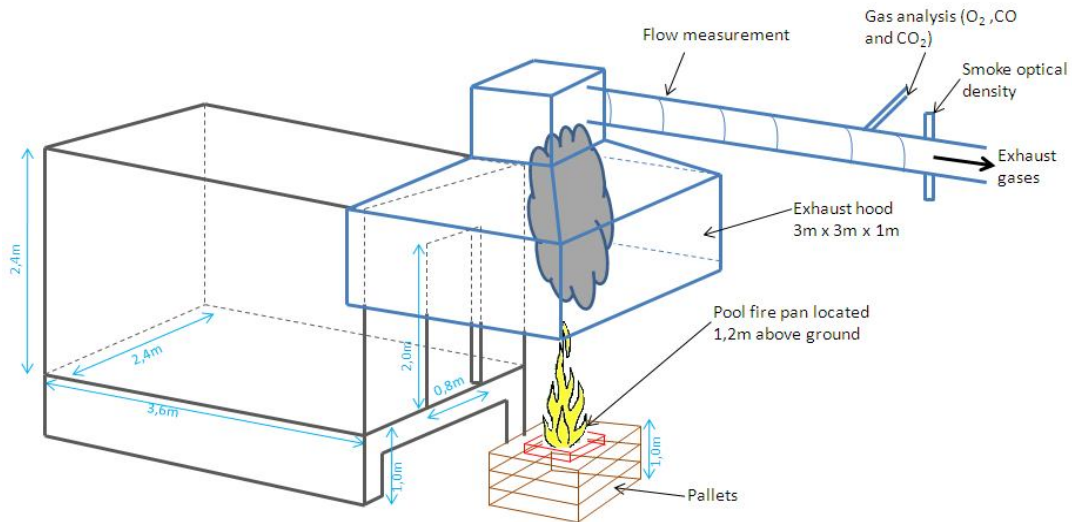
Figure 5-1 *Overall test setup showing ISO room, cone calorimeter and location of pool fire*
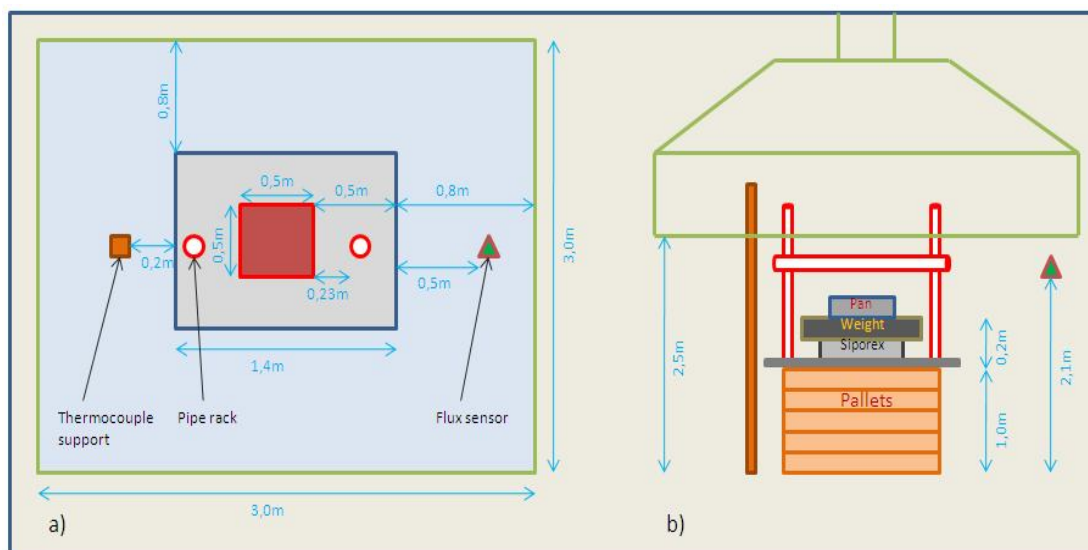
Figure 5-2 *Detail test set-up top view in a) and side view in b)*
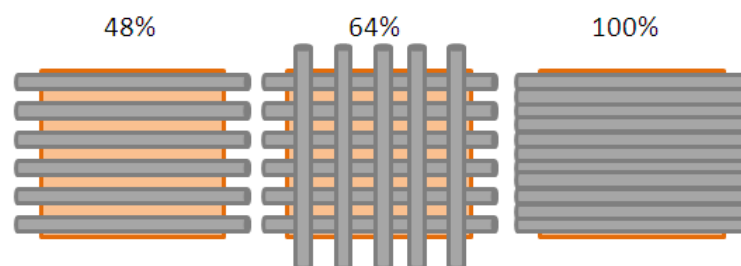
Figure 5-3 *Different obstruction areas used in the experiments*

33
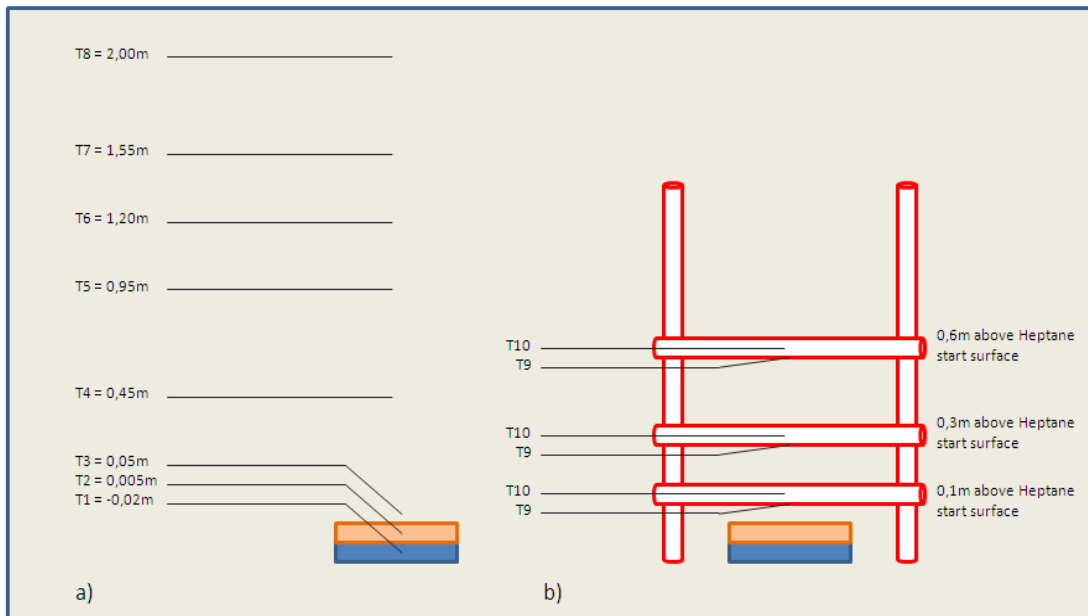
Figure 5-4 *Location of thermocouples in a) and added thermocouples for tests 3-5 in b)*

More information about the measuring equipment can be found in appendix A.

5.3   Results indoor experiments

Summary of indoor experiments are shown in Table 5-1 below.

Table 5-1 *Summary indoor experiments*

Fire experiment	Mass of Heptane (g)	Burning time (s)	Geometry above Heptane pool (m)	Obstruction area (%)	Velocity above pool/flux sensor (m/s)
Exp 1	2600	304	-		-
Exp 2	2600	298	-	-	-
Exp 3	2800	516	0.1	48	-
Exp 4	2800	322	0.3	48	-
Exp 5	2800	302	0.6	48	0.2-0.3/0.15-0.2
Exp 6	2600	520	0.05	48	0.2-0.3/0.15-0.2
Exp 7	2600	334	0.15	48	0.2-0.3/0.15-0.2
Exp 8	2700	300	0.2	48	0.2-0.3/0.15-0.2
Exp 9	2400	300	0.2	64	0.2-0.3/0.15-0.2
Exp 10	2700	454	0.1	64	0.2-0.3/0.15-0.2
Exp 11	2600	434	0.1	100	0.2-0.3/0.15-0.2

Mass loss rate:
It was only possible to measure hectograms (100g) with the available scale. To get reasonable values for use in graphical description of the results it was therefore necessary to calculate the mass loss rate ($\dot{m}$) by considering the average mass loss over a longer time aspect. In this way, the mass loss rate won't give accurate values for every time step, but a good total indication of the mass loss throughout the fire development. Mass loss rate for each time step was estimated based on the changes in mass for a period of 62 seconds, 30 seconds before and after each time step.
Heat Release Rate (HRR):

_____

After analysing the results from both weight measurements and cone calorimeter measurements, the conclusion could be drawn that the values measured with the cone calorimeter were unreasonable high. Looking at experiment 1 the cone calorimeter measured a total energy production of 160MJ. As shown in calculation below this value is approximately 38 percent above maximum energy potential in 2.6kg heptane.

$$\dot{Q}_{total} = m_{\text{heptan}} \cdot \Delta H_{c\text{heptan}} = 2600g \cdot 44{,}6\frac{kJ}{g} = 115\ 960kJ \approx 116MJ$$

Experiment 2 which was performed under exact same conditions gave the same deviation.

From (Jesper Axelsson, 2001) a HRR uncertainness of 10.6 % with 150kW fire and 7.1% with 1MW fire is reported for the room corner test. According the same report the uncertainness in smoke production rate is dependent of the smoke production, where low production has high uncertainness. For instance $0.1m^2/s$ smoke production has 103% uncertainty while $1m^2/s$ production has 11.6 %. This shows that the HRR values measured in the experiments are not just over predicted due to measuring uncertainness (only 10.6%).

Even if the cone calorimeter values are too high, the deviation during same conditions is constant. As shown in Figure 5-5 the ratio between maximum possible HRR for a given mass of heptane divided by the measured HRR in cone calorimeter are from 64-74 percent in all experiments. The main reason for the over predicted values are probably because the cone calorimeter wasn't calibrated according to a calibrating procedure before the experiments. If, for instance, a calibration procedure described by (Javier O.Trevino) had been utilized more reasonable values could have been obtained. It is also possible that it was something wrong with the measuring equipment in the cone calorimeter during the experiments.
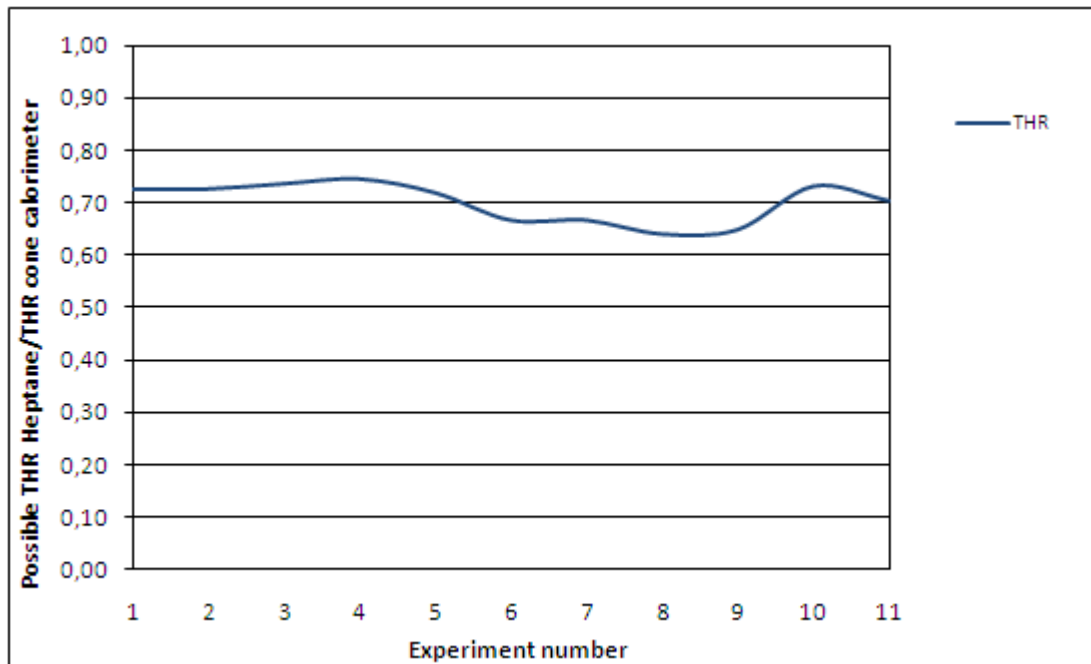
Figure 5-5 _Ratio between maximum total energy for given heptane mass and total energy calculated by cone calorimeter for each experiment_

_____

In Figure 5-6 values from cone calorimeter measurements and mass loss measurements are compared. HRR from mass loss rate is calculated by inserting the measured mass loss rate in equation (2-11), using 100% combustion efficiency (χ). As the figure reveals the cone calorimeter measurements agree quite well with the mass loss measurements after correcting the values according to ratio in Figure 5-5. For experiment 1 this means multiplying all measured cone calorimeter values with 0.72. These experimental values also agree quite well with HRR calculated using proposed values in Table 2-2 together with (χ) of 1 and diameter of 0.56m in equation (2-19) and equation (2-11) .

$$\dot{m}'' = \dot{m}_\infty''(1 - exp(-k\beta D)) = 101 \cdot (1 - exp(-1.1 \cdot 0.56)) \approx 46.4 \ g/s$$
$$\dot{Q}_c = \chi \cdot \Delta H_c \cdot \dot{m}'' \cdot A_f = 1.0 \cdot 44.6 \cdot 46.4 \cdot 0.25 \approx 517.4 \ kW$$
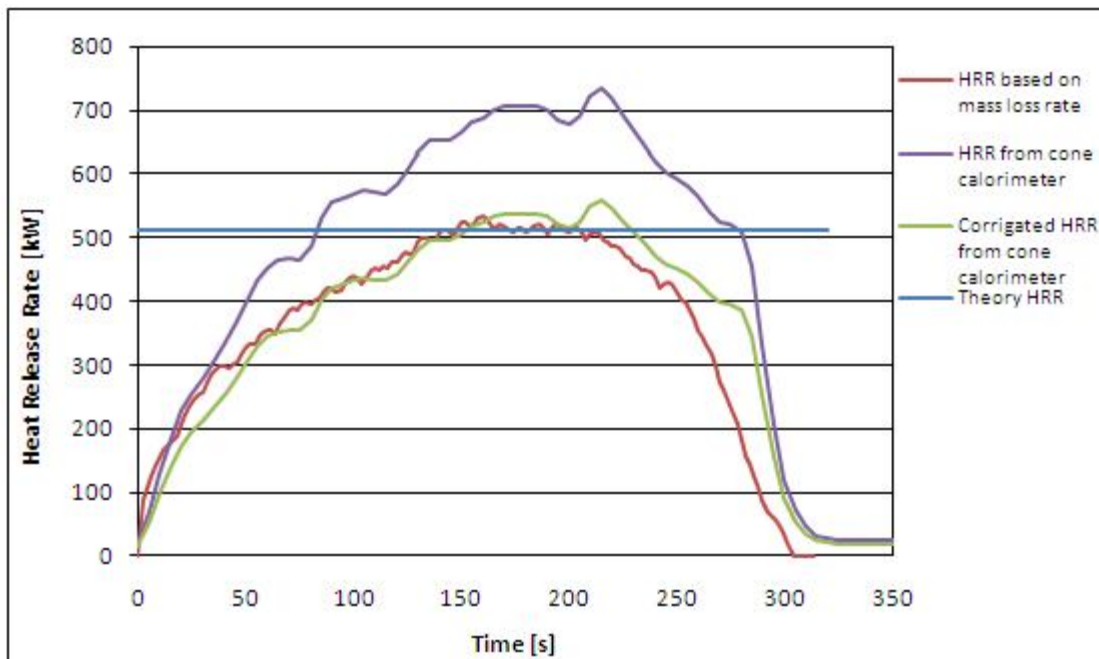
Figure 5-6 *Comparing HRR measured from cone calorimeter with HRR calculated based on mass loss rate in experiment 1, combustion efficiency 100%*

As described in Chapter 2, incomplete combustion where the combustion efficiency (χ) is less than 100% is the reality of a fire scenario. If the cone calorimeter was calibrated and correct HRR values obtained, χ could have been estimated by using $\dot{m}''$ and different χ in equation (2-11) until the values matched the measured one in the cone calorimeter.

Different combustion efficiency values for heptane are reported in literature (see Section 2.4.1). When visual flame length from experiment 1 is compared with calculated flame length using equation (2-22) and (2-23) it seems like the flame length agrees best when using combustion efficiency around 0.7 which gives max HRR of 372.6kW. Maximum mass loss rate in experiment 1 is measured to be 47.7g/sm^2. As calculations below shows, this gives approximately identical flame lengths using equations (2-22) and (2-23);

$$H_f = 0{,}235\dot{Q}_c^{2/5} - 1{,}02D = 0{,}235 \cdot 372{,}6^{2/5} - 1{,}02 \cdot 0{,}56m = 1{,}94m$$

$$H_f = 42D\left(\frac{\dot{m}''}{\rho_a\sqrt{gD}}\right)^{0,61} = 42 \cdot 0,56m\left(\frac{47.7\frac{g}{sm^2}}{1225\frac{g}{m^3}\sqrt{9,81\frac{m}{s^2}\cdot 0,56m}}\right)^{0,61} = 1,93m$$

Changing the HRR to for instance 450kW in the above calculations, flame length is only extended to 2.13m. The combustion efficiency cannot be stated based only on the above calculations. Tewarson (2004) described the relationship between combustion efficiency (χ) and its radiative component (χ) by the equation;

$$\chi_{rad} = -2.88\chi^3 + 3.56\chi^2 - 5.10\chi - 0.002 \tag{5-1}$$

Using χ_{rad} value of 0.30 which is a reasonable value for heptane liquid and also found as a reasonable value in these experiments (described later), the above equation give a value around 0.92.

CO and CO_2, which both are measured by the cone calorimeter, are compared with values from experiments performed by McCaffery and Harkleroad (1989) and values from Table 3-4.14 in (NFPA, 2002), see Table 2-1 for χ values measured in these experiments. By comparing the molar ratio between CO and CO_2 measured in the cone calorimeter in the present work, with the one from the above experiments, these are quite similar, see Figure 5-7.
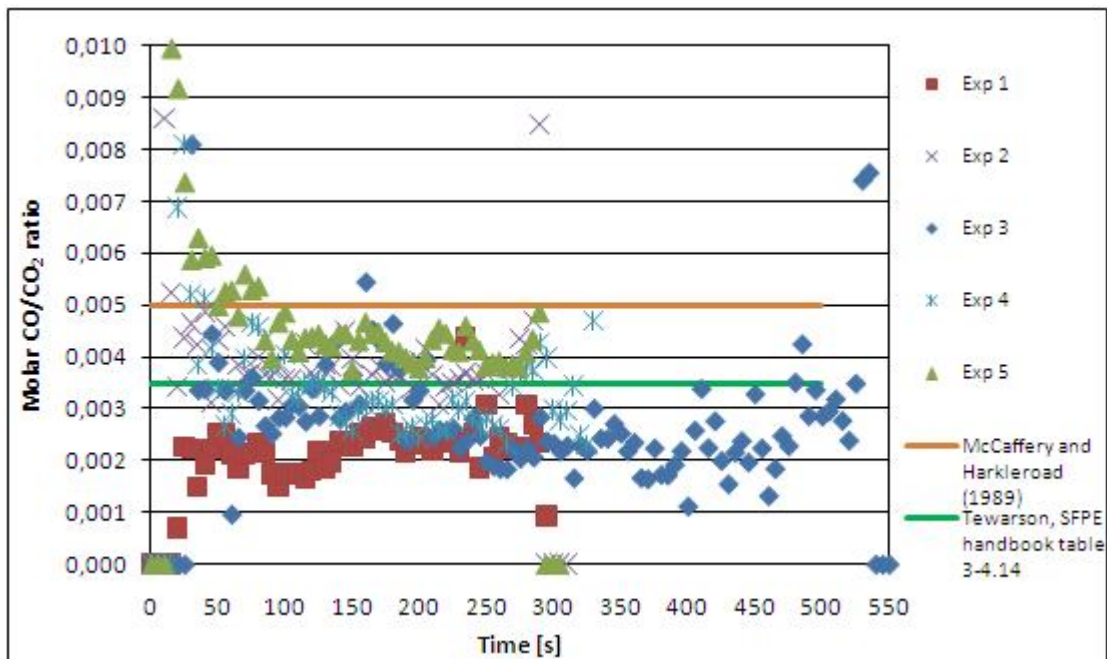
Figure 5-7 *Molar CO/CO$_2$ ratio from experiments 1-5 compared with literature values*

Also the relationship between Extinction coefficient (1/m) and CO/CO_2 are quite similar to heptane values from McCaffery and Harkleroad (1989), see Figure 5-8 and Figure 5-9 below. Values from McCaffery and Harkleroad (1989) are captured from graphs using the software "plot digitizer".

_____
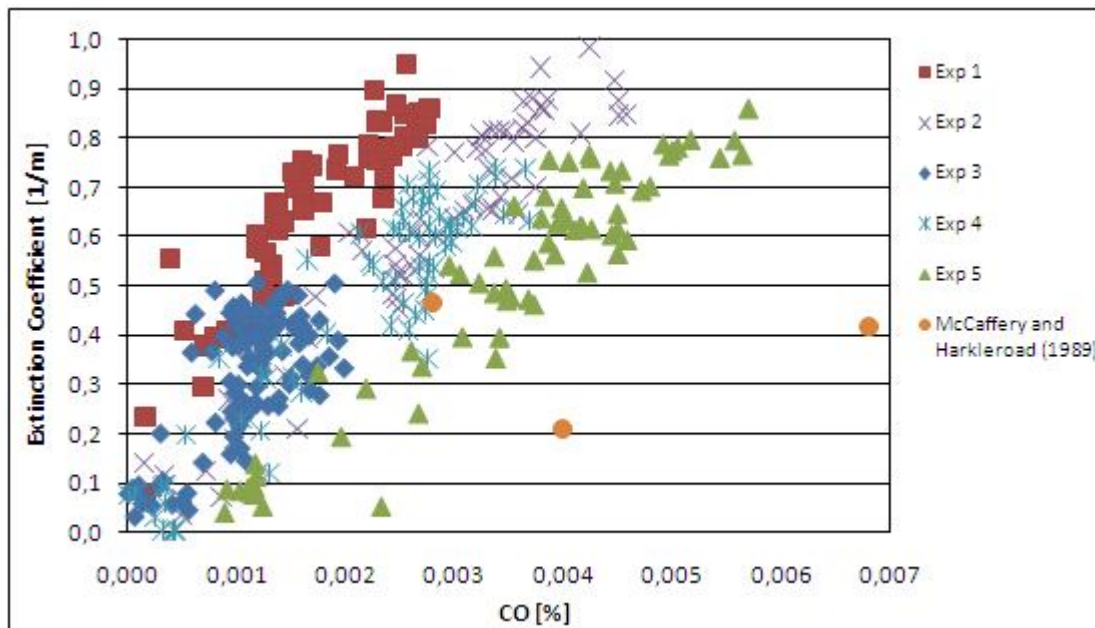
Figure 5-8 _Relationship between smoke and CO in experiments 1-5 compared with literature values_
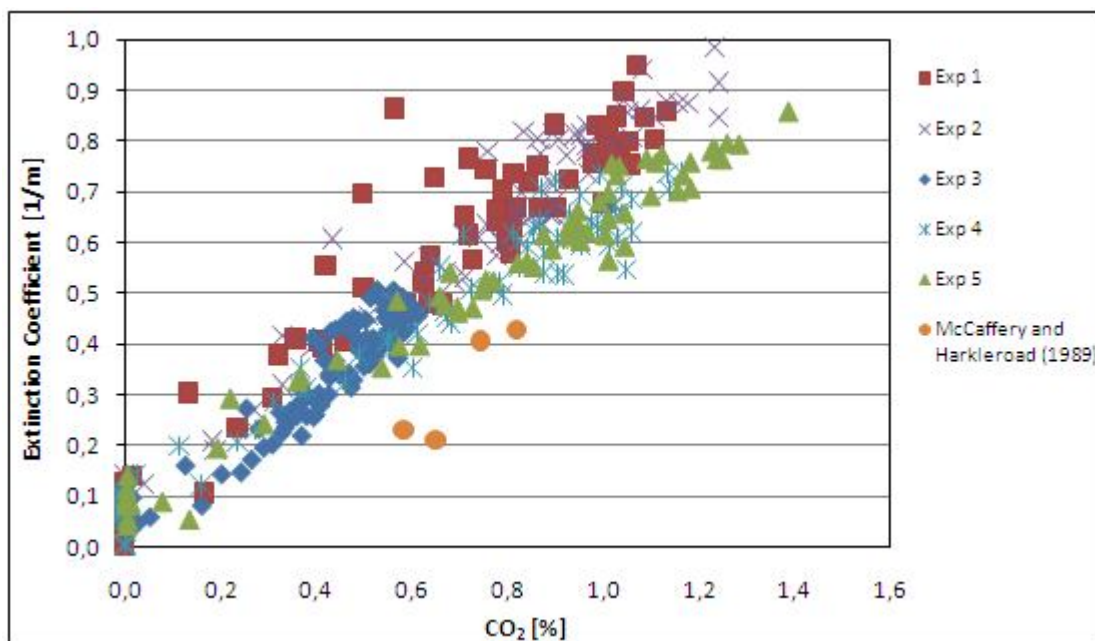
Figure 5-9 _Relationship between smoke and CO₂ in experiments 1-5 compared with literature values_

Smoke Production Rate (SPR) from the experiments is also measured by the cone calorimeter. SPR values from experiments 1-5 are presented in Figure 5-10 below. As the figure shows, heptane values are compared with kerosene- and jet A-1 values from experiments performed during the present work. These experiments are a part of a fellow student, Frode A. Halrynjo thesis, but they were performed in collaboration. Both kerosene and jet A-1 produce significantly smoke than the heptane fires in these experiments. This was also seen in the temperature measurements for kerosene and jet A-1 where both of these are measured in the area 550°C-650°C, while heptane values are measured in the area 700°C-800°C (Figure 5-19).

38
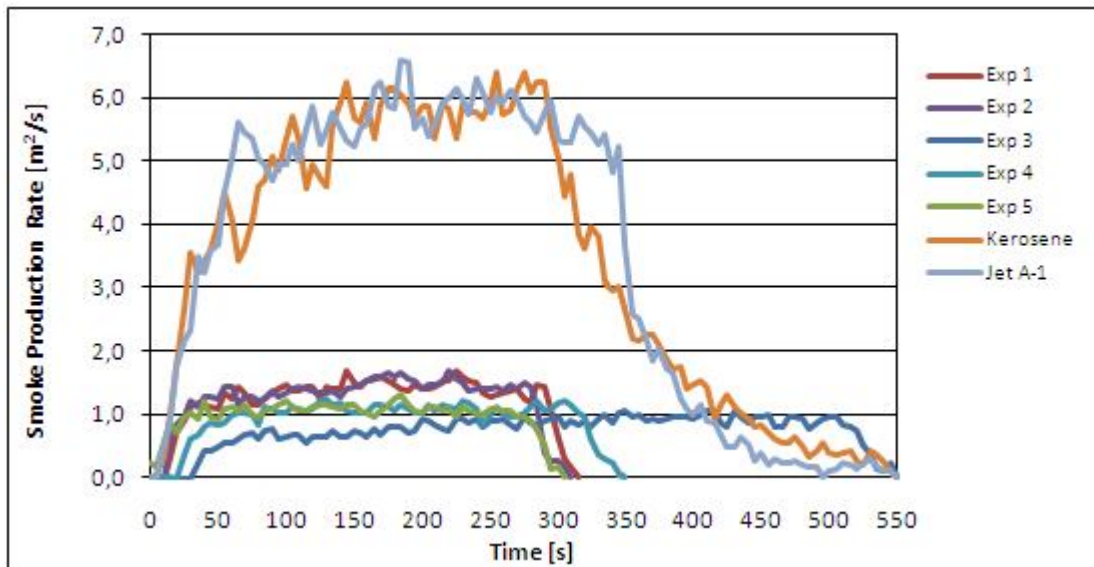
Figure 5-10 *Measured smoke production rate in experiments 1-5 compared with kerosene and jet A-1 values*

Based on the above results, and the fact that the ventilation system in the cone calorimeter probably feeds the fire with enough air, it is assumed that combustion efficiency around 0.9 is reasonable for these experiments. This value is further applied in the presentation of HRR.

After comparing maximum HRR values calculated from mass loss rate with maximum values measured with the cone calorimeter for each experiment, the ratio between the measurement methods seems to be constant, see Figure 5-11. Experiments 6-11 have a lower ratio; this probably because these experiments were performed in another period than the first experiments. In experiment 10 there were some problems with the cone calorimeter measurements which resulted in too high values. Based on this it is concluded that the method calculating the HRR based on average mass loss agree quite well with the measured HRR from the cone calorimeter.
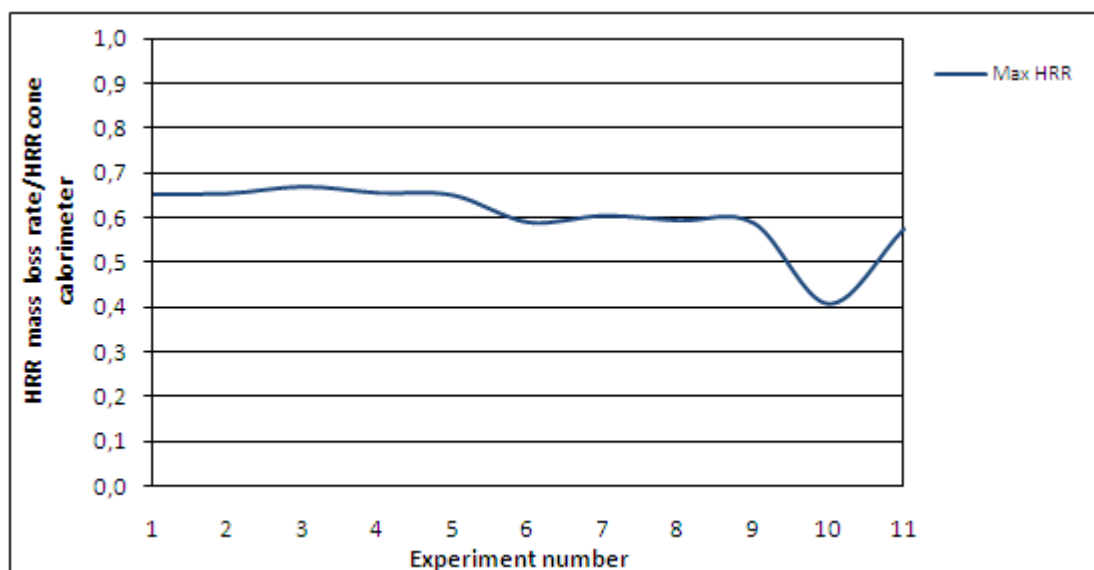
Figure 5-11   *Maximum HRR cone calorimeter measurements compared with mass loss measurements*

39

_____

As shown in Figure 5-12 all experiments except experiment 3, 6, 10 and 11 got stabilized HRR around 450-500 kW when using combustion efficiency of 0.9. In these experiments the pipe obstruction was located quite close to the pool (0.1m and 0.05m) and this resulted in reduced HRR and increased burning time. After analysing the films/tapes from all experiments, it could be seen that the main reason for this reduced HRR is due to the fact that the pipe affects the flame in such way that it burns narrower in the length direction of the pipes. This is shown in Figure 5-13. The pipes did not have this effect on the flame in the other direction (see Figure 5-23) and the effect was largest when the pipes were located close to the pool. It was also tested an increased obstruction percent in 0.1m height above the pool lead to decreased or increased HRR. As Figure 5-14 shows obstruction percent more than 48% did not have considerable effect on the HRR.
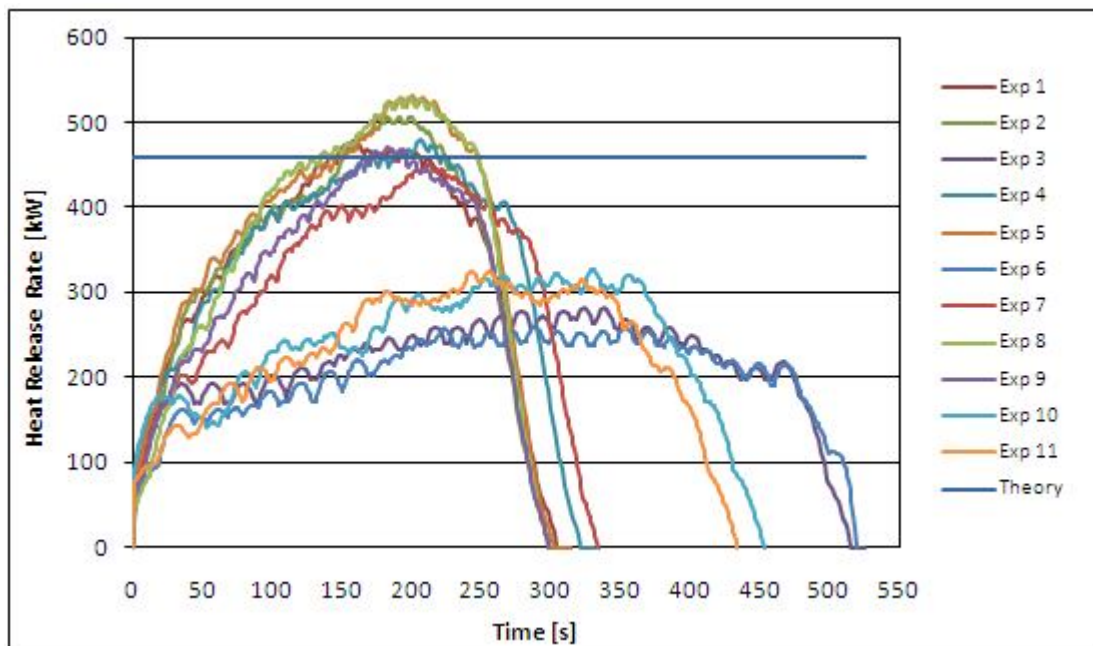
Figure 5-12 *Calculated Heat Release Rate from all experiments using combustion efficiency 0.9*
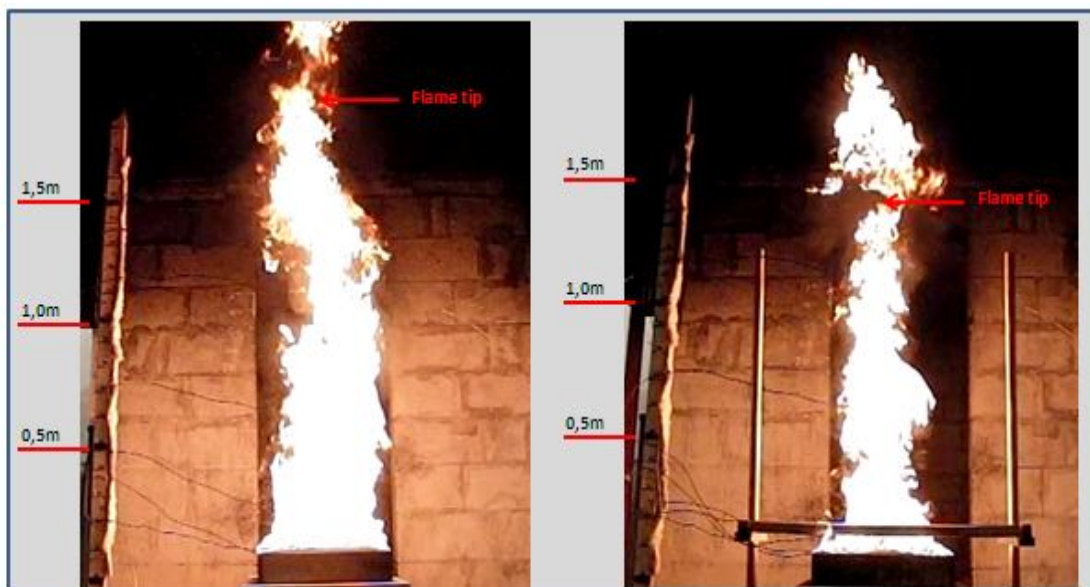
Figure 5-13 *Flame shape: Experiment 1 in left and experiment 3 in right*

40
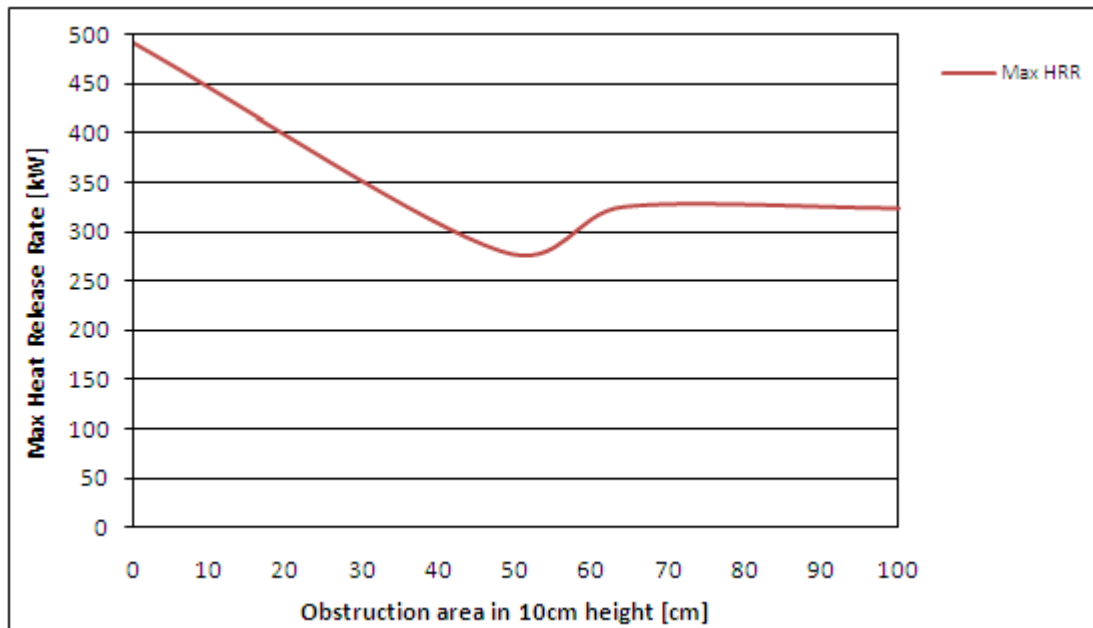
Figure 5-14 *Maximum HRR varying with obstruction area when pipe obstruction is located in 10cm height*

Radiative heat flux (thermal radiation):
Heat flux data measured with the heat flux sensor are compared with values calculated by inserting the measured mass loss rate ($\dot{m}''$) in equation (2-21), using different radiation fractions. In experiment 1 and 2 the radiative heat flux values from the heat flux sensor agrees quite well with values calculated from the equation when using radiation fraction of 0.3. This is illustrated in Figure 5-15, where a radiation fraction of 0.3 in experiment 1 agrees best with experimental values.
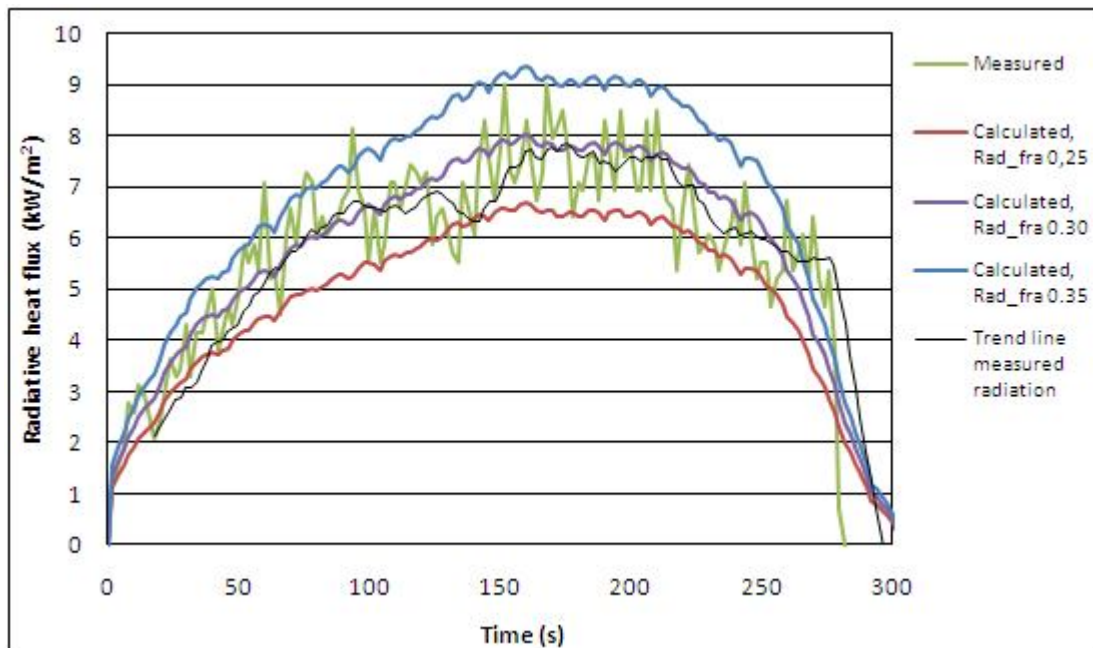
Figure 5-15 *Measured heat flux values compared with calculated values by varying the radiation fraction (χ_{rad}) in experiment 1*

_____

In experiment 3-11 the calculated radiation values by use of equation (2-21) are higher than the measured ones. Even after accounting for the height difference between the flame centre and the flux sensor location (cos θ) the calculated heat flux were too high in these experiments. The main reason for this is probably because the equation doesn't account for the flame shape, only the HRR from the flame and the flame height. The pipe effect leads, as described earlier in this section to a narrower flame. Since this effect works in the direction opposite the flux sensor, the radiation was reduced more in this direction, hence, the low measurements.

After analysing radiative heat flux values from all experiments the same effects as with the HRR is observed. For experiments were pipes are located close to the pool the radiation are considerable reduced. In Figure 5-16 maximum heat flux values for all experiments with 48% pipe obstruction including no obstruction, is illustrated. Heat flux was only measured from one side of the fire and the reduction is therefore probably not the same in the directions where the flame burnt almost without any pipe obstructions.
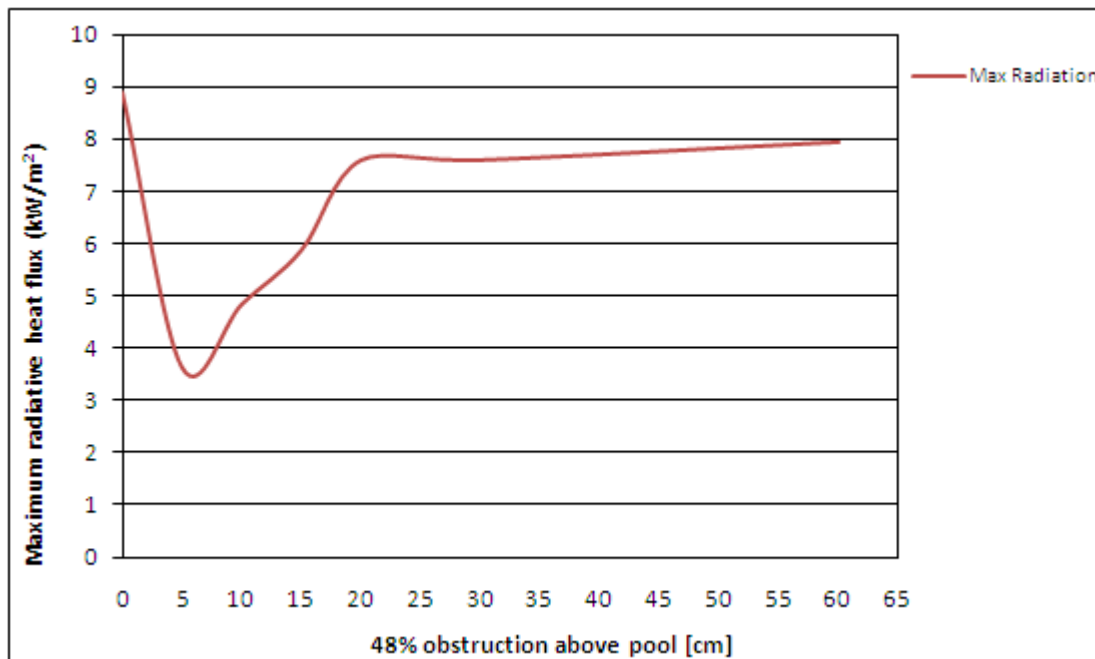
Figure 5-16 *Maximum radiative heat flux values varying with obstruction height*

Uncertainness in the measurements is highest for the lowest measurements. The uncertainly in the measuring data is estimated based on error sources given in Chapter 2 in the heat flux sensors user manual (User manual SBG01, 2008). Initial calibration accuracy is 3%. Non-linearity error (deviation from ideal behaviour since the sensor is calibrated at full range) is assumed to be 2%. But in experiment 3, 6 and 10 where the measurements are around 40-50% of the full scale range to the sensor, the error is assumed to be 5%. Using wind speed of 0.2 m/s (from Table 5-1) and 35°C measured by the flux sensor in equation 2.2.1 and table 2.2.1 both from (User manual SBG01, 2008) the convective error is 1%. Using a 5% radiation error the total uncertainness in the measurements are 11.4%, except from experiment 3 and 6 where it is calculated to 14.7%.

In Figure 5-17 radiative heat flux measurements during fire development in all experiment is illustrated.

_____
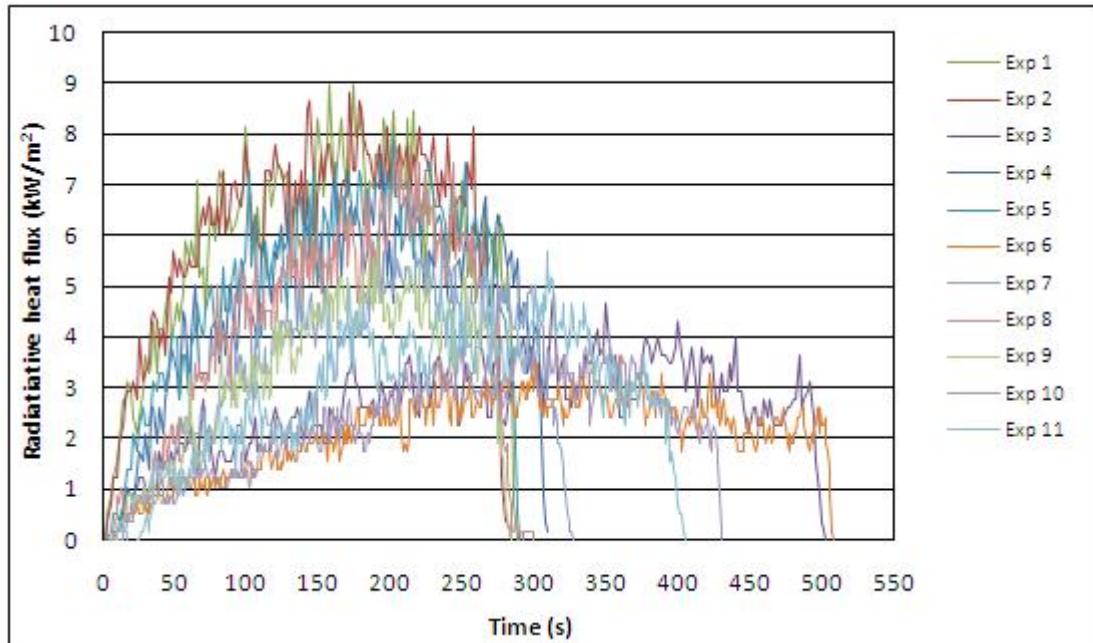
Figure 5-17 *Measured radiative heat flux all experiments*

Flame height:
Maximum flame height from each experiment is observed using a high speed camera. As expected, the flame fluctuated quite much during the experiments. The maximum flame height presented in Table 5-2 is based on observations where the flame was connected about 50 percent of the time in a given time interval. The flame heights were also calculated by using the maximum mass loss rate in equation (2-23) and the maximum HRR based on the mass loss rate in equation (2-22), see Table 5-2 below. A combustion efficiency of about 0.7 utilized in equation (2-22) gave the best results when comparing with visual flame height, while when χ is 0.9 the flame height seems over predicted compared with the observation. Flame height using the mass burning rate in equation (2-23) are close to observations. In Figure 5-13 experiment 1 and 3 are compared in order to visualize the pipe obstruction effect on the flame height.

Table 5-2 *Flame height measurements experiments*

Experiment	Measured flame height (camera)	Flame height calculated using $\chi=0.9$ and $\chi=0.7$ equation (2-22)	Flame height calculated base on using measured mass burning rate in equation (2-23)
1	1.80m-1.90m	2.20/ 1.94m	1.93m
2	1.80m-1.90m	2.26/ 1.99m	2.00m
3	1.40m-1.50m	1.67/ 1.46m	1.39m
4	1.80m-1.90m	2.20/ 1.94m	1.93m
5	1.80m-1.90m	2.32/ 2.04m	2.06m
6	1.40m-1.50m	1.60/ 1.39m	1.18m
7	1.80m-1.90m	2.14/ 1.88m	1.73m
8	1.80m-1.90m	2.32/ 2.04m	1.93m
9	1.80m-1.90m	2.18/ 1.92m	1.84m
10	1.50m-1.60m	1.81/ 1.58m	1.30m
11	1.30m-1.40m	1.80/ 1.58m	1.34m

From the above calculations, a combustion efficiency of 0.9 might seem high, but there is uncertainty in the visual flame length due to the fire fluctuating quite much. The ventilation from the cone calorimeter fed the fire with enough air, this might have resulted in more turbulence and more fluctuations which affected the flame height.

Temperature:
As described in Section 5.2, temperatures were measured in different heights in the flame centre. The temperature results presented below is limited to experiment 1 and 3. The reason for this is that these experiments represent temperatures both with and without pipe obstruction, and it is these experiments that are used in the CFD validation in Chapter 6.
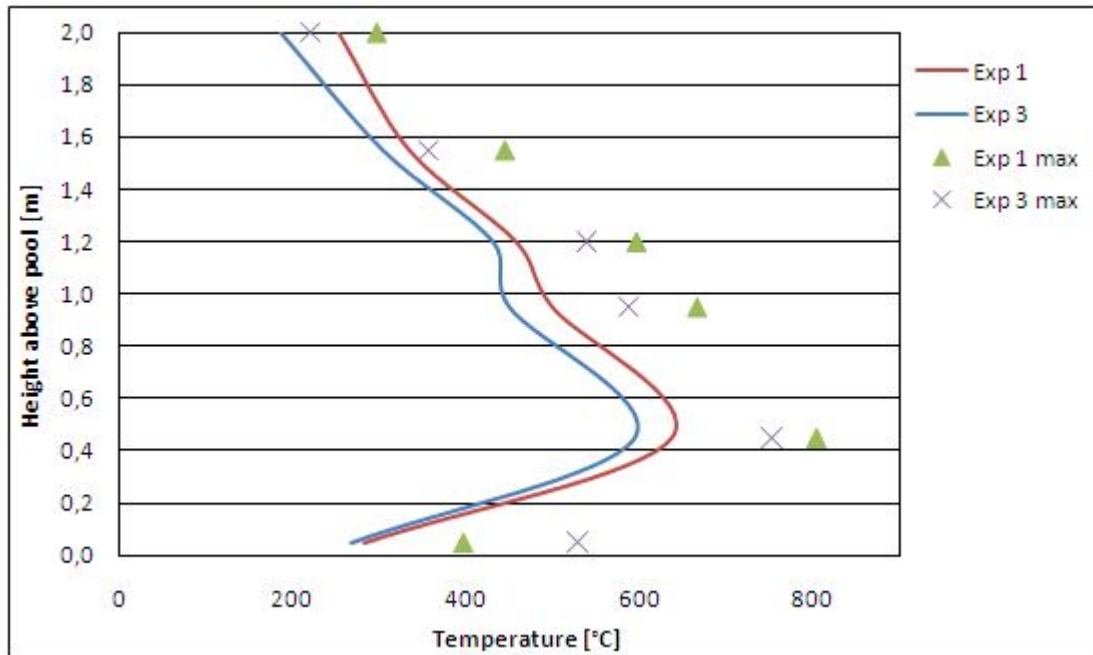
Figure 5-18 *Pipe obstruction effecting average flame temperatures and maximum flame temperatures*

Figure 5-18 presents average flame temperatures compared with maximum flame temperature as a function of flame height during stabilized HRR (Figure 5-12) in experiments 1 and 3. Maximum temperatures are quite high compared with the average temperatures when HRR is stabilized. Looking closer at temperature measurements from experiment 1 in Figure 5-19, the maximum temperatures in the fire (T3-T7) are reached in the growth period of the fire. When the fire grows, the hot flame zone fluctuates around these thermocouples, and this result in high temperatures. After 125 seconds the flame stabilizes and temperatures drop due to the hot flame front fluctuating less around these thermocouples. Similar temperature rise is also observed in the burn out period, but since this period is quite short, the temperature rise is not that high. Thermocouple T8, located at 2.0m, is stable around 250-300°C since the flame front didn't reach this point.
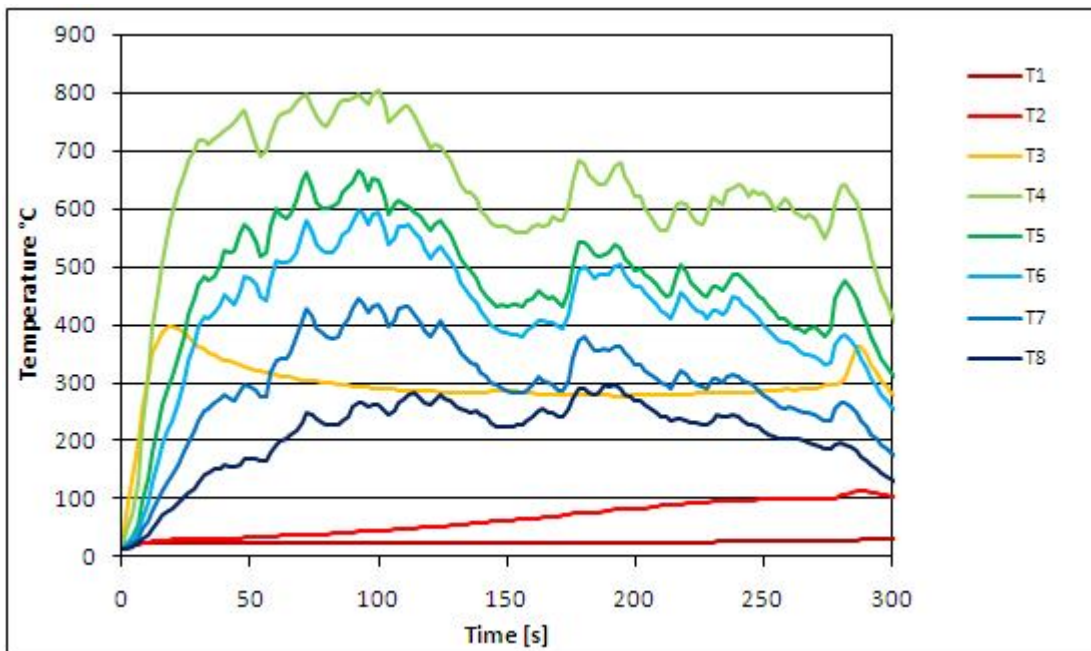
Figure 5-19 *Temperature measurements during experiment 1*

For both experiment 1 and experiment 3, the highest temperatures measured are during the fire growth and burn out period. As Figure 5-20 describes the temperature "jump" in experiment 3 is not as clear as in the fire growth period for experiment 1, but on the other hand, clearer in the burn out period. The low temperature measured from thermocouple T7 (around 300°C), which is located in 1.55m height, indicate that the flame didn't reach this point. This is also in consistence with the flame height observation from the video of the fire.
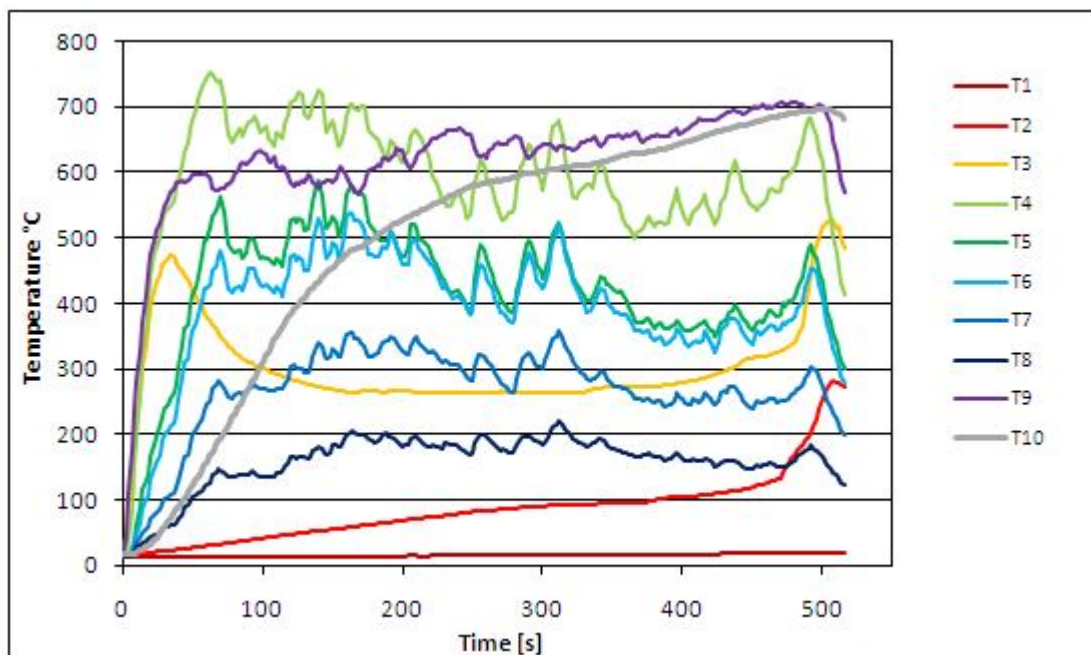
Figure 5-20 *Temperature measurements during experiment 3*

_____

5.4   Outdoor experiments

The outdoor experiments were carried out in the safety centre RESQ located outside Haugesund. A total of 10 pool fire experiments with 0.8m x 0.8m pan and 2 experiments with 1m x 1m pan were performed. Due to limited amounts of heptane fuel, kerosene was also used in these experiments. Figure 5-21 gives an overview of the experimental setup, and a summary of all the experiments is shown in Table 5-3. The main purpose of the outdoor experiments was to identify if there were any relations between the height of the obstruction (pipe rig) and pool diameter.
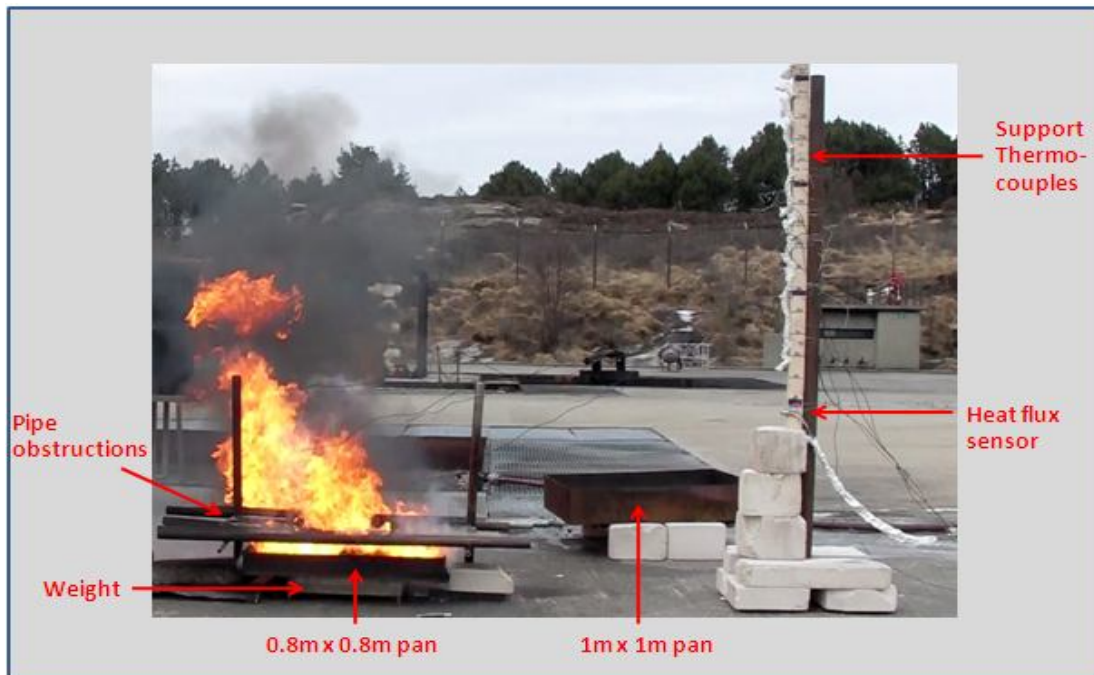
Figure 5-21 *Overview experimental set-up outdoor experiments*

Table 5-3 *Summary outdoor experiments*

Fire experiment	Fuel	Mass of fuel (g)	Pool size (m)	Approximately burning time (s)	48% geometry above pool (m)
Exp 1	Kerosene	6900	0.8x0.8	370	-
Exp 2	Kerosene	8400	0.8x0.8	430	0.1
Exp 3	Heptane	5400	0.8x0.8	290	0.1
Exp 4	Kerosene	6000	0.8x0.8	400	0.15
Exp 5	Kerosene	6100	0.8x0.8	500	0.15
Exp 6	Heptane	5600	0.8x0.8	310	0.15
Exp 7	Kerosene	6300	0.8x0.8	480	0.2
Exp 8	Kerosene	6500	0.8x0.8	420	0.2
Exp 9	Kerosene	6300	0.8x0.8	400	0.3
Exp 10	Heptane	5900	0.8x0.8	360	-
Exp 11	Kerosene	10600	1.0x1.0	400	-
Exp 12	Kerosene	10600	1.0x1.0	300	0.3

In these experiments the mass burning rate was measured based on weight loss. The wind conditions were unstable during the experiments. This resulted in liquid movement inside the pan and gave negative measurement for some time steps. Heat flux measurements were also difficult since the heat flux sensor had to be located opposite to wind direction. In

_____

outdoor pool fires wind is not unusual and, these experiments reveals that the pipe obstruction do not have the same effect when wind is involved. Figure 5-22 shows the maximum HRR for the 0,8m x 0,8m kerosene pan calculated from measured mass loss rate, assuming combustion efficiency of 0.7. As the figure describes, pipe effect on the HRR is minimal.
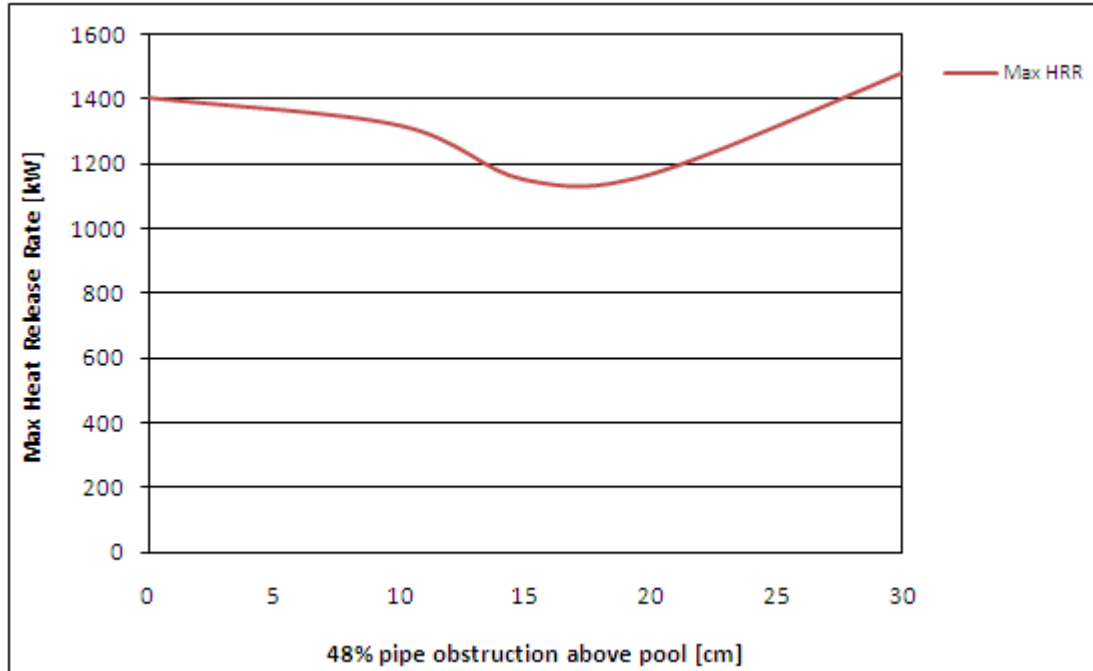

Figure 5-22 _Maximum HRR varying with 48% pipe obstruction in windy conditions_

In the experiments using kerosene as fuel an extra boiling process of the water (below kerosene) was observed. This resulted in "negative" weight measurements at the end of the experiments. When looking at the smoke from the fire in these experiments, which was kind of white, it was clear that more water evaporated.

5.5   Discussion experimental work

The most important observation from the pool fire experiments was that the pipe obstruction close to the pool fire had a decreasing effect on the fire growth when the fire was not affected by wind. This effect resulted in reduced HRR from the fire, reduced radiation to the surroundings and as a natural consequence of this, increased burning time. As described in Section 5.3, the fire only became narrower in the length directions of the pipe obstructions, no changes were observed in the opposite directions, see Figure 5-23 from experiment 10. In the same figure pipes in the opposite direction were included. These were located on top of the other pipes and therefore in an elevation about 0.15m. As plot (b) in Figure 5-23 illustrate, these pipes had no effect on the flame.
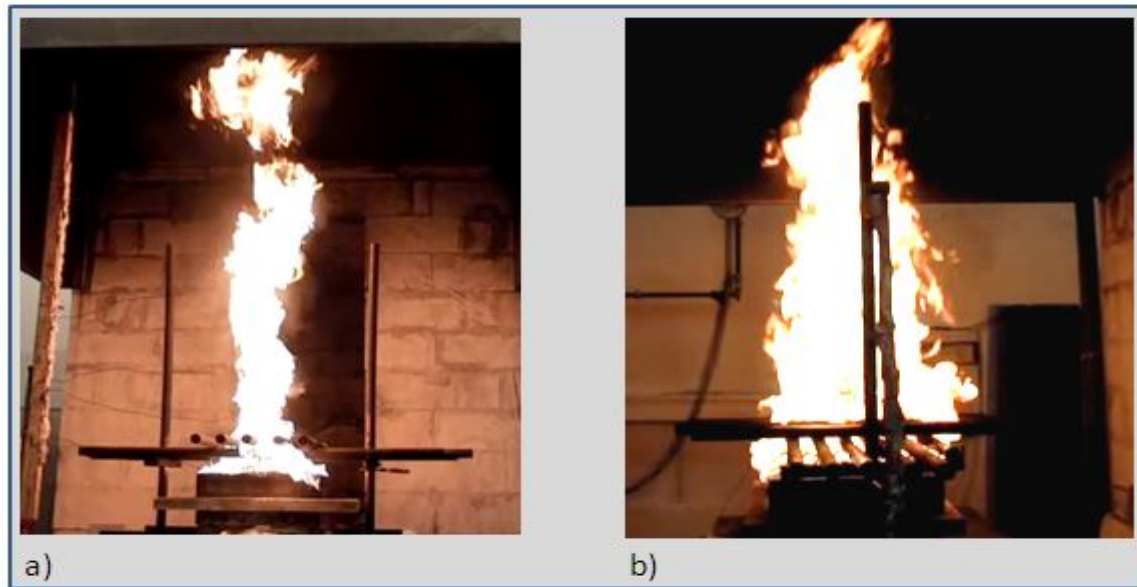
Figure 5-23 *Pool fire narrower in the length direction of the pipes a) but not in the other direction b)*

There are probably several explanations to the obstruction effect observed in the experiments. Table 5.5 in (Drysdale, 1999) shows heat required on pool surface to maintain steady state burning rate and estimated radiant heat transfer from flame to surface for some liquids. According the table kerosene requires 1.05kW to maintain steady burning rate, and it is estimated (experiments performed by Rasbash, 1956) that radiant heat transfer from the flame is 1.08kW. This will also be the case for heptane that is used in experimental work in the present work. If the amount of heat from the flame to the surface is reduced, the fire would reach a point where steady burning is not obtained. The vapour zone observation described by Rasbash (1956) and reported in Drysdale (1999) could explain why this effect mainly was observed when the pipe obstruction were located quite close to the liquid. This cool vapour layer above the pool liquid absorbs radiation from the hot flame and then preventing some of the radiation reaching the surface. This vapour zone varies for different fuels and pool sizes. As described in Figure 5-24 the obstruction area in the length direction of the pipe is high and therefore preventing much of the radiation from the flame. This might have caused the vapour zone absorbing enough radiation so that steady burning rate is reduced. This could result in a narrower flame, reduced flame height and reduced heat release rate. Heat losses to the pipes could also be an explanation why the flame didn't obtain the HRR. Since the pipes reached outside the fire there will be more heat losses in these areas (end of the pool).

Mixing of air into the combustion zone could also be an explanation to reduced HRR. Pipes which are located close to the fire might prevent entrance of air to the combustion zone, and by this reduced combustion efficiency (χ). When looking at Figure 5-7 and Figure 5-10 the CO/CO_2 ratio and smoke production rate (SPR) is not higher in experiment 3 than experiment 1. This indicates that it is the mass burning rate ($\dot{m}''$), which generally is dominated by radiation, that is the factor influencing the HRR, and not the combustion efficiency.
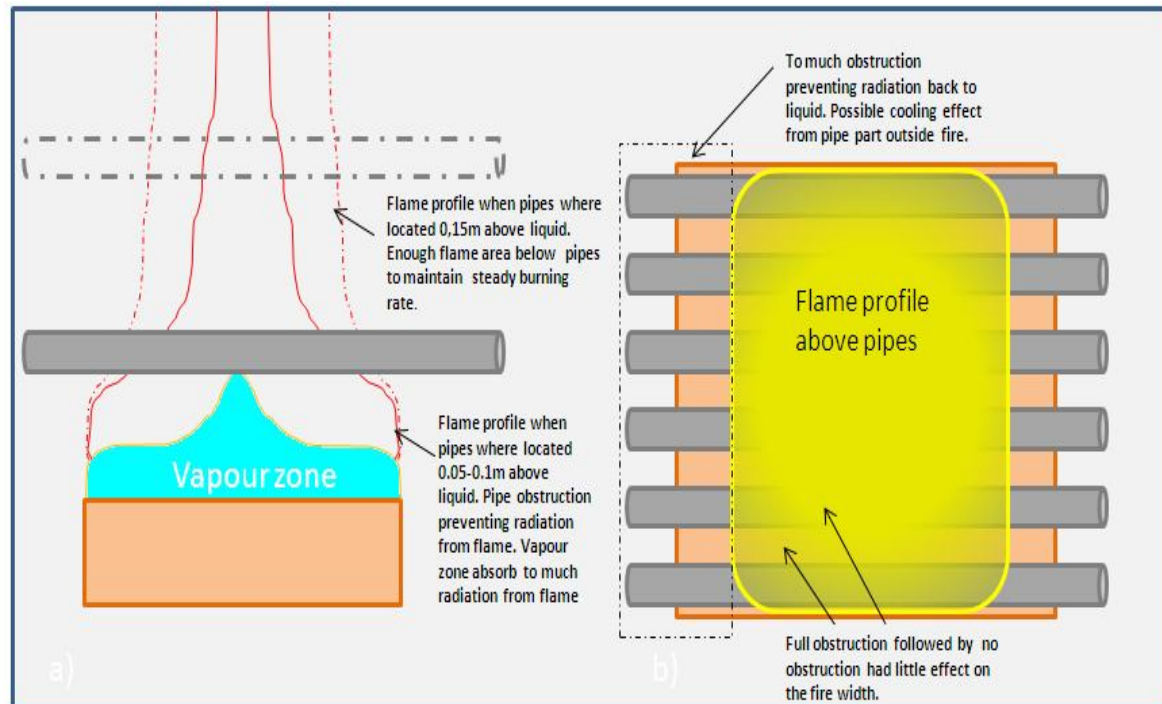
Figure 5-24 *Pipe height effect on pool fire in a) and pool fire structure above pipes in b)*

5.6   Suggested improvements experimental work

When performing outdoor experiments the weather conditions is an important factor that needs to be taken into consideration. The date for performing these experiments was set some time in advance. Days before the experiments the weather condition seemed good. Even if some wind was reported it was decided to perform the experiments. There were also limitations in when to use the test facility and when necessary personnel were available for performing the experiments.

When it comes to the indoor experiments following improvements is suggested:
- Calibrate the cone calorimeter before the experiments, and verify that reasonable values are obtained by running a known test fire.
- Utilization of a scale which has an accuracy of per gram, and not per hectogram as used for the weighing in these experiments.
- Increase the experimental time (amount of fuel) to be sure that steady state is reached. Heptane pool fire experiments performed by (Björklund, 2008) reported higher HRR values than values from experiments performed in the present work. In their HRR calculations a combustion efficiency of 0.92 was used, but it seems like the main effect on the increase HRR is the amount of fuel. Instead of 4 litres of fuel which is used in the present work, they used 15 litres for the same fire area. This lead to increased evaporation (mass loss rate) and by this increased HRR.

6   Simulations

Simulations using FDS and FLACS are compared with experiments performed with regards to this thesis (see Section 5) and some of the pool fire experiments performed by Steckler et al. (1982) and Gutiérrez-Montez et al. (2009). These experiments are mainly chosen because of the detailed descriptions of the experimental set-up and because the measured data is suitable for comparisons with obtained CFD simulations. This chapter constitutes of a description of the experimental setup, input data used in the CFD simulations, results from the simulations and discussion of the results from each experiment.

6.1   Simulations of "Experiments from this thesis (Chapter 5)"

Eleven experiments are performed in the fire laboratory in Haugesund, see Section 5.2, but only experiment 1 and 3 are chosen for further simulation with the CFD models. The main purpose of these simulations is firstly to validate how well CFD models predicted the pool fires (flame, temperature, radiative heat flux), and secondly, to investigate if the pipe obstruction effect from the experiments could be reproduced in the fire models. In simulations of cases with pipe obstruction located above the fire as in experiment 3, the liquid fuel model in FDS is mainly used. This because the fire then develops based on heptane properties (re-radiation from flame to pool surface) and is not controlled as a vent (nozzle) with defined heat release rate or mass loss rate.

The geometries shown in Figure 5-1 - Figure 5-4 are constructed in both CFD programs.

6.1.1   FDS input data

In pool fire simulations with FDS, the fire is both defined by mass loss rate and heat release rate from the experiments, and developed from the liquid fuel model based on evaporation of heptane liquid.

The entire experiment facility is built up in the model, but to reduce the amount of grid cells only the most important part of the facility is used in the simulations, see Figure 6-1.
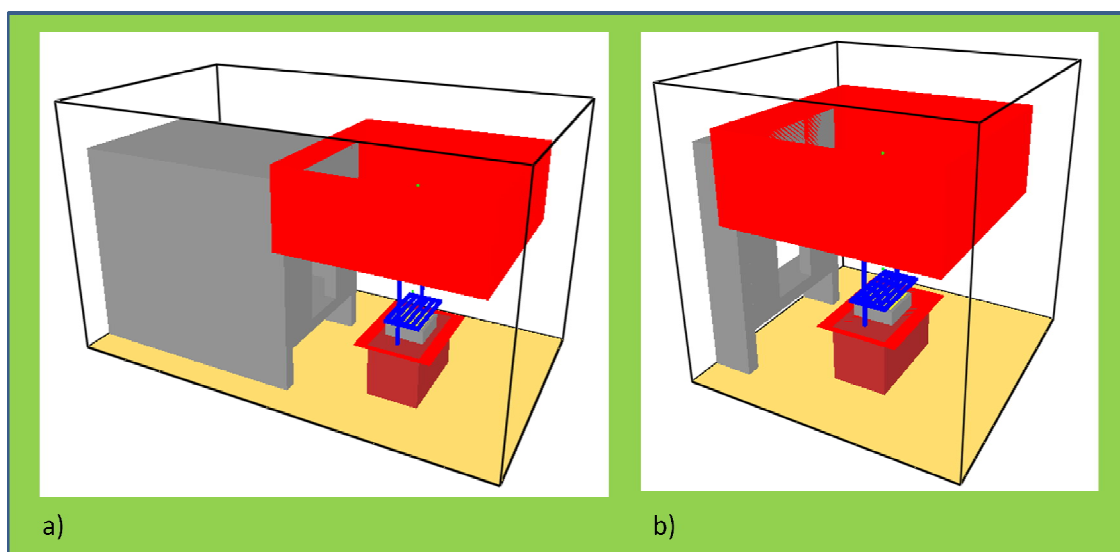
Figure 6-1 _Entire test facility in a) and area used in modelling in b)._

_____

Simulations using Mass Loss Rate (MLR) and Heat Release Rate (HRR):
In the input files a fraction of the maximum MLR and maximum HRR measured from the experiments are applied to describe the fire growth. Since the MLR is measured directly from the experiments this is the most accurate value. The HRR is based on the MLR but it is uncertainty considering the combustion efficiency (χ) which is estimated to be around 0.9 from the experimental work. In this way the MLR from the fire is correct according to the experimental results but there are still other parameters in FDS that affect the results. If the radiation fraction is not defined in input file this fraction is default 0.35 for LES calculations in FDS 5. In the experimental work a radiation fraction of 0.3 gave better results when using the measured MLR in equation (2-21), see Section 5.3. In FDS simulations the fire is defined both based on MLR per unit area (MLRPUA) and HRR per unit area (HRRPUA) using different radiation fraction values and different combustion efficiency values in the HRRPUA simulations.

Simulations where HRR is not defined (liquid fuel model):
For liquid fuels in FDS the evaporation rate of the fuel is as described in Section 3.3.1 governed by the Clausius-Clapeyron equation. When using the liquid fuel model properties of the fuel(s) are given in the input file. Properties listed in Table 6-1 are used in the simulations of these experiments.

Table 6-1 *Input properties using the liquid fuel model in FDS (Engineering Toolbox home page (2011) and Drysdale (1999))*

Property	Used value	Comment
Emissivity	Varying in simulations	Surface emissivity for liquid.
NU_FUEL	1	Account for possible impurities in the liquid that do not take part in the combustion process.
Heat of Reaction	318 kJ/kg	The amount of energy consumed, per unit mass of reactant that is converted into something else.
Conductivity	0.14 W/mK	Thermal conductivity of the liquid.
Specific Heat	2.24 kJ/kgK	Amount of heat per unit mass required raising the temperature by one degree Celsius.
Density	684 kg/m3	Liquid density.
Absorption coefficient	Varying in simulations	Detonate the absorption in depth of thermal radiation. Since liquids do not only absorb radiation on the surface, but rather over a thin layer near the surface, this coefficient has significant effect on the burning rate, ref FDS User Guide Section 8.4.5 (Kevin McGrattan, 2010)
Boiling Temperature	98.4 °C	The temperature at which the vapour pressure of the liquid equals the environmental pressure surrounding the liquid.
Thickness of fuel layer	0.0152m in exp 1 and 0.0164m in exp 3.	Defines how thick the fuel layer is.

According to the FDS User Guide the convection of the liquid is important, but it is not considered in the model. It is also stated that the pyrolysis model of evaporating liquid fuels is recommended for research use only, due to the evaporation rate is strongly grid

dependent. Wakatsuki et al. (2008) observed that an accurate description of radiative transfer in fires requires temperature-dependent absorption coefficients for all fuels and decomposition products present in significant concentrations. In the verification part of FDS, absorption coefficient 40 1/m is used for an ethanol pan fire. The ethanol value is discussed on FDS official home page, and according to one of the authors of the FDS User Guide (Hostikka, 2007) this value is a pure "best fit" value to match the ethanol experiment. He also says that there are still many physical phenomena in pool fires that are not taken into account by FDS and some of these effects may now have been "lumped" to the number 40 for the ethanol experiment.

However, in this thesis the liquid fuel model is tested to verify the prediction of the simple experiments carried out, and to see whether the pipe effect observed in the experiments are reproduced in the simulations. This is done by defining equal liquid properties in both cases. Properties from Table 6-1 together with variation in absorption coefficient and emissivity to the heptane liquid is used in the simulations.

Mesh (grid cells):
Only one mesh (not multiple meshes) with uniform grid cells is used. Grid sizes of 20cm, 10cm, 5cm and 2.5cm are tested out to verify the grid sensitivity of the simulations.

Measurements:
Temperature and radiative heat flux measurements are defined as "THERMOCOUPLE" and "RADIATIVE HEAT FLUX GAS" in the input files. More information about these measuring methods is given in Section 3.3.1.

Table 6-2 *Properties used for the exhaust hood*

Thickness [mm]	Density [kg/m3]	Thermal conductivity [W/Km]	Specific heat [J/kgK]	Emissivity [-]
6	7800	45	460	0.3

An example input files for the liquid fuel model is attached in appendix C.

6.1.2   FLACS input data

In FLACS simulations, the fuel is added by using jet nozzles and the mass rates correspond to those obtained in the experiments. It is possible to model pool leaks in FLACS, but the modelling of the heat feedback, which determines the evaporation rate is premature (Lokna, 2008). The pool model in FLACS is therefore not used in this work. The following inputs are used in the simulations:

Fuel evaporation model (the fire):
Evaporation of liquid fuel leak is modelled by 25 jet nozzles where each nozzle has area of $0.00758m^2$ to fit into a defined grid cell for the fire. Each nozzle releases 1/25 of the total mass flow rate measured in the experiments. Vertical "jet" nozzles, horizontal "jet" nozzles by defining four leak direction (x,-x,y,-y) from each nozzles and a combinations are tested to verify what leakage method predicting the best results. It is also possible to control the leaks in FLACS by modifying the CL-files for each leakage, but in this thesis the leakages are defined to match the maximum mass loss rate (steady state).
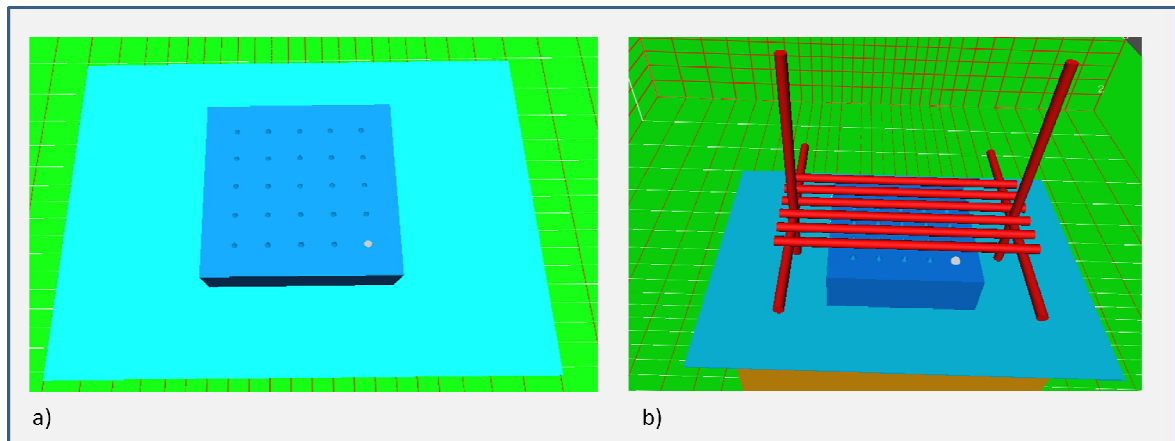
_____

Figure 6-2 *CASD plot of the 25 jet leaks in a) and experiment 3 with pipe obstructions in b)*

Mesh (grid cells):
The grid around the fire is uniform with 10cm size. Outside the fire region the grid cells are stretched towards the boundaries.

Measurements:
Temperature and radiative heat flux measurements are done by defining monitor points.

6.1.3   Results FDS simulations

Simulations using Mass Loss Rate (MLR) and Heat Release Rate (HRR):
When defining the fire as a MLRPUA or HRRPUA fraction, the fire developed exactly like the heptane pool fire from the experiments. Using MLRPUA gives the most correct description of the fire since mass loss rate was measured directly in the experiments and heat release rate were calculated based on mass loss rate by assuming combustion efficiency (χ).

In these simulations the main focus is therefore to verify if FDS would predict the radiative heat fluxes and temperatures measured in the experiments by defining the fire correctly. It is also in interest to compare the two methods, MLRPUA and HRRPUA, to verify what combustion efficiency values assumed in the HRR that gives most equal results.

Table 6-3 *MLRPUA and HRRPUA values used in simulations*

Exp	Maximum measured mass loss rate (g/s)	MLRPUA (kg/sm^2)	HRRPUA (χ=0.7)	HRRPUA (χ=0.8)	HRRPUA (χ=0.9)	HRRPUA (χ=1)
1	11.94	0.0477	1490.5	1703.4	1916.4	2129.3
3	7.0	0.028	873.6	998.5	1123.3	1248.1

Radiative heat flux measurements using; HRR with different mix in combustion efficiency (χ) and Radiation Fraction (R_F), and using MLR with different R_F is shown in Figure 6-3. In these simulations a relatively coarse grid (20cm) is used, but grid sensitivity analysis shows that these simulations are not very grid dependent when it comes to radiative heat flux, see Figure 6-4 and Figure 6-5. Monitor points in FDS measures heat flux from the whole grid cell where the monitor point is located. The monitor point is located at 2.45 in y-direction. From the defined mesh this means that heat flux is calculated in 2.3-2.5m for 20cm cells, 2.4-2.5m for 10cm cells and 2.45-2.5m for 5cm cells. It then

seems like the 5cm grid cells measure radiative hat flux a little further away from the fire and this could be the reason why this value is a little lower than the other grid cells. As Figure 6-3 indicated when using MLR with R_F of 0.3 the heat flux is over predicted compared with the experimental values. By correcting the R_F to 0.27 the simulated and measured heat flux are almost identical. The figure also shows that using χ of 0.7 in combination with R_F of 0.3 the simulated heat flux value is under predicted compared with the measurements. By changing the χ to 0.9 the heat flux values agrees well with the measurements. The combination where χ is 0.8 and R_F is 0.35 also gives good results.
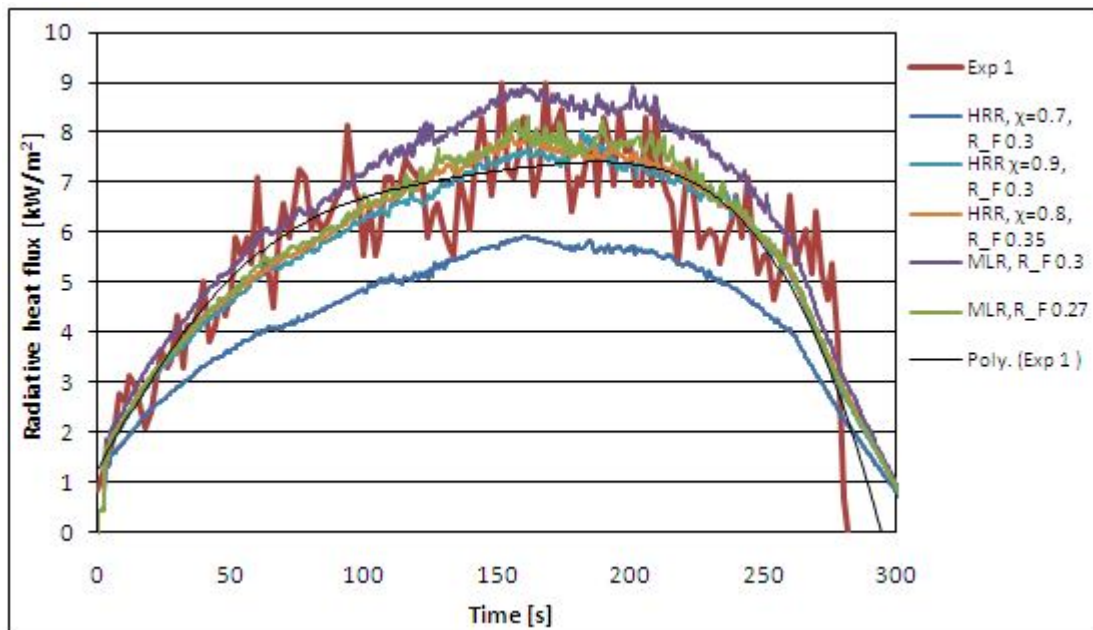
Figure 6-3 *Radiative heat flux measurements from Experiment 1 compared with radiative heat flux measured in FDS using 20cm grid cells, HRR or MLR defined and variation in combustion efficiency χ and Radiation Fraction (R_F)*
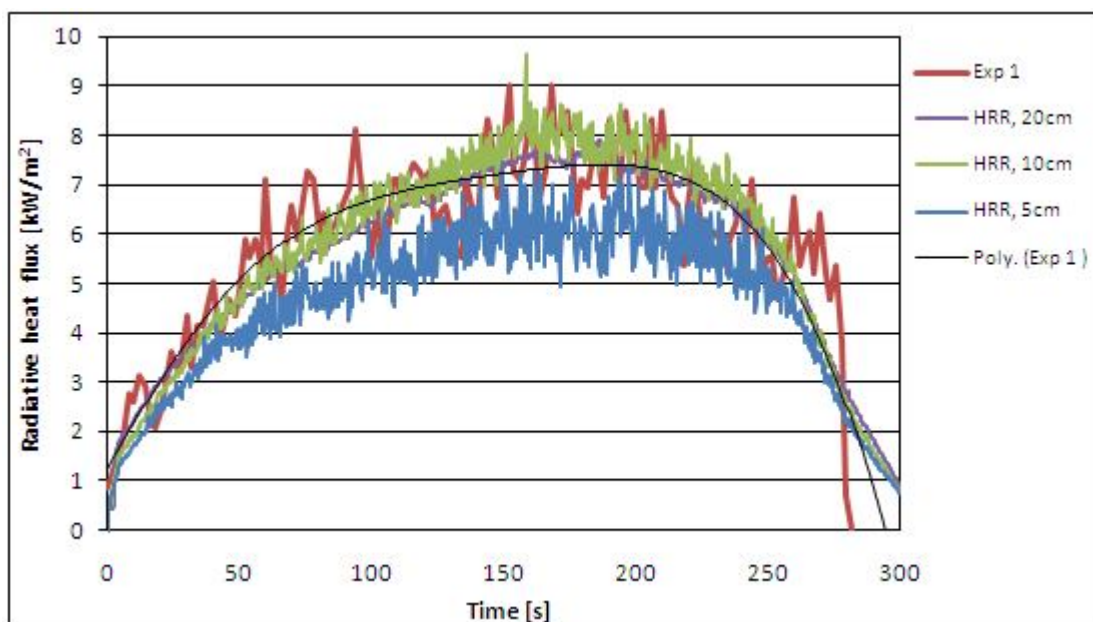
Figure 6-4 *Grid dependency radiative heat flux measurements FDS simulations, using HRR with efficiency (χ) of 0.9 and Radiation Fraction (R_F) of 0.3*

55
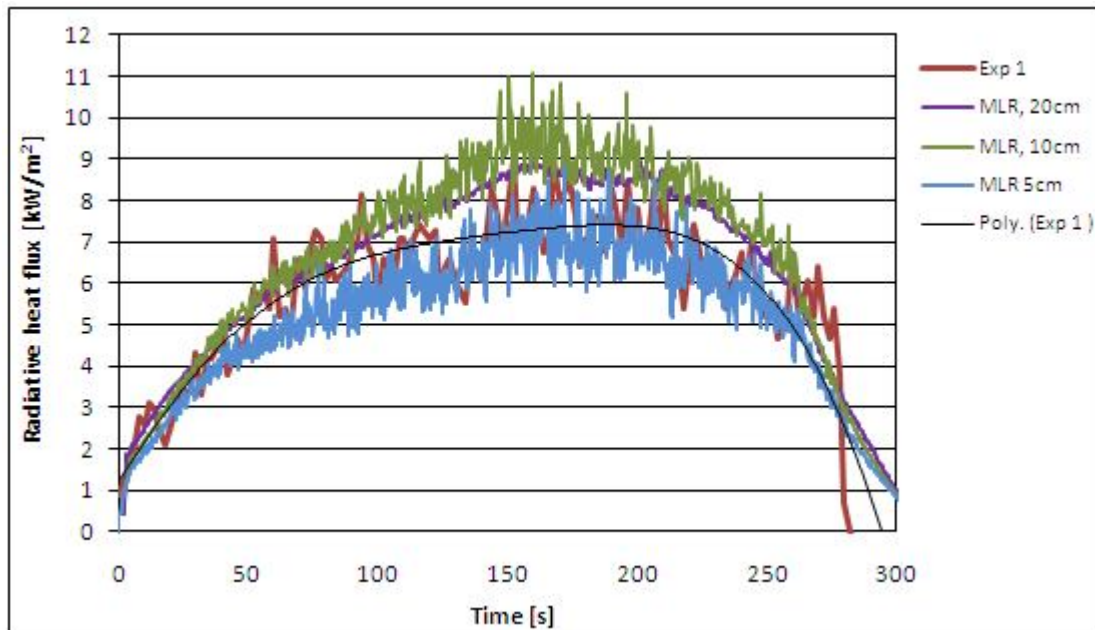
Figure 6-5 *Grid dependency radiative heat flux measurements FDS simulations, using Mass Loss Rate (MLR) and Radiation Fraction (R_F) value 0.3*

Figure 6-6 illustrates average flame temperatures (100-250s) in experiments 1 compared with average flame temperature calculations from FDS simulations using 20cm grid cells. The fire is defined by HRR or MLR with a mix in combustion efficiency (χ) and Radiation Fraction (R_F) that gave the best heat flux results described above.
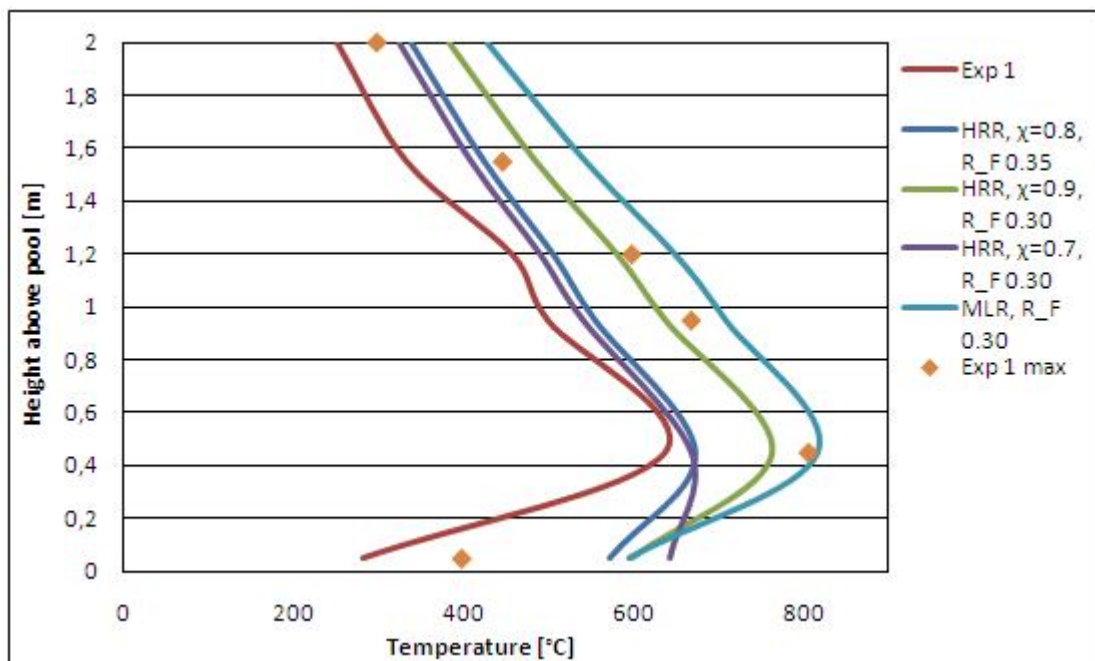
Figure 6-6 *Average flame temperatures from experiment 1 (100-250s) compared with average flame temperatures in FDS simulations (20cm grid, HRR or MLR defined)*

As the above figure shows, the flame temperature predicted in FDS using relatively coarse grid do not differ much from experimental data. When HRR is defined FDS values are between the average-and maximum flame temperature measurements, while using MLR

56

the predicted temperatures are somewhat higher. When the grid cells were refined the temperature fluctuated more and higher temperature with more divagation from experimental results is observed, see Figure 6-7 and Figure 6-8.
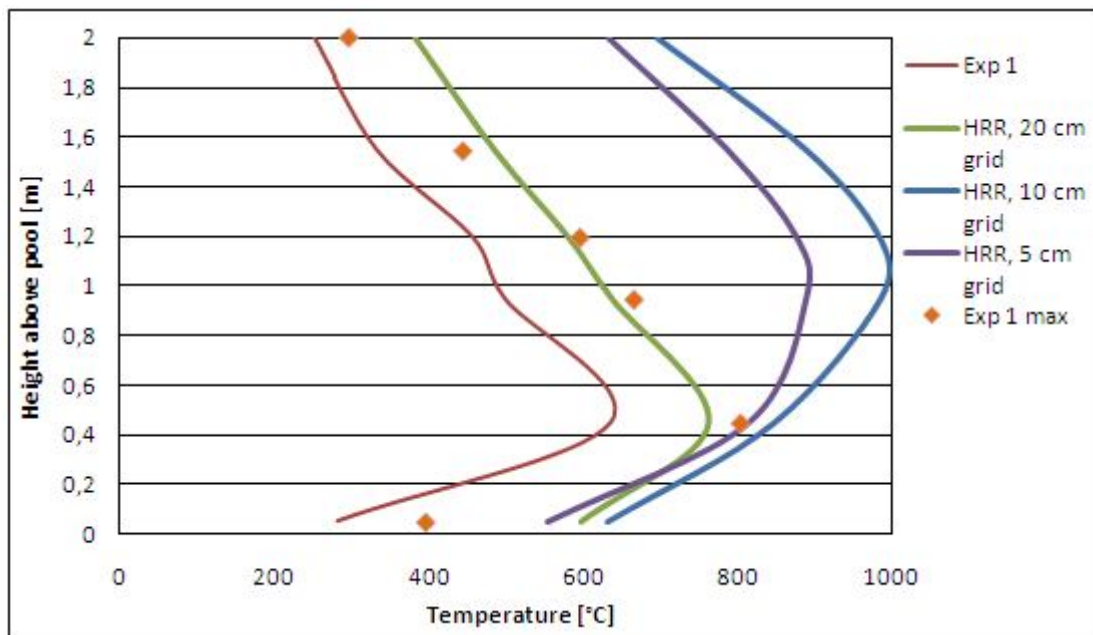
Figure 6-7 *Grid sensitivity average temperatures from experiment 1 when HRR is defined with χ=0.9 and R_F=0.30*
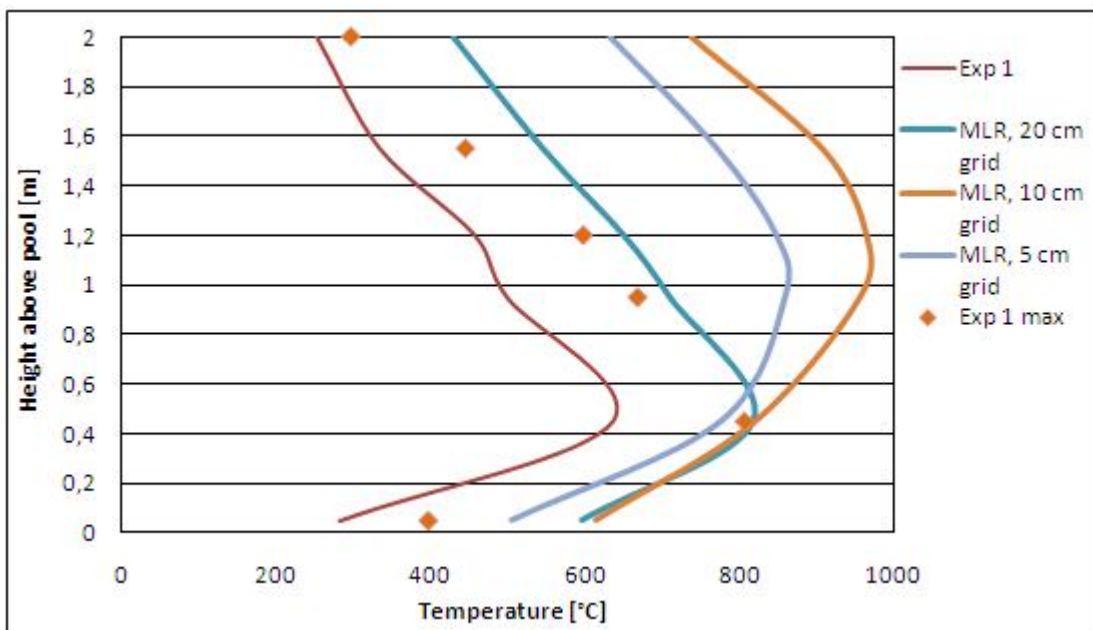
Figure 6-8 *Grid sensitivity average temperatures from experiment 1 when MLR is defined using R_F=0.30*

Refined grid should generally give better temperature measurements. But when the grid is changed, the area where the temperature is measured is changes due to the fact that FDS measure temperature in the grid cell where the monitor point is located. When studying only the flame and its temperature, grid cells of 5cm are still quite coarse.

_____

Simulations when the pool fire is not defined (liquid fuel model)
Since it is stated in the FDS User Guide that this model is very grid dependent, this was the first to be verified when using the model. In these experiments heptane values from Table 6-1 are used together with an absorption coefficient value of 40 1/m and emissivity of 1, which predicted good results for the ethanol liquid experiment, as described in the FDS User Guide.
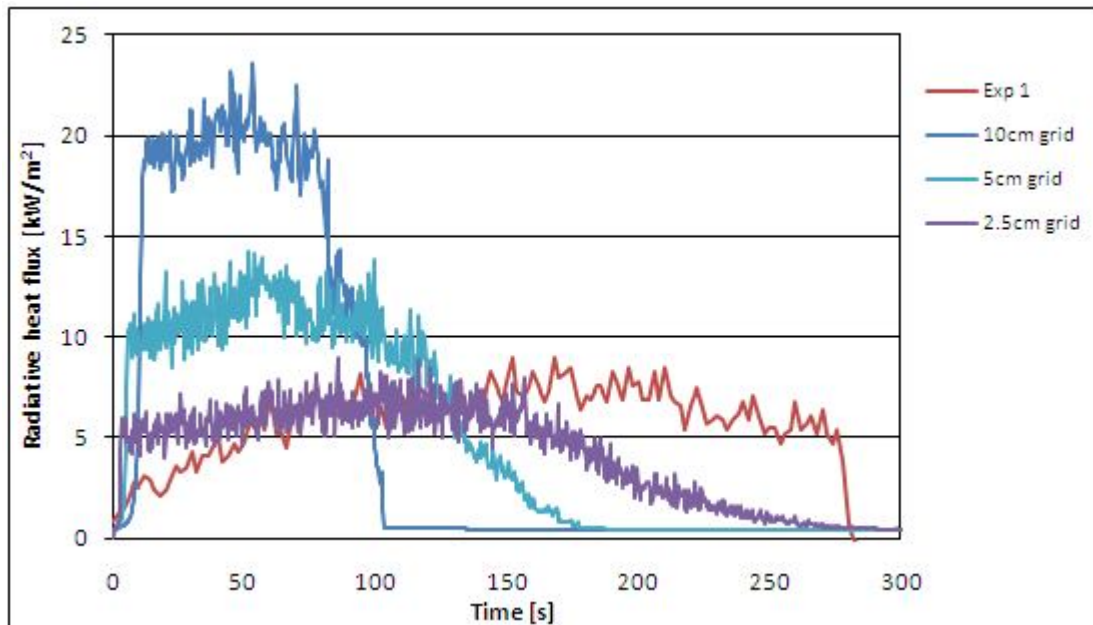
Figure 6-9 *Grid sensitivity radiative heat flux measurements using the liquid fuel model Experiment 1)*
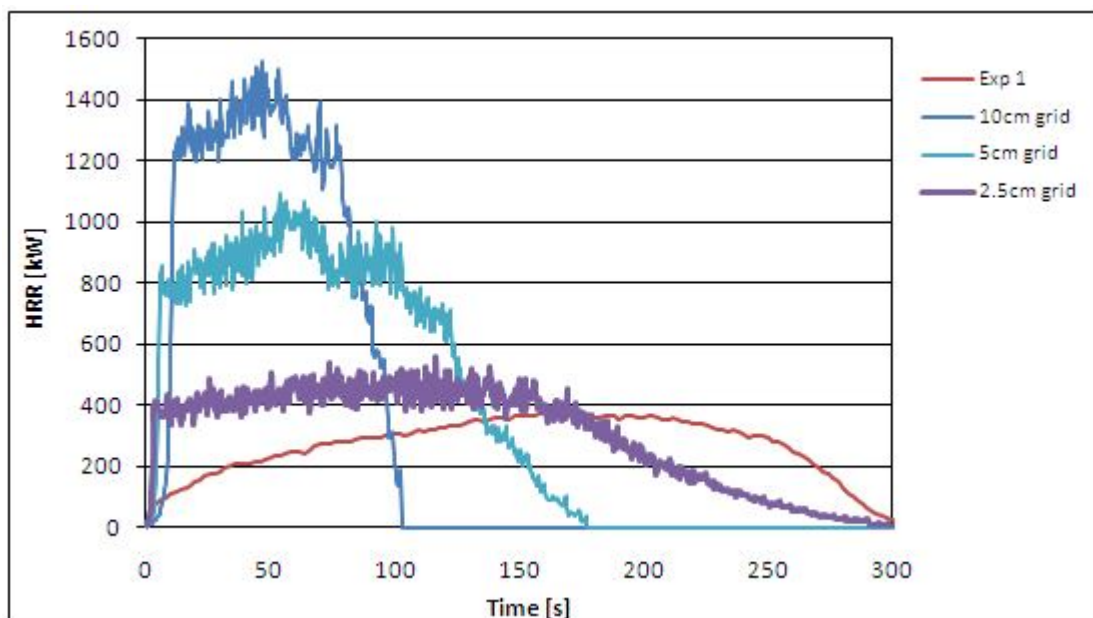
Figure 6-10 *Grid sensitivity heat release rate measurements using the liquid fuel model (Experiment 1)*

Results from simulations shows that HRR and radiative heat flux from the fire varied a lot for different grid cells sizes. Coarser grid cells gave most overestimated results. As Figure

_____

6-9 and Figure 6-10 shows results near the experimental values was only obtained when using 2.5cm grid cells. In these simulations the domain was decreased due to limitations in computer capacity running the simulation. This may have affected the results.

When it comes to the pipe effect (experiment 3) only simulations using 2.5cm grid cells with absorption coefficient value of 40 1/m and emissivity of 1(-) is performed. The fire is unchanged from experiment 1 since the main reason for these experiments was to see if the reduced HRR and reduced radiative heat flux observed in the experimental work also could be seen in the simulations.
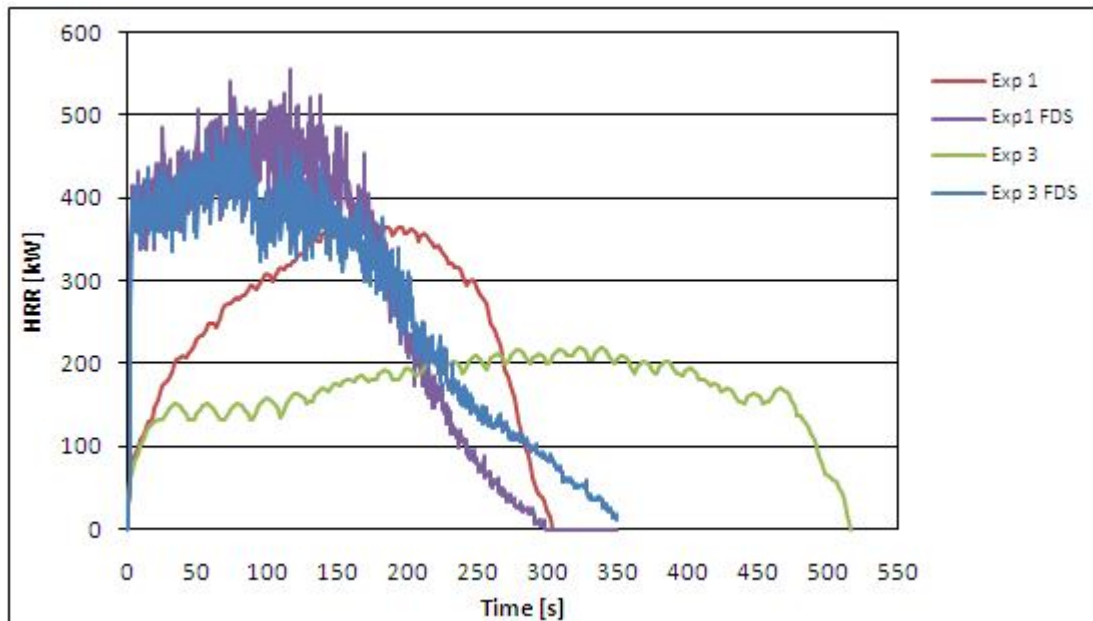
Figure 6-11 *Heat release rate predicted by the liquid fuel model in experiments with and without pipe obstruction*

As Figure 6-11 above illustrate, the pipe effect on the HRR is little compared to the experimental observation. The pipes lead to little reduction in HRR and heat flux. Additionally, the fire lasted longer, but still, it differed much from the experimental results. When looking at temperature plot from both simulations (Figure 6-12), the pipe effect leading to a narrower flame in only one direction during the fire development in experiment 3, are seen.
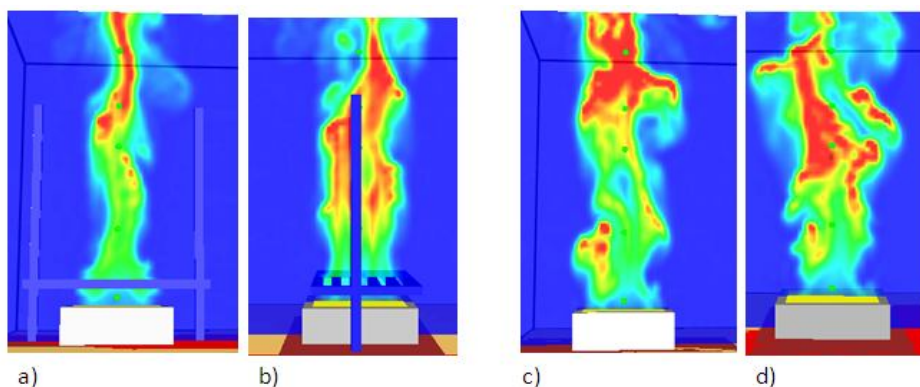
Figure 6-12 *Temperature plots from experiment 3 in a) and b), and plots from experiment 1 in c) and d)*

_____

Reduced grid cells gave reduction in HRR and radiative heat flux, and as Figure 6-13 shows the same trend is observed for the temperature in the flame.
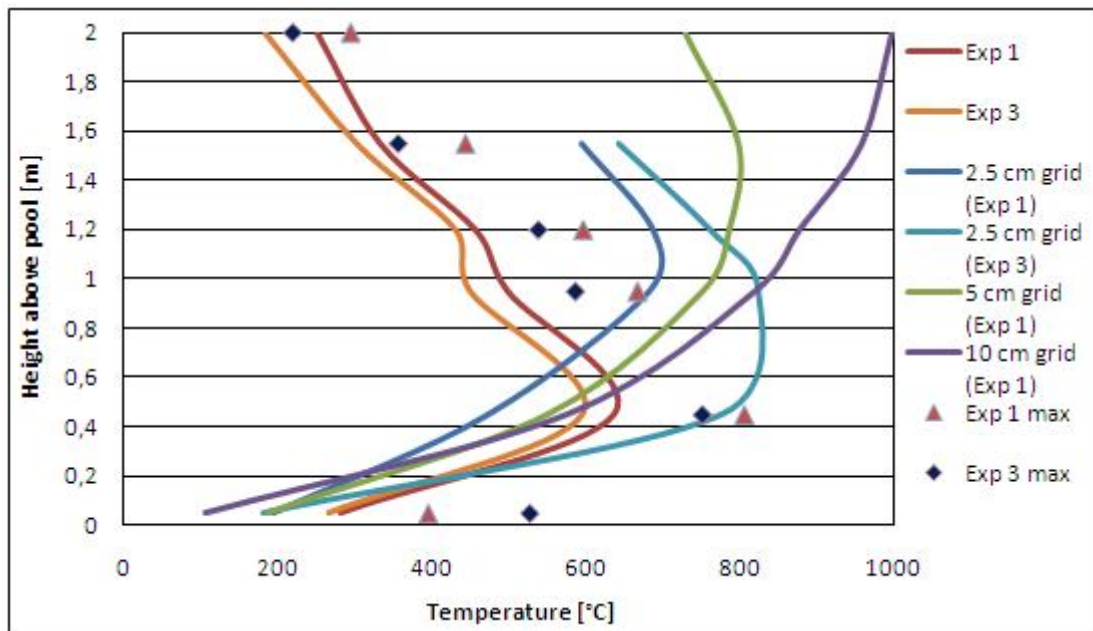

Figure 6-13 *Comparing average temperature measurements (100-250s) with and without pipe obstructions using the liquid fuel model*

In order to verify how changes in absorption coefficient and emissivity affect the HRR from the fire, several simulations using 10cm grid cells were performed. After testing a large number of combinations, also by varying the NU_FUEL, the conclusion is that by changing these variables there are minor changes in results from simulations performed, see Figure 6-14.
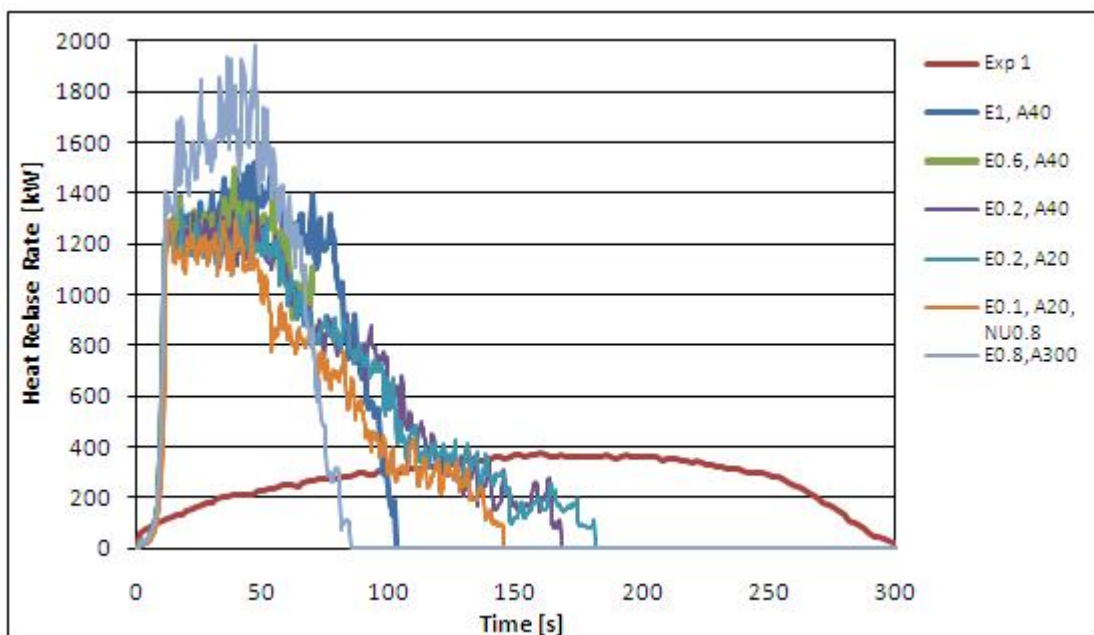
Figure 6-14 *HRR affected by using different Adsorption coefficient (A) and different Emissivity (E) in experiment 1*

_____

6.1.4   Results FLACS simulations

In FLACS simulations the jet nozzles representing the pool fire are tested as different leaks to determine which method predict results most equal to the experimental values. As described earlier, it is known that the 6-flux radiation model does not predict spatial distribution of radiation correctly, and a ray tracing radiation model is under development in FLACS. Only temperature measurements are therefore compared to experimental results for FLACS.
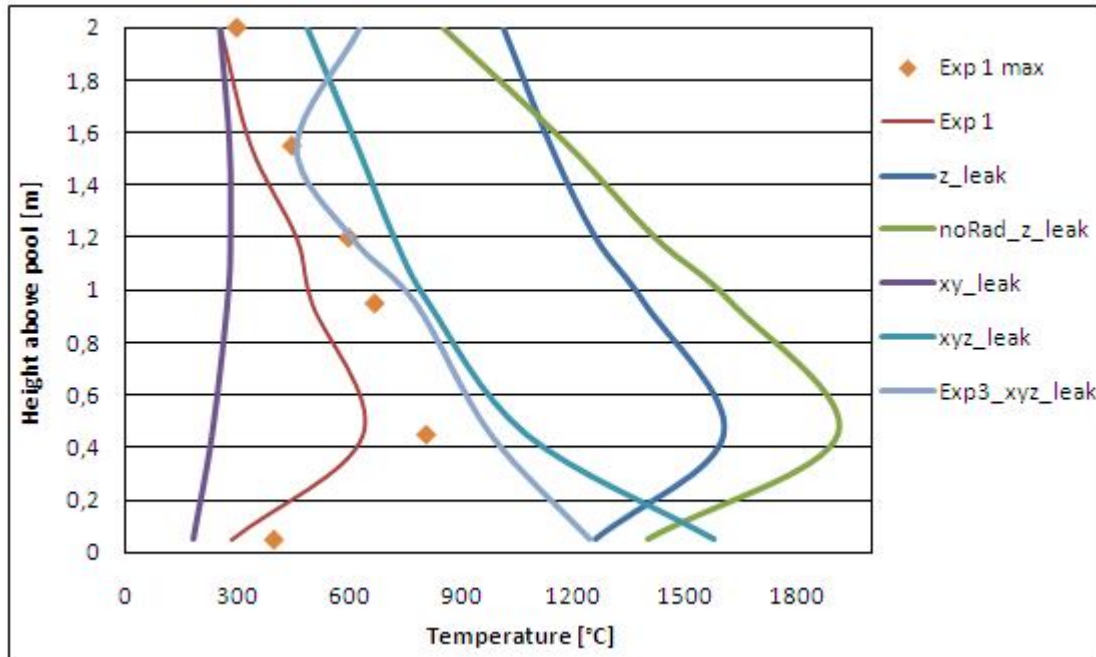

Figure 6-15 *Temperature measurements from experiment 1 and 3 compared with FLACS results using different leak directions, 6-flux radiation model and no radiation model*

From the temperature results in Figure 6-15 following is identified when specifying the pool fire with jet nozzles in FLACS:
- When vertical jet nozzles (z-direction) are used, the simulated flame temperatures are higher than the experimental values even though the leak velocity is low (0.96 mm/s). Deviation from the experimental values decreases with increased distance from the release. The deviation increases further, except for at the highest thermocouples, when no radiation model is used.
- Horizontal jet nozzles underestimate the flame temperature in the flame center. In this case the jet has zero velocity in z-direction and buoyancy is therefore the driven force. The main reason for these low temperature values are probably because the fire becomes too wide and too little fuel rises from the centre of the fire where the measuring points is located.
- Combination of horizontal and vertical jet nozzles resulted in over-predicted temperatures, mainly close to the leak. Temperatures at the second lowest thermocouple are not far away from the maximum experimental one. The leak velocity is here 0.029 mm/s.
- The pipe obstruction (experiment 3) reduced the average flame temperatures for all monitor points except the upper most.

_____

6.1.5   Discussion FDS and FLACS simulations

As expected it is not easy to compare flame properties from experiments with numerical simulations. In FDS simulations, results from radiative heat fluxes are quite good compared with experimental results when the fire is defined by Mass Loss Rate (MLR) or Heat Release Rate (HRR). By using MLR directly from the experiments and radiation fraction value around 0.30 (agreed well in experiments) the heat flux from FDS simulations are almost equal to the experimental values. Also by using combustion efficiency of 0.9 (recommended from experiments) and radiation fraction of 0.3 FDS heat flux results are close to experimental. By changing grid size, only small changes in heat fluxes are observed.

Flame temperatures are more sensitive to grid changes. Finer grid resolution probably predicts better flame temperatures. But it must be aware that monitor points in FDS also are sensitive to grid change since they measure temperature inside the whole grid cell where the monitor point is located. It has also been verified that simulations using the liquid fuel model, where FDS calculates the evaporation, is grid dependent which also is stated in the FDS User Guide. From the simulations performed in this thesis results close to the experimental values are only obtained by reducing the grid sufficiently. Little effect is observed when adsorption coefficient and emissivity of the liquid is changed.

When pipes are introduced above the fire some effect is observed in the FDS simulations. Flame width, HRR and radiation are slightly reduced but not as much as the reduction observed in the experiments.

In FLACS, the best way to simulate the pool fire from the experiments is by using a combination in vertical and horizontal jet nozzles. By testing different combination in horizontal leakages improved values could probably been obtained but this has not been further tested.

_____

6.2   Simulations of "The Murcia Atrium Test"

The Murcia Atrium Fire Tests have been carried out by Gutiérrez-Montes et al. (2009) in the atrium of the Centro of Technologico del Metal, in Murcia, Spain. The experimental facility consists of a prismatic structure of 19.5m x 19.5m x 17.5m and a pyramidal roof raised 2.5m in the centre, see Figure 6-16 below. In the experimental work two different heptane fire sizes, 0.92m and 1.17 circular pans with 0.25m depth, are tested, but only test 3 (from the experiments) with natural ventilation is simulated with the CFD models.
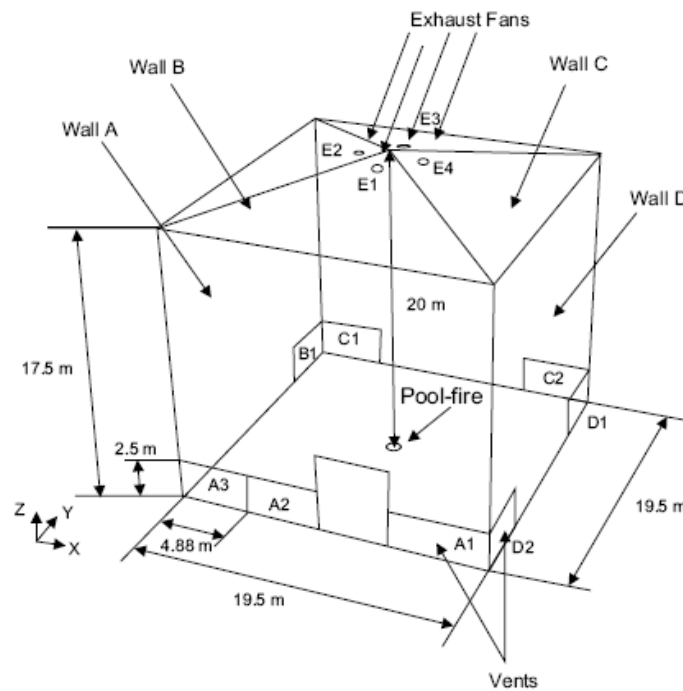
Figure 6-16 *Layout and main dimensions of the Murcia test facility from (Gutiérrez-Montes, Sanmiguel-Rojas et al., 2009)*

The mass loss rate was not measured by weight loss in the experiments (limitation of available balance). Average mass loss rate ($\dot{m}_{avg}$) of each test was measured as a total mass of fuel burnt divided by the burning time. The evaluation of the instantaneous mass loss rate was recovered from the measurements of mass loss in a smaller pool fire, 0,55m diameter. Then that evolution is normalized as:

$$S\dot{\omega}(t) = \frac{\dot{m(t)}}{(\dot{m}_{avg})}$$

(6-1)

The normalized evolution was then used to calculate the mass loss rate of each of the fire test and the heat release rate calculated using combustion efficiency (χ_{eff}) of 0.85 in the following equation:

$$\dot{Q}_c = \dot{m}_{avg} \cdot \chi_{eff} \cdot \Delta H_c$$

(6-2)

The HRR results from the experimental work using equation (6-1) and (6-2) is described in Figure 6-17 below. HRR value from the 2.34MW fire (test 3) is collected from the graph using the free software Plot Digitizer 2.4.0.
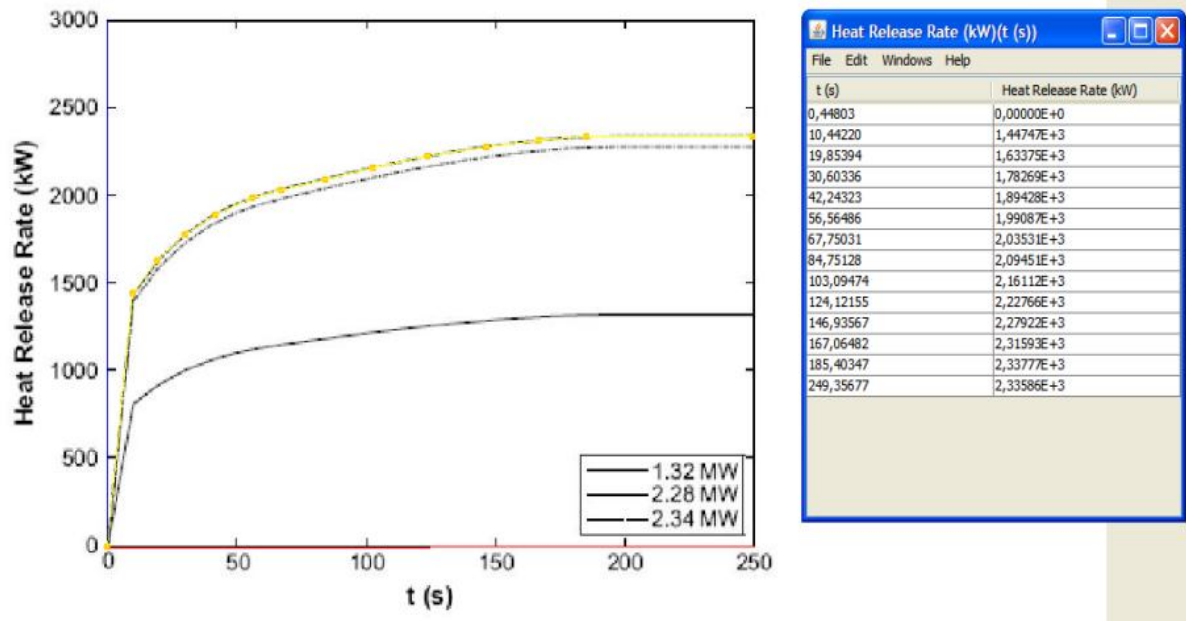
_____

Figure 6-17 *Heat Release Rate calculated based on equation (6-2) in left and values collected from the 2.34MW line using Plot Digitizer 2.4.0 in right.*

Following other inputs are stated from the fire tests:

Table 6-4 *Properties of walls and floor from (Gutiérrez-Montes, Sanmiguel-Rojas et al., 2009)*

Properties	Walls and roof	Floor
Thickness [mm]	6	Not defined. 200mm used.
Density [kg/ m³]	7800	1860
Thermal conductivity [W/mk]	45	0.72
Specific heat (Heat capacity) [J/kgK]	460	780
Emissivity [-]	0.3	-

Vents (at the bottom of the atrium):
  - Width 4.88m
  - Height 2.50m.

Exhaust Fans (at the roof):
  - Circular with 0.56m diameter and it is 1.75m from the centre of the fans to the centre on the atrium.

6.2.1   FDS input data

In addition to input given in Section 6.2 following inputs are specified in the FDS simulations:

Fuel evaporation model (the fire):
As recommended by Gutiérrez-Montes et al. (2009) a radiative fraction of 0.35 is used in these simulations. The fire is modelled as a square pool instead if circular, but in the same location and with the same area as in the experimental work. This gives the following values for the fire:

_____

- 1.17m diameter (test 3) gives area of: $A = \frac{\pi d^2}{4} = \frac{\pi \cdot (1.17m)^2}{4} = 1.075m^2$, and length of 1.0368m of each side.
- Fire growth is described as a fraction of the steady state heat release rate (2,34MW gives 2176.7MW/m^2 for 1.075m^2 area) from the experiment. As described in Section 6.3.1 the program "Plot Digitizer" is used to estimate these values.

Exhaust Fans (at the roof):
In the FDS simulations the fans are modelled as square holes instead if circular holes. They are modelled in the same location with the following size:

- 0.56m diameter gives area of: $A = \frac{\pi d^2}{4} = \frac{\pi \cdot (0,56m)^2}{4} = 0.2463m$, and length of 0.4963m for each side.

Mesh (grid cells):
Only uniform grid cells are used. Grid sizes of 52cm, 39cm and 26cm are tested out to verify the grid sensitivity of the simulations.

Measurements:
Only temperature, using "THERMOCOUPLES", is measured in the simulations. More information about this measurement method is given in Section 3.3.1.

6.2.2   FLACS input data

The FLACS input file is mainly created by Olav Roald Hansen working at Gexcon AS, but some modification is performed. In addition to input given in Section 6.2 following are specified in the FLACS simulations:

Fuel evaporation model (the fire):
Evaporation of liquid fuel leak is modelled by 12 jet nozzles where each nozzle has an area of 0.02m^2 to fit into a defined grid cell in the fire. Each nozzle releases heptane in all horizontal directions (-x, x, -y, y) which means that there is 48 leaks. This gives following flow rate from each leak:

$$\dot{m} = \frac{\dot{q}}{\Delta H_c} = \frac{2340 \frac{kJ}{s}}{44,6 \frac{kJ}{g}} = 52,466 \frac{g}{s} = \frac{0,05246 \frac{kg}{s}}{48 \text{ nozzles}} = 0,0011 \frac{kg}{s} \text{ pr nozzle.}$$

Mesh (grid cells):
The grid around the fire is uniform in x-and y direction with 21.4 cm size. Outside the fire the grid cells are stretched towards the boundaries.

Measurements:
Temperature is defined as monitor points.

_____

6.2.3   Results FDS and FLACS simulations

In the simulations performed most of the measuring points from the experimental work are included, but only temperature measurements in different heights above the pool fire centre are presented in the results below.

In the FDS simulations different grid sizes are simulated in order to consider grid dependency. Simulations performed by Gutiérrez-Montes et al. (2009) concluded that using 150 grid cells in each direction provided good accuracy. In the present work, simulations are only performed with quite coarse grid cells where the smallest cells are 0.26 m (80 cells in each direction). In the FLACS simulations the grid dependency is not verified. Smallest grid cells are localized around the fire (0.21m in x and y direction) and cells are stretched further away from the fire source. Total amount of grid cells in FLACS and FDS simulations using the finest grid are:

FDS: 0.26m uniform grid cell size (512000 cells)
FLACS: 236600 grid cells

In Figure 6-18 to Figure 6-21 temperature measurements from the experiments is compared with FDS simulations and FLACs simulations. After performing FDS simulations with different grid sizes the conclusion is that there is not a large temperature difference amongst these simulations. In the figures below FDS simulations are presented only with 0.26m grid size except from Figure 6-21 where 0.39m grid size gave results closer to experimental results. The reason for this is probably due to the location of the grid cells. With 0.39m grid cells the monitor point is located at a height between 19.5m and 19.89m, while with 0.26m grid cells the monitor point is located at a height between 19.5 and 19.26m. This means that for 0.26m cells the temperature is measured in a lower height giving a lower temperature. From the results it is also clear that something went wrong with the FLACS simulation just before 600 seconds. Even so, the FLACS simulations are quite close to the FDS and experimental results except from the measuring point closes to the fire (Figure 6-18).
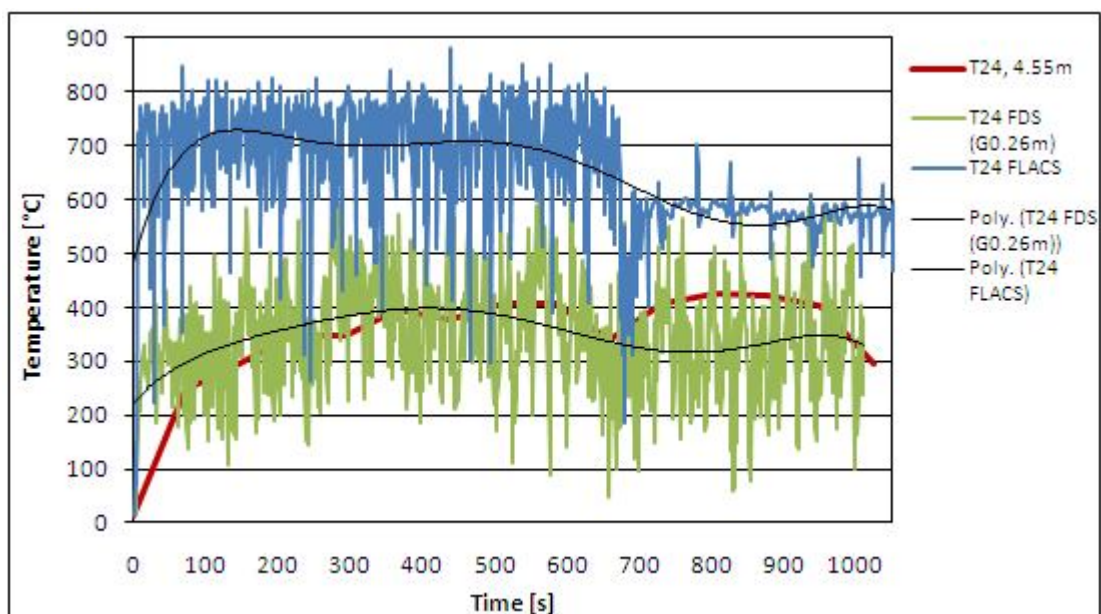

Figure 6-18 *Temperature measurement 4.55m above pool centre compared with FLACS and FDS simulations*
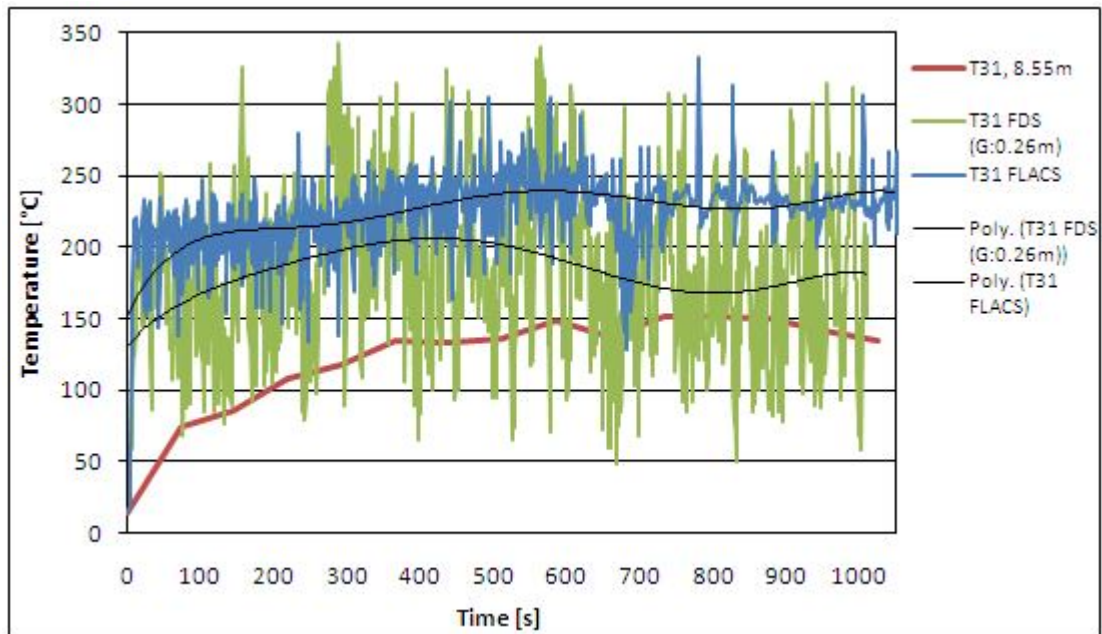
_____

Figure 6-19 *Temperature measurement 8.55m above pool centre compared with FLACS and FDS simulations*

From the figures above and below it is clear that the estimated temperature from the simulations is closer to the experimental temperature measurements far away from the fire source. An exception from this is the FDS results in Figure 6-18 where these are quite close to the experimental results.
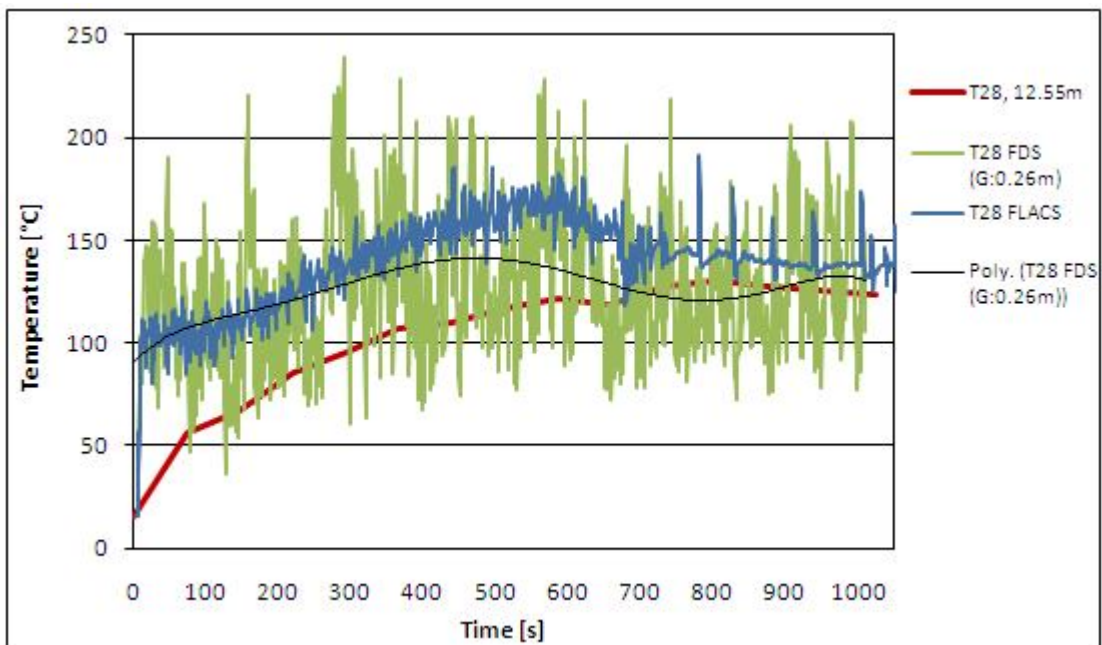

Figure 6-20 *Temperature measurement in 12.55m above pool centre compared with FLACS and FDS simulations*

_____
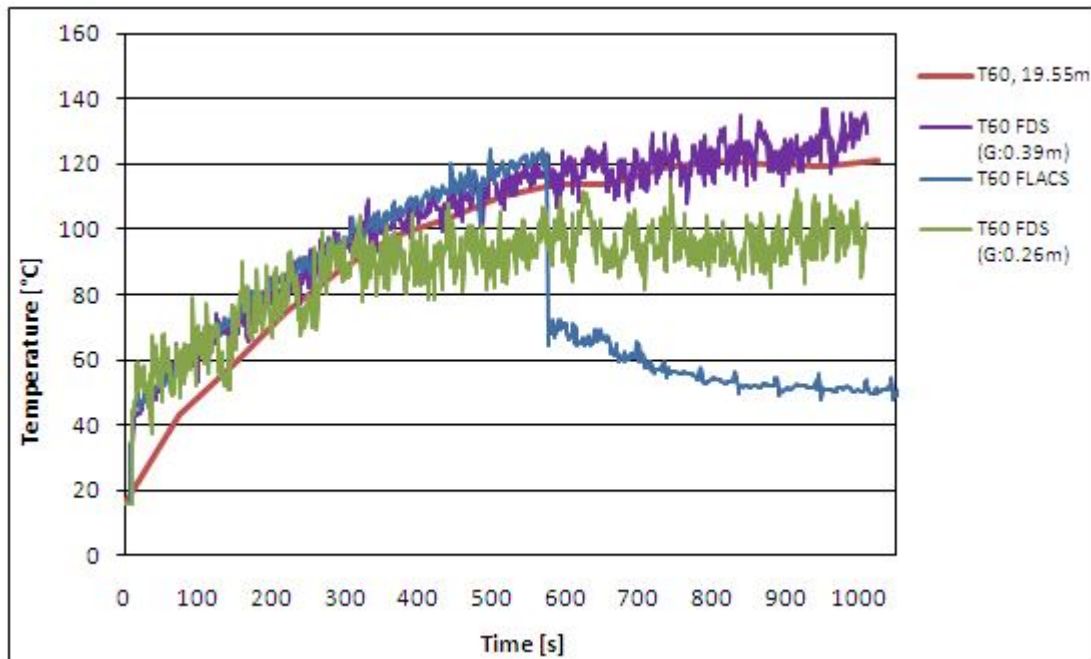
Figure 6-21 *Temperature measurement in roof (19.55m) compared with FLACS and FDS simulations*

6.2.5   Discussion FDS and FLACS simulations

Considering that the grid was quite coarse in both FLACS and FDS simulations the results from the simulations are not very far from the experimental values. Refining the grid cells, especially around the fire, would probably lead to better results but also extend the simulation time. Not surprisingly, the deviation from experimental results is largest close to the fire source, and temperatures close to the roof are almost identical with the experiments.

_____

6.3   Simulations of "Flow induced by a Fire in a Compartment"

Steckler et al. (1982) performed a total of 55 full-scale steady-state experiments in order to study the flow induced by a simulated pool fire in a compartment. Only fire test 160 and 710 described in (Steckler, Quintiere et al., 1982) are simulated in this thesis. The test facility consists of a room with geometry 2.8m x 2.8m x 2.08m with adjustable door opening possibilities. In the chosen fire test the door was fully open with 1.83m height and 0.74m width. The compartment lightweight walls and ceiling were covered with ceramic fibre insulation board, this to establish near-steady conditions within 30 minutes. The layout of the room is illustrated in Figure 6-22.
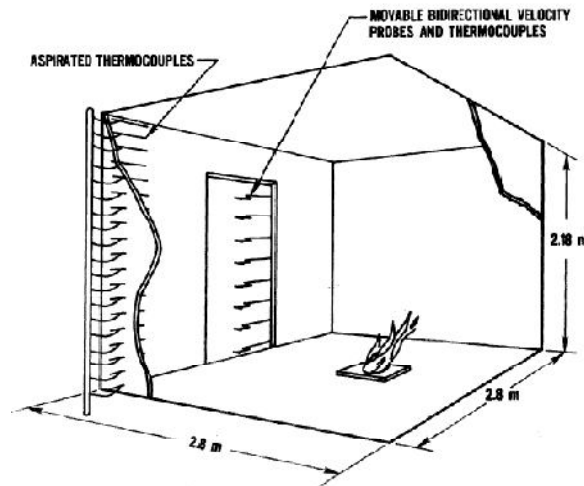
Figure 6-22 *Experimental arrangement from (Steckler, Quintiere et al., 1982).*

Temperature and velocity was measured in the door opening using aspirated thermocouples and velocity bi-directional probes. Temperature was also measured in the "point" corner of the room at a distance of 0.305 from right-and left wall.

A circular methane gas burner with effect of 62.9 kW was used in the experiments. In the simulated fire tests the burner was located in the middle of the room (location A). The only difference between the two simulated experiments is the location of the burner. Where the burner is near flush in one of the experiment and raised in the other, see Figure 6-23.
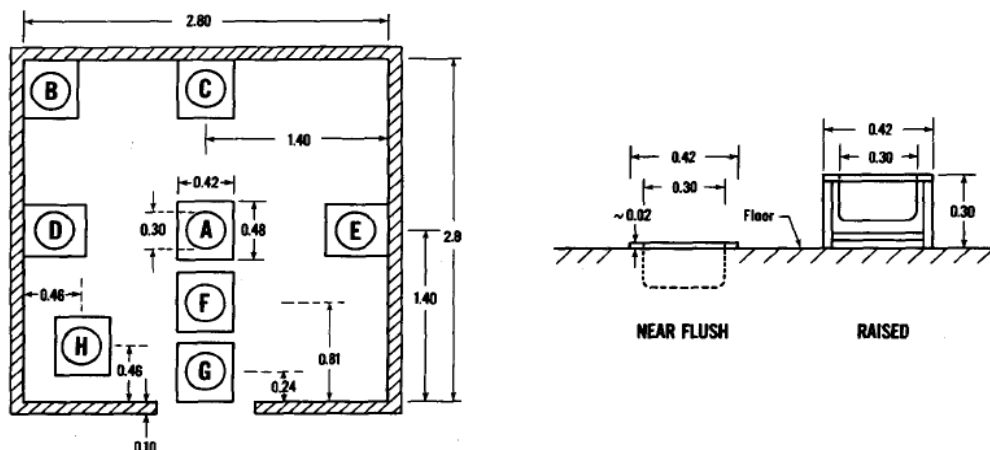

Figure 6-23 *Gas burner location with dimensions in (m) from (Steckler, Quintiere et al., 1982).*

_____

Properties of ceramic fibre insulation board (FIB) and the Lightweight concrete walls (LWC) are not stated in the experimental data. Values in Table 6-5 is used in the experiments.

Table 6-5 *Properties of ceramic fibre insulation board (FIB) and the Lightweight concrete walls (LWC) from Table 2.1 in (Drysdale, 1999)*

Properties	FIB	LWC
Thickness [mm]	12.7(Kwon, Dembsey et al., 2007)	100
Density [kg/ m^3]	229	500
Thermal conductivity [W/mk]	0.041	0.15
Specific heat (Heat capacity) [J/kgK]	2090	1000
Emissivity [-] (Infrared-Services)	0.85	0.92

6.3.1   FDS input data

In addition to input given in Section 6.3 following are specified in the FDS simulations:

Fuel evaporation model (the fire):
The fire is modelled as a square pool instead if circular, but in the same location and with the same area

- 0.3 m diameter gives area of: $A = \frac{\pi d^2}{4} = \frac{\pi \cdot (0.3m)^2}{4} = 0.0707 m^2$, and length of 0.266m for each side.

- Steady state fire with following fire effect per square metre : $\frac{62.9kW}{0.0707m^2} = 889.7 \frac{kW}{m^2}$

Mesh (grid cells):
Only uniform grid cells are used. Grid sizes of 20cm, 10cm and 5 cm are tested out to verify the grid sensitivity of the simulations.

Measurements:
Both temperature, using "THERMOCOUPLES", and velocity, using "VELOCITY" is measured in the simulations. More information about these measuring methods is given in Section 3.3.1.

6.3.2   FLACS input data

The FLACS simulations are performed in corporation with Deiveegan Muthusamy who's work with fire development of FLACS at Gexcon AS. In addition to input given in Section 6.3 following is specified in the FLACS simulations:

Fuel evaporation model (the fire):
Evaporation of liquid fuel leak is modelled by 4 jet nozzles where each nozzle has area of 0.0176715m^2 to fit into a defined grid cell for the fire. Each nozzle releases 1/4 of the total mass flow rate given as:

$$\dot{m} = \frac{\dot{q}}{\Delta H_c} = \frac{62.9 \frac{kJ}{s}}{50,0 \frac{kJ}{g}} = 1.258 \frac{g}{s} = \frac{0,001258 \frac{kg}{s}}{4 \text{ nozzles}} = 0,00003145 \frac{kg}{s} \text{ pr nozzle.}$$

Mesh (grid cells):
The grid around the fire is uniform in x and y direction with 15.6cm size. Outside the fire the grid cells are stretched towards the boundaries.

Measurements:
Temperature and velocity is defined as monitor points.

6.3.3   Results FDS and FLACS simulations

Results from simulations with FLACS and FDS are presented below. In the FDS simulations different grid cells are tested to verify grid dependency. This has not been performed in the FLACs simulations where good results are obtained for the tested mesh. From the FDS simulations with different grid cell sizes the best results are obtained with 5cm grid cells, which is the smallest grid simulated.

Door centre temperatures measured with FDS and FLACS (Figure 6-24 and Figure 6-25) agree quite well with experimental measurements. As the figures shows the upper layer temperature values measured with FDS deviate some from the experimental one, while FLACS results match the experimental values for the whole doorway temperature profile. According Section 14.2.1 (Kevin McGrattan, 2010) in the FDS User Guide the temperature values are calculated in the grid cell where the thermocouple is located and not specific for the thermocouple location. This could affect the temperature results. Smaller grid cells would probably improve the FDS simulations but the simulation time using 5cm grid is already time demanding. Amount of grid cells used in FLACS and FDS are:

FLACS: Burner location A (31920 grid cells) and location AR (20520 grid cells).
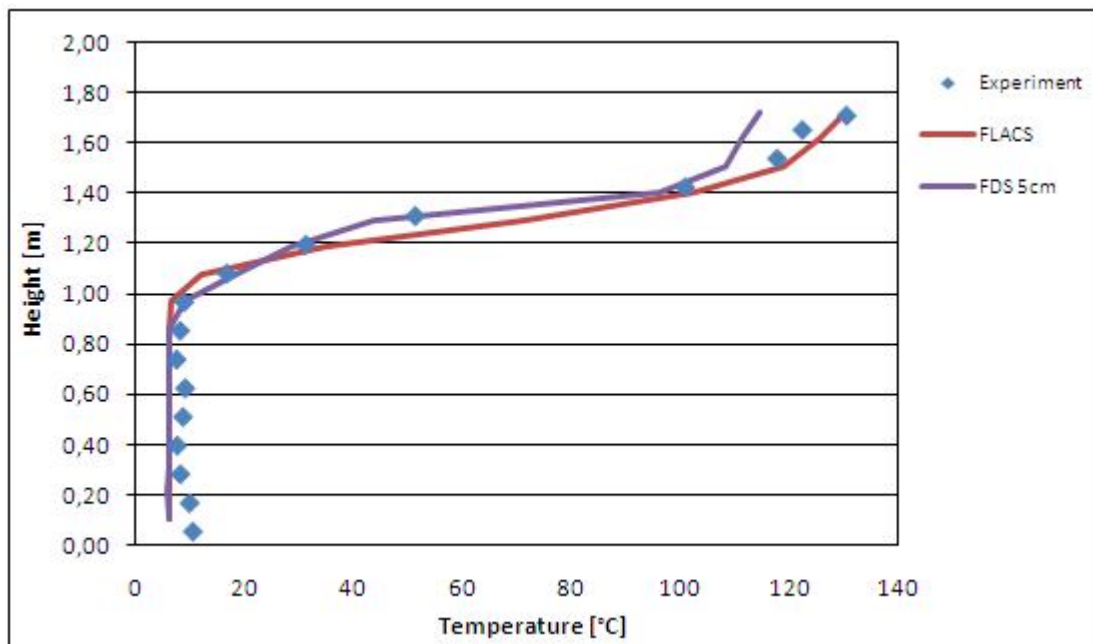*FDS:* Burner location A and AR 5cm grid (768000 grid cells) and 10cm grid (96000 grid cells).

Figure 6-24 *Comparing measured temperature values (door centre) with FDS and FLACS simulations, raised burner (AR)*
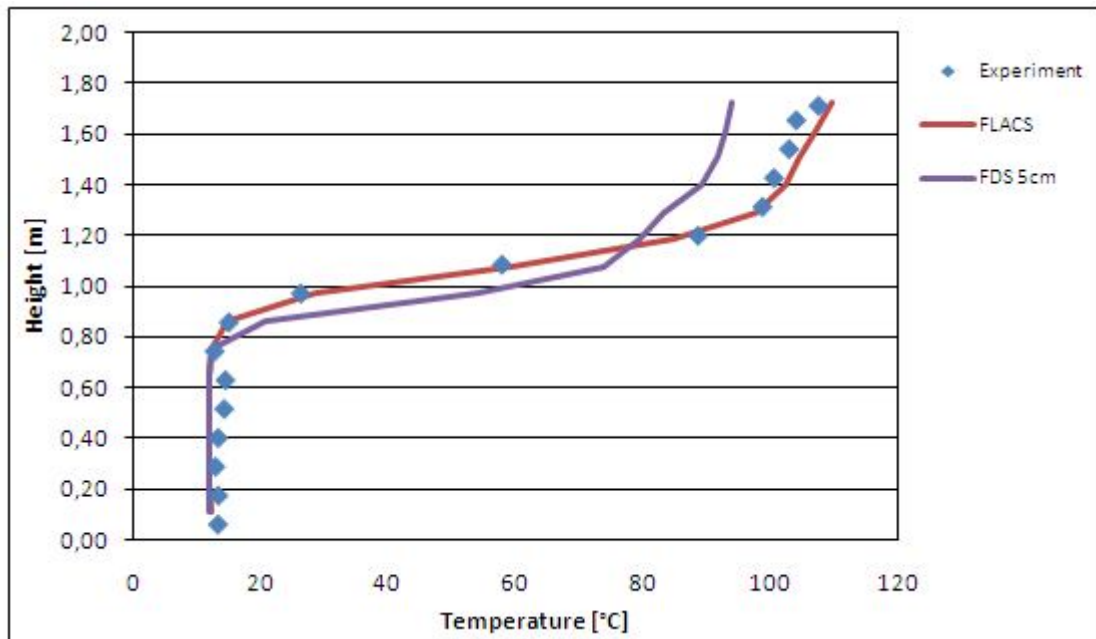
Figure 6-25 *Comparing measured temperature values (door centre) with FDS and FLACS simulations, flush burner (A)*

From room corner temperature measurements deviation in the highest thermocouples is still observed for the FDS simulations. FLACS predicts quite good results for these measurements see Figure 6-26 and Figure 6-27. The figures also shows that FDS predicts the lowest temperatures quite good while FLACS have little temperature rise until about 70-80 centimetre height (smoke layer). The temperature rise in this height probably comes from radiation from the hot smoke layer and from the fire, which the 6-flux radiation model in FLACS does not predict well.
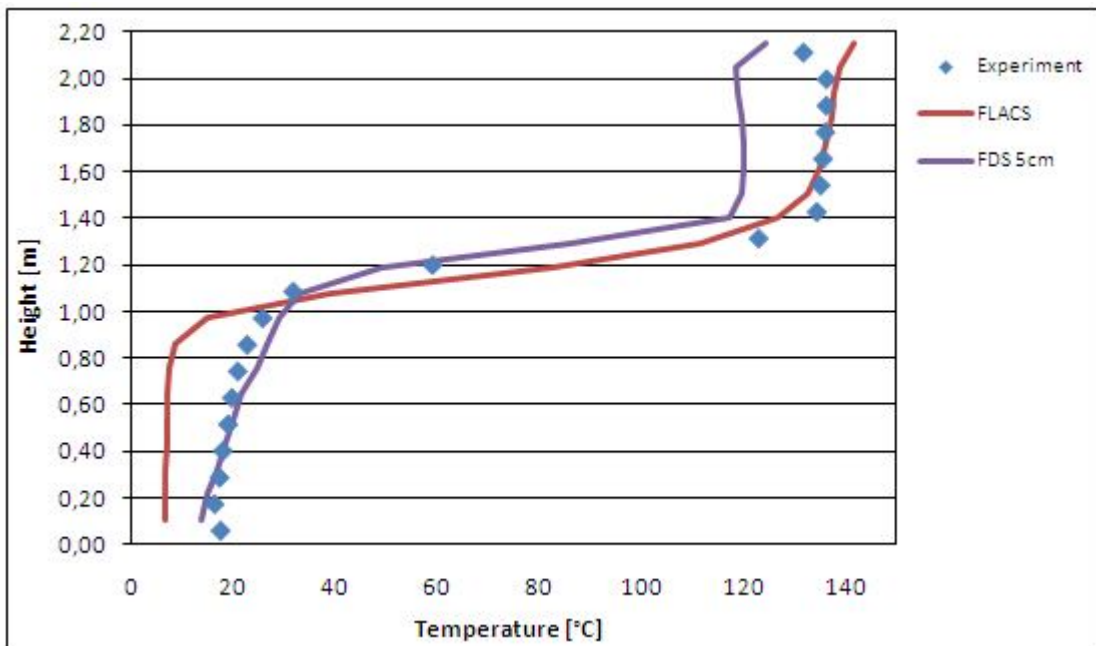

Figure 6-26 *Comparing measured temperature values (room corner) with FDS and FLACS simulations, raised burner (AR)*
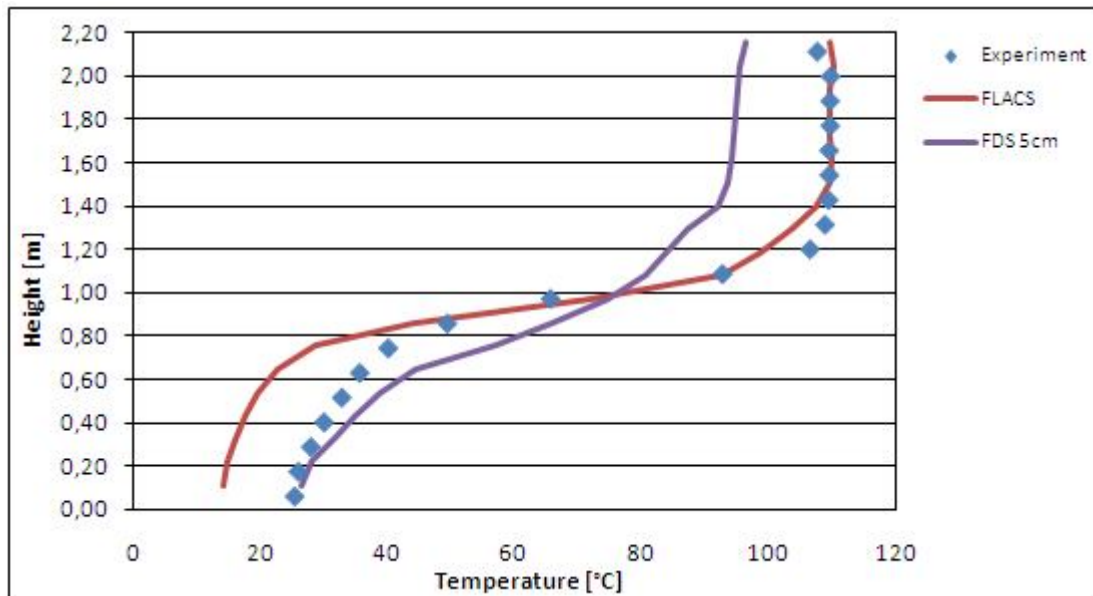
72

_____

Figure 6-27 *Comparing measured temperature values (room corner) with FDS and FLACS simulations, flush burner (A)*

When it comes to velocity measurements in the door opening both FLACS and FDS gave quite good results for all measuring points except the uppermost one, see Figure 6-28 and Figure 6-29. At this point none of the simulations programs predicted the high velocity measured in the experiment. One of the reasons for this could be the location of the measuring point. In the experimental data the location between the measuring points is 0.114m and the highest thermocouple is located 0.057m from the door top. In the simulations with FLACS a start height of 0.1077m was chosen and the same locations were used in FDS simulations. Because of this, the highest thermocouple is located at 1.7232 m instead of 1.767m. For FDS simulations using 5cm grid this means that the velocity is calculated in grid cell 1.7m to 1.75m instead of grid cell 1.75 to 1.8m which could describe some of the deviation.
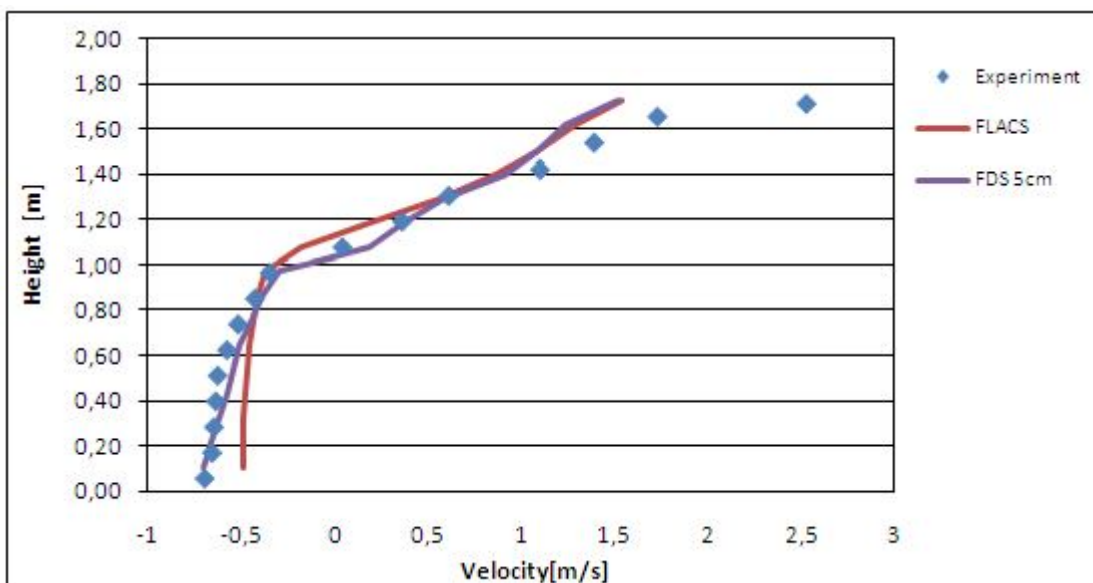

Figure 6-28 *Comparing measured velocity values (door centre) with FDS and FLACS simulations, raised burner (AR)*
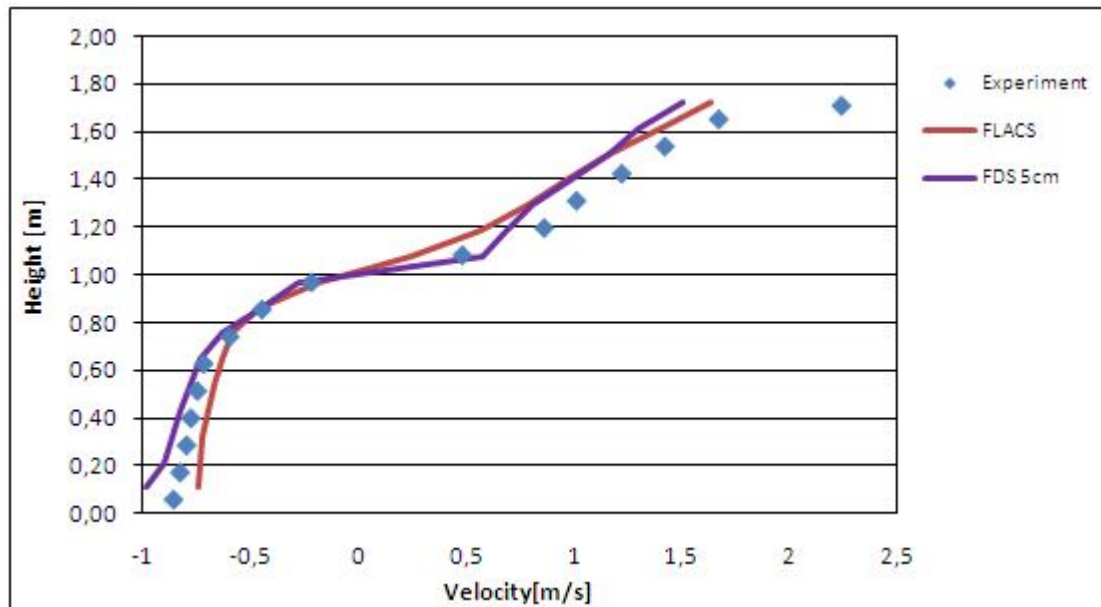
_____

Figure 6-29 *Comparing measured velocity values (door centre) with FDS and FLACS simulations, flush burner (A)*

6.3.4   Discussion FDS and FLACS simulations

In these experiments temperature profile and velocity profile of hot smoke gases leaving a room and cold air entering the room is examined. Both FLACS and FDS predict quite good results in these simulations. While FLACS seems to predict the temperatures in the hot smoke layer better than FDS, the temperatures at low location inside the room is closer the experimental. Since FLACS simulation is only performed with one grid size it cannot be concluded that this is the case in most simulations. The low measuring points are located below the smoke layer where the temperature rise is mainly due to radiation. Since FLACS simulations are performed using the old 6-flux radiation model this could be one of the explanations to the temperature deviation. Regarding velocity measurements both simulations programs gave good results except for the velocity in the highest point in the door opening. The main reason for this deviation could be the location of the measuring point in the simulations where especially the top measuring points are located to low in the simulations. And as shown in the simulation plot from FDS below (Figure 6-30), minor movement in vertical or horizontal direction in this area leads to drastic changes in velocity.

If considering amount of grid cells used, FLACS obtained quite good results with relative few grid cells compared with FDS. The smallest grid cells in the FLACS simulation was 15.6cm around the fire. FDS simulations with 16cm grid cells were tested, but because of the measuring method FDS use this resulted in equal values for measuring point located within one grid cell. Anyway, there is no direct context between amount of grid cells and simulation time when comparing FLACS and FDS.
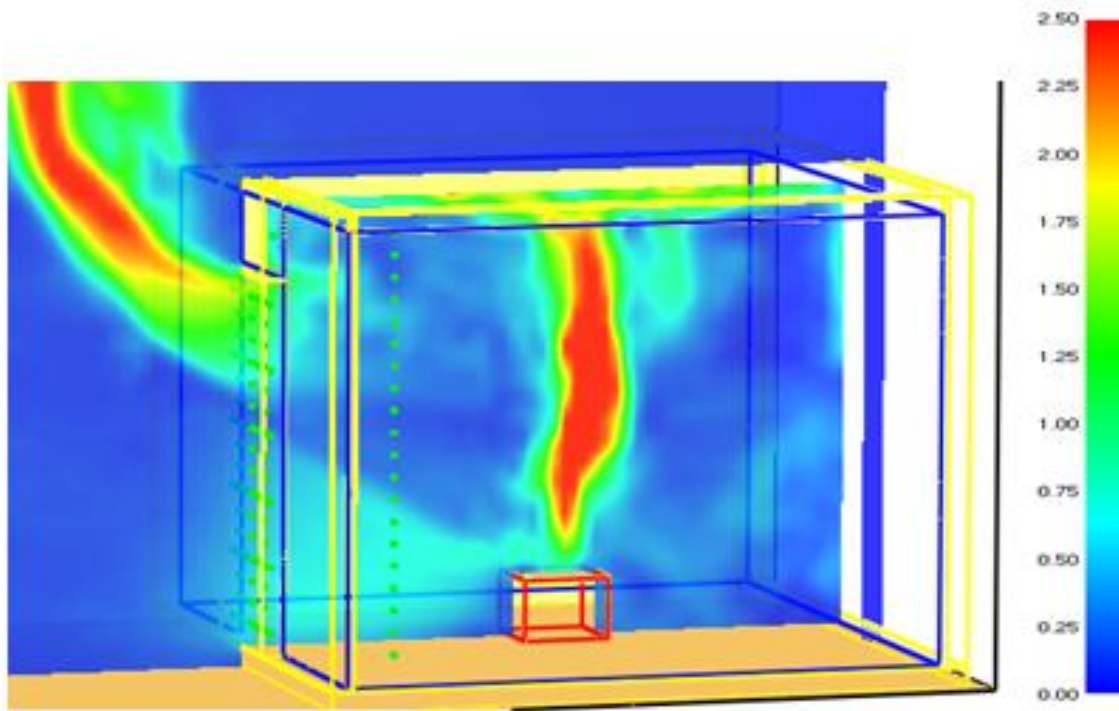
Figure 6-30 *Simulation plot from FDS simulation 5cm grid cells, fire location AR*

_____

7   Conclusion

Pool fires are studied through experimental work and CFD simulation using FLACS and FDS. The major findings from this work are listed below.

Experiments showed that:
- Pipe obstructions close to the pool fire has a decreasing effect on the fire growth when the fire is not influenced by cross-wind. Obstructions resulted in reduced heat release rate from the fire, reduced radiation to the surroundings and as a naturally consequence of this, increased burning time.
- Maximum temperature measured in the flame center was in the region 700-800°C. A combustion efficiency of 0.90 and radiation fraction around 0.30 is found reasonable for the heptane indoor experiments without pipe obstruction.

CFD simulations using FDS showed that:
- Temperature and velocity in a fire plume (hot smoke) is predicted quite well. In cases with temperature change in small areas (near roof) the size of the grid is of high importance due to the temperature is measured for the entire grid cell where the measuring point is located. This applies also to temperatures in flames.
- Heat flux values are close to experimental measurements when the fire is defined by Mass Loss Rate (MLR) or Heat Release Rate (HRR). When using measured MLR, a radiation fraction around 0.30 instead of default value of 0.35 gave heat flux values closer to experimental results. FDS simulations using combustion efficiency (χ) of 0.90 when defining the HRR, resulted in heat flux values close to experimental.
- The liquid fuel model, where evaporation rate is calculated by FDS, is quite grid dependent as stated in the FDS User Guide. From simulations of experiments performed in the present work, small grid cells are required to get results even close to experimental one.
- The pipe obstruction effects from the experimental work are less explicit in the simulations. Some reduction in HRR and heat flux is observed, but the main finding is the narrow flame shape equal to the one from the experiments.
- Studying flame properties requires small grid cells. The domain of interest is only divided into one mesh (grid cell area) in the present work. Using multiple meshes (more than one grid area) with decreased grid cells around the fire would probably improve the results.

CFD simulations using FLACS showed that:
- When running FLACS-Fire with the 6-flux radiation model, temperature and velocity in a fire plume (hot smoke) is predicted quite well. Below smoke layer, and around the fire, temperature deviates more from experimental values. This is probably due to limitations in the radiation model. A ray tracing model, which soon will be in place, will probably perform better.
- In cases where the fire itself is not of interest (fire plume) the fire can be modelled as vertical jet nozzles. When using vertical jet nozzles temperatures in the fire are quite high even if the leak velocity is low. Simulating the fire with horizontal jet nozzles or a combination of horizontal and vertical jet nozzles resulted in flame temperatures closer to experimental results in the present work.

78

_____

8   Recommendations for further work

The R&D work with FLACS-Fire is an ongoing process where the fire model continuously improves. One major change is the new radiation model, which soon is ready for use. It was desirable to test out this model in the present work, but the model was not ready for these kinds of simulations yet. In order to validate this model against pool fires, it is recommended to run the simulations performed in this thesis, as well as experiments listed in Chapter 4. Since the present simulations contain smaller pool fires and mainly indoor experiments, it should be focused more on bigger pool fire experiments with good radiative heat flux measurements.

In indoor pool fires, toxic gases as carbon monoxide may cause critical situations and death. The amount of these gases in the combustion products are measured in the experiments performed in the present work, but no comparison against the fire models is performed. This could be of interest in further research.

Further work with modelling of heat feedback on liquid pools located below flames is also recommended. This will give a more realistic pool fire scenario than using "jet" nozzles. This is especially important in situations where radiation from a surrounding smoke layer or surrounding equipment have an influence on the fuel evaporation rate from the pool.

9   References

(2011). "The Engineering Toolbox ". from http://www.engineeringtoolbox.com/.

(FDS official website). from http://fire.nist.gov/fds/documentation.html.

0803, U. M. S. m. v. (2008). Hukseflux Thermal Sensors SBG01 manual version 0803.

Ansys "Ansys home page (Fire & Smoke Propagation)."

Björklund, A. L. a. A. (2008). Smoke Spread and Gas Temperatures during
Fires in Retail Premises - Experiments and
CFD Simulations. Fire Technology
SP report 2008:55. S. T. R. I. o. Sweden. Sweden**:** 178.

Casal, E. P. a. J. (2008). Evaluation of the effects and consequences of major accidents in industrial plants. Amsterdam ; Boston, Elsevier.

Chatris, J. M., J. Quintela, J. Folch, E. Planas, J. Arnaldos and J. Casal (2001). "Experimental study of burning rate in hydrocarbon pool fires." Combustion and Flame **126**(1-2): 1373-1383.

Computit.   "Computit   home   page   (product   &   services)."   from http://www.computit.no/en/Product_+_services/KFX/Application_areas/.

D.A. Crowl and J.F. Louvar (1990). "Chemical Process Safety. Fundamentals with Applications." Englewood Cliffs: Prentice Hall.

Drysdale, D. (1999). An introduction to fire dynamics. Chichester ; New York, Wiley.

FARLEX "The free dictionary (http://www.thefreedictionary.com/fire)."

Gexcon-Software (2007). FLACS Manual v.0.0 Test release (FLACS fire).

Gutiérrez-Montes, C., E. Sanmiguel-Rojas, A. Viedma and G. Rein (2009). "Experimental data and numerical modelling of 1.3 and 2.3 MW fires in a 20 m cubic atrium." Building and Environment **44**(9): 1827-1839.

Hagen, B. C. (2004). "Grunnleggende brannteknikk."

Hamins, A., M. Klassen, J. Gore and T. Kashiwagi (1991). "Estimate of flame radiance via a single location measurement in liquid pool fires." Combustion and Flame **86**(3): 223-228.

Hasib, R., R. Kumar, Shashi and S. Kumar (2007). "Simulation of an experimental compartment fire by CFD." Building and Environment **42**(9): 3149-3160.

Hostikka,   S.   (2007).   "Mark   Mail   answer."   from http://markmail.org/message/26zskd6ayfvuguxf).

HSE-gov-UK (2011). "Internet page: http://www.hse.gov.uk/offshore/strategy/jet.htm."

_____

Infrared-Services. "Infrared Services' WebSite." from http://www.infrared-thermography.com/material-1.htm).

Javier O.Trevino, A. F. G., MarcL. Jansens "SIMPLIFIED CALIBRATION PROCEDURE FOR LARGE SCALE OXYGEN CONSUMTION CALORIMETER."

Jesper Axelsson, P. A., Anders Lönnermark, Patrick Van Hees, Ingrid Wetterlund (2001). Uncertainties in measuring heat and smoke release rates in the Room/Corner Test and the SBI. Borås, SP Swedish National Testing and Research Institute**:** 47.

Jill M. Suo-Anttila, L. A. G. (July 2001). "Thermal Measurements from a Series of Tests with a Large Cylindrical Calorimeter on the Leeward Edge of a JP-8 Pool Fire in Cross-Flow." SANDIA REPORT: 184.

Kevin McGrattan, R. M., Simo Hostikka, Jason Floyd (2010). FDS user guide (NIST publication).

Koseki, H. and G. W. Mulholland (1991). "The effect of diameter on the burning of crude oil pool fires." Fire Technology **27**(1): 54-65.

Kwon, J.-W., N. Dembsey and C. Lautenberger (2007). "Evaluation of FDS V.4: Upward Flame Spread." Fire Technology **43**(4): 255-284.

Lokna, J. I. (2008). Evaluation of pool fire modelling in FLACS. Bergen, [J.I. Lokna]**:** IX, 62 s.

McCaffrey, B. J. and M. Harkleroad (1989). "Combustion efficiency, radiation, co and soot yield from a variety of gaseous, liquid, and solid fueled buoyant diffusion flames." Symposium (International) on Combustion **22**(1): 1251-1261.

Miles Greiner, A. S.-A. (August 2004). "Validation of the Isis-3D Computer Code for Simulating Large Pool Fires under a Variety of Wind Conditions." Journal of pressure vessel technology **126**: 9.

Muñoz, M., J. Arnaldos, J. Casal and E. Planas (2004). "Analysis of the geometric and radiative characteristics of hydrocarbon pool fires." Combustion and Flame **139**(3): 263-277.

Muñoz, M., E. Planas, F. Ferrero and J. Casal (2007). "Predicting the emissive power of hydrocarbon pool fires." Journal of Hazardous Materials **144**(3): 725-729.

Muthusamy, D. (2011). "Implementation of Radiative Transfer Calculations in the FLACS."

Muthuswamy, D., O. R. Hansen, P. Middha and M. R. a. D. Willoughby (2011). "Modelling of Hydrogen Jet Fires using CFD." (Gexcon AS, Bergen).

Naeem Iqbal, M. H. S. (2004). Fire Dynamics Tools (FDTs):Quantitative Fire Hazard, Analysis Methods for the,U.S. Nuclear Regulatory Commission, Fire Protection Inspection

Program. Washington, DC 20555-0001, U.S. Nuclear Regulatory Commission, Office of Nuclear Reactor Regulation**:** Chapter 3.

NFPA (2002). SFPE handbook of fire protection engineering. Quincy, Mass.
Bethesda, Md., National Fire Protection Association ;
Society of Fire Protection Engineers.

Nilsen, C. (2010). "Jet diffusion flames in FLACS Fire."

Norsok(S-001) (2008). "Norsok S-001 "Technical Safety"."

Norway, P. S. A. (2010). from http://www.ptil.no/innretningsforskriften/category380.html.

Planas-Cuchi, E. and J. Casal (1998). "Flame temperature distribution in a pool-fire." Journal of Hazardous Materials **62**(3): 231-241.

Planas-Cuchi, E., J. Casal, A. Lancia and L. Bordignon (1996). "Protection of equipment engulfed in a pool fire." Journal of Loss Prevention in the Process Industries **9**(3): 231-240.

Scandpower, D. (2001). HUMAN RESISTANCE AGAINST THERMAL EFFECTS, EXPLOSION EFFECTS, TOXIC EFFECTS AND OBSCURATION OF VISION.

Simo Hostikka, M. K. J. V. (2001). "Experimental Study of the Localized Room Fires, NFSC2 Test Series." VTT Research Notes 2104.

Steckler, K. D., J. G. Quintiere and W. J. Rinkinen (1982). Flow induced by fire in a compartment**:** 106.

Tewarson, A. (2004). "Combustion efficiency and its radiative component." Fire Safety Journal **39**(2): 131-141.

Van Maele, K. and B. Merci (2006). "Application of two buoyancy-modified k-[epsilon] turbulence models to different types of buoyant plumes." Fire Safety Journal **41**(2): 122-138.

Wakatsuki, K., G. S. Jackson, J. Kim, A. Hamins, M. R. Nyden and S. P. Fuss (2008). "'Determination of Planck Mean Absorption Coefficients for Hydrocarbon Fuels'." Combustion Science and Technology **180**(4): 616 — 630.

Warnatz, J., U. Maas and R. W. Dibble (2006). Combustion : physical and chemical fundamentals, modeling and simulation, experiments, pollutant formation. Berlin ; New York, Springer.

Weckman, E. J. and A. B. Strong (1996). "Experimental investigation of the turbulence structure of medium-scale methanol pool fires." Combustion and Flame **105**(3): 245-266.

Wen, J. X., K. Kang, T. Donchev and J. M. Karwatzki (2007). "Validation of FDS for the prediction of medium-scale pool fires." Fire Safety Journal **42**(2): 127-138.

9   References

_____

Appendix A – Experimental apparatuses/Certificates

Equipment	Type	Section
Heat flux sensor	SBG01 - Water Cooled Heat Flux Sensor According to Schmidt-Boelter	A.1
Thermo camera	Fluke Ti20 Thermal Imager	A.2
Weight	VEGA (weight indicator, VDI 137)	A.3
Velocity	VelociCalc Plus Meter (Model: 8386-M-S)	A.4
High speed camera	Casio Exilim EX-F1	A.5
Cone calorimeter equipment	According to "ISO 9705 Room-Corner test"	A.6

A. 1 Heat flux sensor

Figure A-1 *SBG01 -10 Heat Flux Sensor with certificate of calibration*

A. 2 Fluke Ti20 Thermal Imager

Figure A-2 *Fluke Ti20 Thermal Imager with thermal specifications*

A

_____

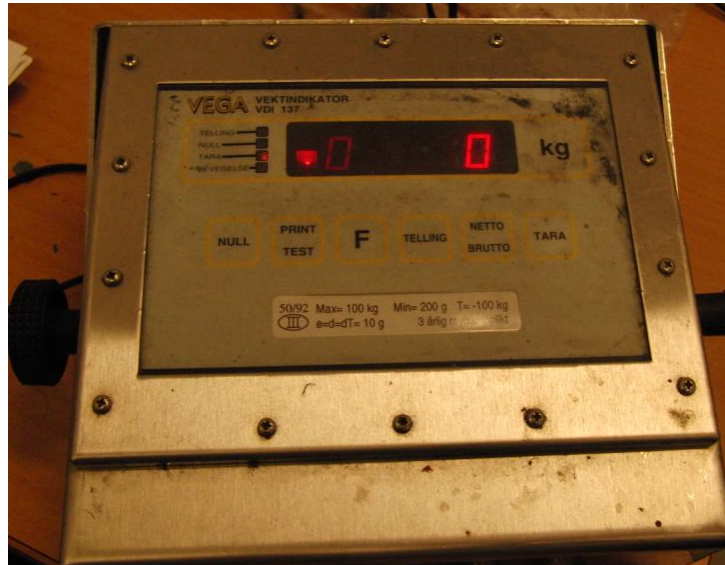**A. 3 VEGA (weight indicator, VDI 137)**

Figure A-3 *VEGA (weight indicator, VDI 137)*

A. 4 VelociCalc Plus Meter (Model: 8386-M-S)

Figure A-3 *VelociCalc Plus Meter (Model: 8386-M-S)*

_____

A. 5 Fluke Ti20 Thermal Imager

Figure A-4 *Fluke Ti20 Thermal Imager*

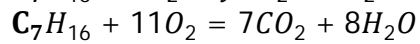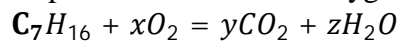## A. 6 Cone calorimeter with analysing equipment

Figure A-4 *Cone calorimeter with analysing equipment*

C

D

Appendix B – Calculations

D. 1 Calculating Heptane stociometric ratio

Heptane combustion in oxygen:

$$C_7H_{16} + xO_2 = yCO_2 + zH_2O$$
$$C_7H_{16} + 11O_2 = 7CO_2 + 8H_2O$$

Oxygen-fuel mass ratio is then:

$$\frac{m_{O_2}}{m_{C_7H_{16}}} = \frac{2 \cdot 16\frac{g}{mol}}{7 \cdot 14\frac{g}{mol} + 16 \cdot 1\frac{g}{mol}} = 3,52$$

Mass % oxygen in air is:

$$\frac{0,21 \cdot O_2}{0,79 \cdot N_2 + 0,21 \cdot O_2} = \frac{0,21 \cdot 2 \cdot 16\frac{g}{mol}}{0,79 \cdot 2 \cdot 14\frac{g}{mol} + 0,21 \cdot 2 \cdot 16\frac{g}{mol}} = 0,233$$

Heptane/air stociometric ratio is then:

$$\frac{\Delta H_c}{r} = \frac{44600\frac{kJ}{kg}}{3,52 \cdot \frac{1}{0,233}} = \textbf{2952, 2kJ/kg}$$

E

F

Appendix C – Example FDS input file using liquid fuel model

```
&HEAD CHID='pool_fire exp1', TITLE='pool fire exp1' /

&MESH IJK=80,80,80, XB=4.0,6.0,0.5,2.5,1.0,3.0 /

&RADI RADIATIVE_FRACTION = 0.3/

&TIME T_END=350. /
&MISC TMPA=20./

&MATL ID              = 'STEEL SHEET'
      EMISSIVITY      = 0.3
      DENSITY         = 7800.
      CONDUCTIVITY    = 45.0
      SPECIFIC_HEAT   = 0.46 /

&MATL ID              = 'CONCRETE ISO'
      EMISSIVITY      = 0.93
      DENSITY         = 1860.
      CONDUCTIVITY    = 0.72
      SPECIFIC_HEAT   = 0.78/

&SURF ID              = 'ISO ROOM'
      MATL_ID         = 'CONCRETE ISO'
      THICKNESS       = 0.20
      COLOR           = 'GRAY' /

&SURF ID              = 'HOLE'
      POROUS          = .TRUE.   /
      VOLUME_FLUX     = -5.6
      COLOR           = 'BLUE'

&SURF ID              = 'PALLET'
      COLOR           = 'BROWN' /

&SURF ID              = 'HOOD'
      MATL_ID         = 'STEEL SHEET'
      THICKNESS       = 0.006
      COLOR           = 'RED' /

&SURF ID              = 'RIG'
      MATL_ID         = 'STEEL SHEET'
      THICKNESS       = 0.006
      COLOR           = 'BLUE' /

Fire
&MATL ID                     = 'HEPTANE LIQUID'
      EMISSIVITY             = 1.0
      NU_FUEL                = 1.0
      HEAT_OF_REACTION       = 318.
      CONDUCTIVITY           = 0.14
      SPECIFIC_HEAT          = 2.24
      DENSITY                = 684.
      ABSORPTION_COEFFICIENT = 40
      BOILING_TEMPERATURE    = 98.4 /

&SURF ID                = 'HEPTANE POOL'
      FYI               = '4 l of heptane in a 0.5 m x 0.5 m pan'
      COLOR             = 'YELLOW'
      MATL_ID           = 'HEPTANE LIQUID','STEEL SHEET','CONCRETE ISO'
      THICKNESS         = 0.0152,0.006,0.05/Thickness heptane measured based onn mass 2,6kg and density 684 kg/m3.
      TMP_INNER         = 14. / From measurements experiments.

&VENT XB= 4.85, 5.35, 0.95, 1.45, 1.20,1.20, SURF_ID='HEPTANE POOL' /

&VENT MB='YMIN',SURF_ID='OPEN' / Mesh side open, Air supply to mesh.
&VENT MB='YMAX',SURF_ID='OPEN' / Mesh side open, Air supply to mesh.
&VENT MB='XMIN',SURF_ID='OPEN' / Mesh side open, Air supply to mesh.
&VENT MB='XMAX',SURF_ID='OPEN' / Mesh side open, Air supply to mesh.
&VENT MB='ZMAX',SURF_ID='OPEN' / Mesh side open, Air supply to mesh.

ISO room
&OBST XB= 0.00, 3.60, 0.00, 0.20, 0.00, 3.40, SURF_ID='ISO ROOM' / South wall
&OBST XB= 0.00, 3.60, 2.20, 2.40, 0.00, 3.40, SURF_ID='ISO ROOM' / Nort  wall
&OBST XB= 3.40, 3.60, 0.20, 2.20, 0.00, 3.40, SURF_ID='ISO ROOM' / East wall
&OBST XB= 0.00, 0.20, 0.20, 2.20, 0.00, 3.40, SURF_ID='ISO ROOM' / West wall
&OBST XB= 0.20, 3.40, 0.20, 2.20, 0.80, 1.00, SURF_ID='ISO ROOM' / Floor
&OBST XB= 0.20, 3.40, 0.20, 2.20, 3.20, 3.40, SURF_ID='ISO ROOM' / Roof

&HOLE XB= 3.35, 3.65, 0.20, 2.20, 0.00, 0.80,/ Below ISO room east wall
&HOLE XB= 3.35, 3.65, 0.80, 1.60, 1.00, 3.00, / Door

Exhaust hood
&OBST XB= 3.61, 3.616, -0.30, 2.70, 2.50, 3.80, SURF_ID='HOOD' / west side
&OBST XB= 6.61, 6.616, -0.30, 2.70, 2.50, 3.80, SURF_ID='HOOD' / east side
&OBST XB= 3.61, 6.61, -0.294, -0.30, 2.50, 3.80, SURF_ID='HOOD' / South side
&OBST XB= 3.61, 6.61, 2.70, 2.706, 2.50, 3.80, SURF_ID='HOOD' / North side
&OBST XB= 3.61, 6.616,-0.294, 2.706, 3.80, 4.00, SURF_ID='HOOD' / Top

&HOLE XB= 3.61, 6.616,-0.3, 2.706, 3.70, 4.2,    / Ventilation
&OBST XB= 4.6,5.6, 0.7,1.7, 3.80, 3.80, SURF_ID='HOLE'   / Ventilation

Support fire (Pallets)
&OBST XB= 4.70, 5.50, 0.50, 1.90, 0.00, 1.00,  SURF_ID='PALLET' / Pallets
&OBST XB= 4.50, 5.70, 0.40, 2.00, 1.00, 1.006, SURF_ID='HOOD' / Plate
&OBST XB= 4.80, 5.40, 0.90, 1.50, 1.006,1.200, SURF_ID='ISO ROOM' / Siporex+weight (concrete)

The Rig
OBST XB= 5.05, 5.10, 0.70, 0.75, 1.00, 2.40, SURF_ID='RIG' / Foot   (Use 50mm square pipes)
OBST XB= 5.05, 5.10, 1.65, 1.70, 1.00, 2.40, SURF_ID='RIG' / Foot
OBST XB= 4.85, 5.40, 0.70, 0.75, 1.30, 1.35, SURF_ID='RIG' / Foot
OBST XB= 4.85, 5.40, 1.65, 1.70, 1.30, 1.35, SURF_ID='RIG' / Foot
OBST XB= 4.85, 4.90, 0.70, 1.70, 1.30, 1.35, SURF_ID='RIG' / Pipe
OBST XB= 4.95, 5.00, 0.70, 1.70, 1.30, 1.35, SURF_ID='RIG' / Pipe
OBST XB= 5.05, 5.10, 0.70, 1.70, 1.30, 1.35, SURF_ID='RIG' / Pipe
OBST XB= 5.15, 5.20, 0.70, 1.70, 1.30, 1.35, SURF_ID='RIG' / Pipe
OBST XB= 5.25, 5.30, 0.70, 1.70, 1.30, 1.35, SURF_ID='RIG' / Pipe
OBST XB= 5.35, 5.40, 0.70, 1.70, 1.30, 1.35, SURF_ID='RIG' / Pipe

Output data
&SLCF PBX=5.1, QUANTITY='TEMPERATURE' /
&SLCF PBY=0.95, QUANTITY='TEMPERATURE' /
&SLCF PBY=1.20, QUANTITY='TEMPERATURE' /
&SLCF PBY=1.45, QUANTITY='TEMPERATURE' /
&SLCF PBY=2.45, QUANTITY='TEMPERATURE' /
&SLCF PBY=3.20, QUANTITY='TEMPERATURE' /
&SLCF PBX=5.1, QUANTITY='visibility' /
&SLCF PBX=5.1, QUANTITY='HRRPUV' / Heat Release Rate per Unit Volume
&SLCF PBX=5.1, QUANTITY='MIXTURE_FRACTION' /

Overall energy budget (HRR fire+losses)is generated automatical in FDS.

Temperature measurements
&DEVC ID='T3'  XYZ=5.1,1.2,1.25, QUANTITY='TEMPERATURE' / 5 cm above heptane layer
&DEVC ID='T4'  XYZ=5.1,1.2,1.65, QUANTITY='TEMPERATURE' / 45 cm above heptane layer
&DEVC ID='T5'  XYZ=5.1,1.2,2.15, QUANTITY='TEMPERATURE' / 95 cm above heptane layer
&DEVC ID='T6'  XYZ=5.1,1.2,2.40, QUANTITY='TEMPERATURE' / 120 cm above heptane layer
&DEVC ID='T7'  XYZ=5.1,1.2,2.75, QUANTITY='TEMPERATURE' / 155 cm above heptane layer
&DEVC ID='T8'  XYZ=5.1,1.2,3.20, QUANTITY='TEMPERATURE' / 200 cm above heptane layer

Radiation measurement
&DEVC ID='R1'  XYZ=5.1,2.45,2.12, QUANTITY='RADIATIVE HEAT FLUX GAS',  IOR=-2, /

&TAIL /
```

H

Appendix D – Various experimental data